UNIVERSIDADE FEDERAL DO RIO GRANDE DO SUL

INSTITUTO DE PESQUISAS HIDRÁULICAS

PROCESSOS HIDROLÓGICOS E HIDRÁULICOS EM GRANDES ÁREAS INUNDÁVEIS: ASSIMETRIA DE HIDROGRAMAS E SIMULAÇÃO MATEMÁTICA

Ayan Santos Fleischmann

Dissertação submetida ao Programa de Pós-Graduação em Recursos Hídricos e Saneamento Ambiental da Universidade Federal do Rio Grande do Sul como requisito parcial para a obtenção do título de Mestre em Recursos Hídricos e Saneamento Ambiental

Orientador: Prof. Dr. Rodrigo Cauduro Dias de Paiva

Co-Orientador: Prof. Dr. Walter Collischonn

Banca examinadora

Adriano Rolim da Paz	UFPB
Joel Avruch Goldenfum	UFRGS
Fernando Mainardi Fan	UFRGS

Porto Alegre, 10 de março de 2017.

p
p l
p l u
p l u v
p l u v i
p l u v i a
f l u v i a l
f l u v i a l
f l u v i a l
f l u v i a l
f l u v i a l
f l u v i a l

(Augusto de Campos)

Agradecimentos

Ficam aqui registrados meus sinceros agradecimentos a todos aqueles que contribuíram de alguma forma para esta pesquisa.

Aos professores e amigos Walter Collischonn e Rodrigo Paiva, pelos ensinamentos sobre hidrologia e sobre como fazer pesquisa, pela orientação e ótima convivência nos últimos anos.

Aos professores Fernando Fan e Anderson Ruhoff, aos amigos do grupo de pesquisa em Hidrologia de Grande Escala, em especial a Siqueira (grande amigo, e a quem devo grande parte de meu conhecimento em programação), Pedro, Mino, Paulo, Bibiana, Sly, Germano, João Paulo, Hugo, Anderson, Alice e Arthur, e a todos meus amigos de modo geral, do IPH, da graduação e do colégio, pela ótima parceria do dia-a-dia e pelas profícuas discussões hidrológicas (e tantas outras).

Aos colegas e pesquisadores de Toulouse, Adrien Paris, Marielle Gossett, Sylvain Biancamaria e Stephane Calmant, que me proporcionaram o contato com a bacia do rio Níger.

Ao CNPq pelo financiamento, e à UFRGS e ao Instituto de Pesquisas Hidráulicas, seus funcionários e à sua estrutura que me permitiram a realização deste trabalho.

À minha mãe, Nádia, por ter me apresentado ao mundo da pesquisa, pelos cafés em Ibiraquera, e por tudo o mais que me fez chegar até aqui; a meu pai, Rogério, pela parceria sempre atenta e carinhosa; e a toda minha família, que sempre me apoiou.

À minha namorada Camila, companheira e parceira de tantas belas aventuras e alegrias.

Resumo

Grandes áreas inundáveis prestam importantes serviços ambientais, como manutenção da biodiversidade e regulação de clima, cheias e ciclos biogeoquímicos, e estão presentes nas mais variadas regiões geográficas, desde úmidas áreas tropicais como a Amazônia, até locais áridos como os grandes deltas internos da África. Complexos processos hidrológicos e hidrodinâmicos ocorrem nestas áreas, onde existe intensa interação entre áreas inundadas, biosfera e atmosfera, e onde ocorrem alterações significativas das ondas de cheia que são por elas propagadas sazonalmente. Neste contexto, o presente trabalho apresenta, através de dois métodos distintos, formas com que podemos aprofundar nosso conhecimento da dinâmica destas grandes áreas inundáveis. Inicialmente, é abordado o efeito causado pela interação rio-planície de inundação na forma dos hidrogramas. Constatou-se, através de observação de diversos hidrogramas defluentes de grandes sistemas inundáveis, que a ascensão destes é tipicamente mais lenta que a recessão, caracterizando uma assimetria negativa. Então, a partir de uma série de abordagens numéricas, analíticas e empíricas, mostrou-se que a este fenômeno é decorrente da inversa relação entre velocidade da onda de cheia (celeridade) e vazão que ocorre nestes ambientes devido ao armazenamento nas planícies. Um estudo de caso com os principais rios da Amazônica evidenciou a relevância da avaliação de assimetria de hidrogramas para compreensão da dinâmica hidrológica em regiões inundáveis. A segunda etapa deste trabalho consistiu no aprimoramento e validação de um modelo acoplado hidrológico-hidrodinâmico distribuído para simulação de bacias com grandes áreas inundáveis, capaz de modelar matematicamente a dinâmica existente e a aumentar nossa capacidade preditiva da inundação destas regiões. Foi realizada uma aplicação na bacia do Alto Rio Níger, no Oeste da África, onde está localizado o Delta Interno do Níger, uma vasta planície no Deserto do Sahel inundada sazonalmente, e onde importantes perdas por evaporação ocorrem. O modelo desenvolvido representou de forma satisfatória vazões, níveis e áreas inundadas ao longo da região, permitindo a identificação de processos relevantes na inundação do Delta. O acoplamento entre uma representação explícita da hidrodinâmica dos canais da planície (armazenamento, bifurcações, remanso) e o balanço vertical hidrológico (infiltração de água da planície para o solo e evapotranspiração) mostrou-se necessário para o satisfatório resultado do modelo. Assim, com esta pesquisa, acredita-se que novos elementos foram contribuídos para a compreensão da hidrologia de grandes áreas inundáveis, a partir da identificação do importante efeito da interação rio-planície na assimetria de hidrogramas, e do desenvolvimento de técnicas de modelagem matemática que evidenciaram a relevância da representação de interações entre hidrologia e hidrodinâmica em modelos de grandes escala.

Abstract

Large floodable areas provide important environment services, such as biodiversity maintenance and regulation of climate, floods and biogeochemical cycles, and are present throughout different geographical settings, from tropical, wet areas like the Amazon, to arid ones such as the large African Inner deltas. Complex hydrologic and hydrodynamic processes occur in these areas, such as an intense interaction between flooded areas, biosphere and atmosphere, and alterations of flood waves that propagate through it. In this context, this study presents, through two distinct methods, ways with which we can deepen our understanding of the dynamics of such floodable areas. Firstly, the effect of river-floodplain interaction on hydrograph shape is addressed. It was noted, by observing a series of hydrographs routed through floodable systems, that hydrograph ascension is typically slower than the recession, characterizing a negative skewness. Then, through a series of numerical, analytical and empirical approaches, it was shown that this phenomenon exists due to the inverse relationship between flood wave speed (celerity) and discharge that occurs in these environments because of floodplain storage. A case study in main Amazon Basin tributaries was performed and indicated the relevance of hydrograph skewness evaluation for comprehension of hydrological dynamics in floodable areas. The study second step consisted in the development and validation of a distributed, coupled hydrologic-hydrodynamic model for simulation of basins with large floodable areas, able to mathematically model and to improve our prediction capacity of flooding in these areas. An application was performed in Upper Niger River, West Africa, where the Niger Inland Delta is located, which is a vast floodplain in the Sahel Desert that is seasonally flooded, and where important evaporation losses occur. The developed model satisfactorily represented discharges, levels and flooded areas across the basin, allowing the identification of relevant flooding processes in the Delta. The coupling between explicit representation of floodplain channel hydrodynamics (storage, bifurcations, backwater) and vertical hydrological balance (floodplain water infiltration into soil column, and evapotranspiration) proved a necessary model structure for the satisfactorily obtained results. Finally, with this research, we understand that new elements were contributed to the comprehension of hydrology of large floodable areas, from the identification of the river-floodplain interaction effects on hydrograph skewness to the development and application of mathematical modelling techniques, showing the relevance of the interaction between hydrology and hydrodynamic in such areas.

Sumário

1 Apresentação

1.1 Introdução e justificativa

Áreas inundáveis podem ser definidas como "ecossistemas na interface entre ambientes terrestres e aquáticos, continentais ou costeiros, naturais ou artificiais, permanentemente ou periodicamente inundados por águas rasas ou com solos encharcados, doces, salobras ou salgadas, com comunidades de plantas e animais adaptadas à sua dinâmica hídrica" (Junk et al., 2015). Representam extensas partes de bacias hidrográficas, prestando diversos serviços ambientais como retenção de sedimentos, recarga de aquíferos, estocagem de carbono, manutenção de biodiversidade, regulação de clima e fornecimento de produtos vegetais (Whalen, 2005; Fan & Miguez-Macho, 2011; Junk et al., 2015). Na América do Sul, por exemplo, existem diversas regiões onde centenas de quilômetros quadrados são sazonal ou permanentemente inundadas (Figura 1.1). São áreas de extrema diversidade de vegetação, onde em muitos casos se encontra um mosaico de florestas alagáveis e secas, savana e vegetações hidrófilas (Junk et al., 2015). O relevo é tipicamente plano, sendo o solo do tipo hidromórfico, e onde níveis freáticos elevados auxiliam na manutenção das áreas inundadas. Na área central da Bacia Amazônica, por exemplo, cerca de oito mil lagos estão presentes, e cerca de 17% da região está coberta por áreas inundáveis (Latrubesse, 2012; Alsdorf, 2003; Melack & Hess, 2010). Nestas áreas, os ecossistemas se desenvolvem e se adaptam aos ciclos sazonais de inundação (Junk et al., 1989). Há também áreas inundáveis em grandes regiões semi-áridas, como nos grandes deltas internos da África (deltas do Níger e do Okavango), onde a inundação é causada por águas precipitadas em áreas a centenas de quilômetros de distância, gerando abundância de alimentos e biodiversidade.

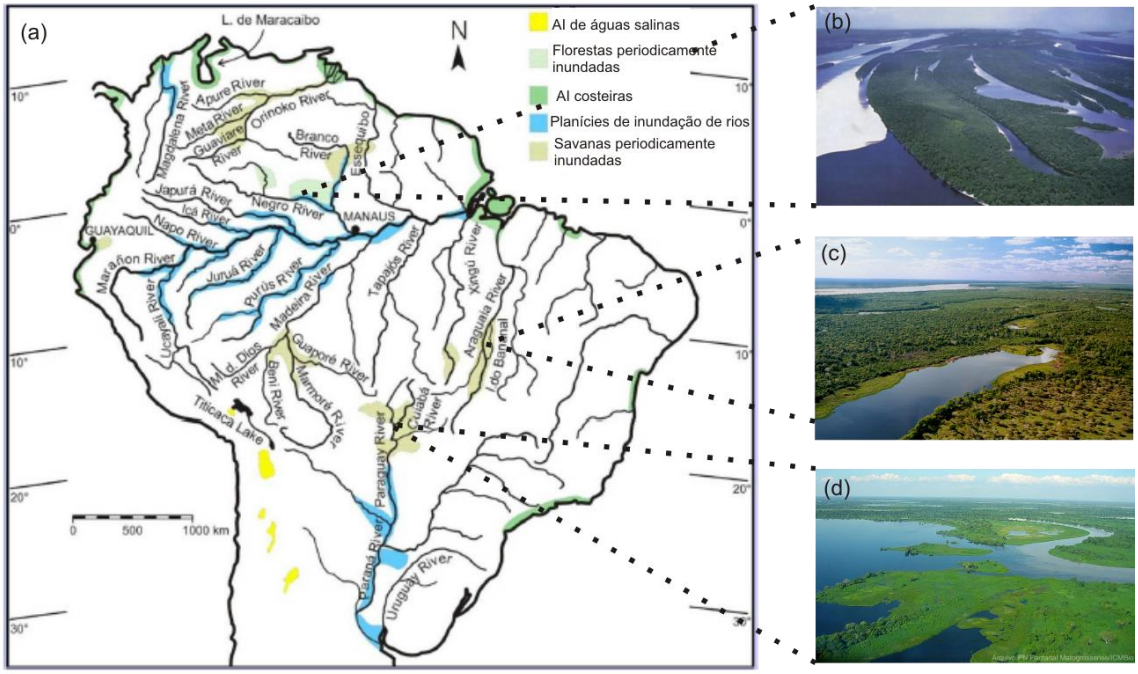

Figura 1.1. (a) Localização das principais áreas inundáveis (AI) da América do Sul. Fonte: Junk et al., 2015. (b) Arquipélago de Mariuá, no Rio Negro, Amazônia. Fonte: Latrubesse & Stevaux, 2008. (c) Ilha do Bananal, no rio Araguaia. Fonte: Pavan, 2016 (d) Pantanal, no Rio Paraguai. Fonte: Brasil, 2016.

Dependendo da origem das águas causadoras da inundação, as áreas inundáveis podem ser classificadas como planícies de inundação, onde o extravasamento direto de água dos rios é o processo dominante, ou como áreas interfluviais, cuja inundação é causada por fenômenos hidrológicos locais, como chuva incidente diretamente na região causando saturação do solo e grandes áreas de alagamento. Estes processos podem também ocorrer simultaneamente. Além disso, áreas inundáveis de pequenas bacias hidrográficas têm um comportamento bastante distinto daquelas de grandes bacias (e.g. Bacia Amazônica, Bacia do Rio Araguaia), onde os volumes de água que chegam aos rios nas partes mais baixas são a integração de diversos processos que ocorreram a montante. Hidrogramas em rios pequenos tendem a apresentar picos bastante aleatórios, enquanto em grandes rios estes refletem a natureza integradora da grande bacia (Junk et al., 2015).

Muitas destas grandes áreas inundáveis possuem baixa cobertura de observações in situ, seja pelo difícil acesso ou pela grande área coberta. Assim, surge a necessidade de se desenvolver técnicas alternativas que permitam inferir sobre processos que ocorram nestas áreas. Recentemente, grandes avanços em medições por sensoriamento remoto têm sido realizados, sendo hoje possível obter medições a cada poucos dias de extensões de áreas inundadas (Schumann et al., 2009; Rast et al,. 2014).

No entanto, ainda é difícil obter informação sobre certas variáveis de forma distribuída na bacia hidrográfica, além de haver a necessidade de se prever respostas a

eventuais mudanças climáticas, de uso e ocupação do solo e de implementação de reservatórios, entre outros tipos de análises de impactos ambientais. Para isto, a modelagem matemática surge como uma ferramenta de grande potencial. Esforços da comunidade científica têm permitido o desenvolvimento de modelos hidrológicos e hidrodinâmicos de grande escala que representem, por exemplo, a complexidade dos fluxos bidimensionais de água nestas áreas inundáveis, a interface de troca com os grandes rios, bem como processos hidrológicos como evapotranspiração e infiltração de água no solo (Paz et al., 2011; Neal et al., 2012a; Yamazaki et al., 2014). O investimento nestas técnicas permitirá o avanço na nossa capacidade de compreensão e predição dos fenômenos relacionados a estas áreas. Isto proporcionaria um manejo mais eficiente destas regiões, bem como um maior domínio sobre o impacto destas nos diversos serviços prestados, como regulação do clima e de cheias.

Neste cenário, este trabalho utiliza dados observados in-situ, observações de sensoriamento remoto e aperfeiçoamentos de técnicas de modelagem hidrológica de grande escala para contribuir à compreensão de processos hidrológicos e hidráulicos de grandes áreas inundáveis. São estudados a relação entre rio e planície de inundação, os efeitos desta relação na resposta hidrológica da bacia, e algumas formas que podemos ter para diferenciar tipos de áreas inundáveis, como as regiões interfluviais, inundadas por processos locais, e as planícies de inundação ao longo de rio, inundadas pelo extravasamento de água destes. Além disso, são desenvolvidas técnicas de modelagem matemática de grande escala que aumentem nossa capacidade preditiva dos processos ocorrentes nestas áreas. O modelo desenvolvido é então calibrado e validado para a bacia do Alto Rio Níger, que contém a região sazonalmente inundável do Delta Interno do Níger, uma das maiores planícies inundáveis da África, sendo então utilizado para demonstrar importantes interações entre hidrologia (infiltração, evapotranspiração) e hidrodinâmica (armazenamento em planícies, efeitos de remanso, propagação em canais de planícies) ao longo desta área.

1.2 Compreensão de processos hidrológicos e hidráulicos de grandes áreas inundáveis: exemplo da área inundável do Delta Interno do Níger

Para finalizar a apresentação do objeto de estudo deste trabalho, na Figura 1.2 estão apresentados hidrogramas observados ao longo do Rio Níger, na África, a montante e a jusante da grande área inundável do Delta Interno do Níger, uma vasta planície no Deserto do Sahel onde mais de 10.000 km² são inundados sazonalmente devido às águas oriundas do alto Rio Níger (Figura 1.2b). A montante, em Koulikoro, o hidrograma apresenta um típico padrão sazonal, com vazões de pico atingindo mais de 4.500 m³/s nos meses de Setembro; no entanto, à medida que a onda de cheia é propagada ao longo do rio, o hidrograma sofre importantes alterações: inicialmente, a atenuação devido ao Delta Interno é evidente, e a jusante da região (estação de Diré), vazões de pico não excedem mais de 2.000 m3/s. Processos de armazenamento,

infiltração e evaporação nas planícies atuam ativamente. Outro aspecto é também marcante: o hidrograma torna-se mais suave, com menos variações de alta frequência como observado em Koulikoro; mesmo as pequenas oscilações existentes no período de águas baixas devido à regularização de vazões a montante de Koulikoro são atenuadas. Além disso, outra característica, menos evidente, surge: o hidrograma em Diré possui uma peculiar assimetria negativa, com uma ascensão mais lenta que a recessão; mais a jusante, em Ansongo, esta assimetria torna-se ainda mais negativa. Cabe salientar que neste trecho Diré-Ansongo, localizado a jusante do Delta Interno do Níger, uma larga planície de inundação de cerca de 4 km de largura também existe.

Neste contexto, surgem as seguintes questões científicas, abordadas nesta dissertação:

- Existe alguma relação entre a assimetria negativa de hidrogramas e a interação entre rio e planícies de inundação? **(Capítulo 3)**

- Quais os processos hidrológicos e hidrodinâmicos que atuam nas grandes áreas inundáveis (e.g., armazenamento, evaporação e infiltração em planícies), e como eles interagem, a ponto de transformar expressivamente os hidrogramas observados? **(Capítulo 4)**

- Como a simulação matemática integrada de processos hidrológicos e hidrodinâmicos melhora a representação da dinâmica de inundação destes sistemas? **(Capítulo 4)**

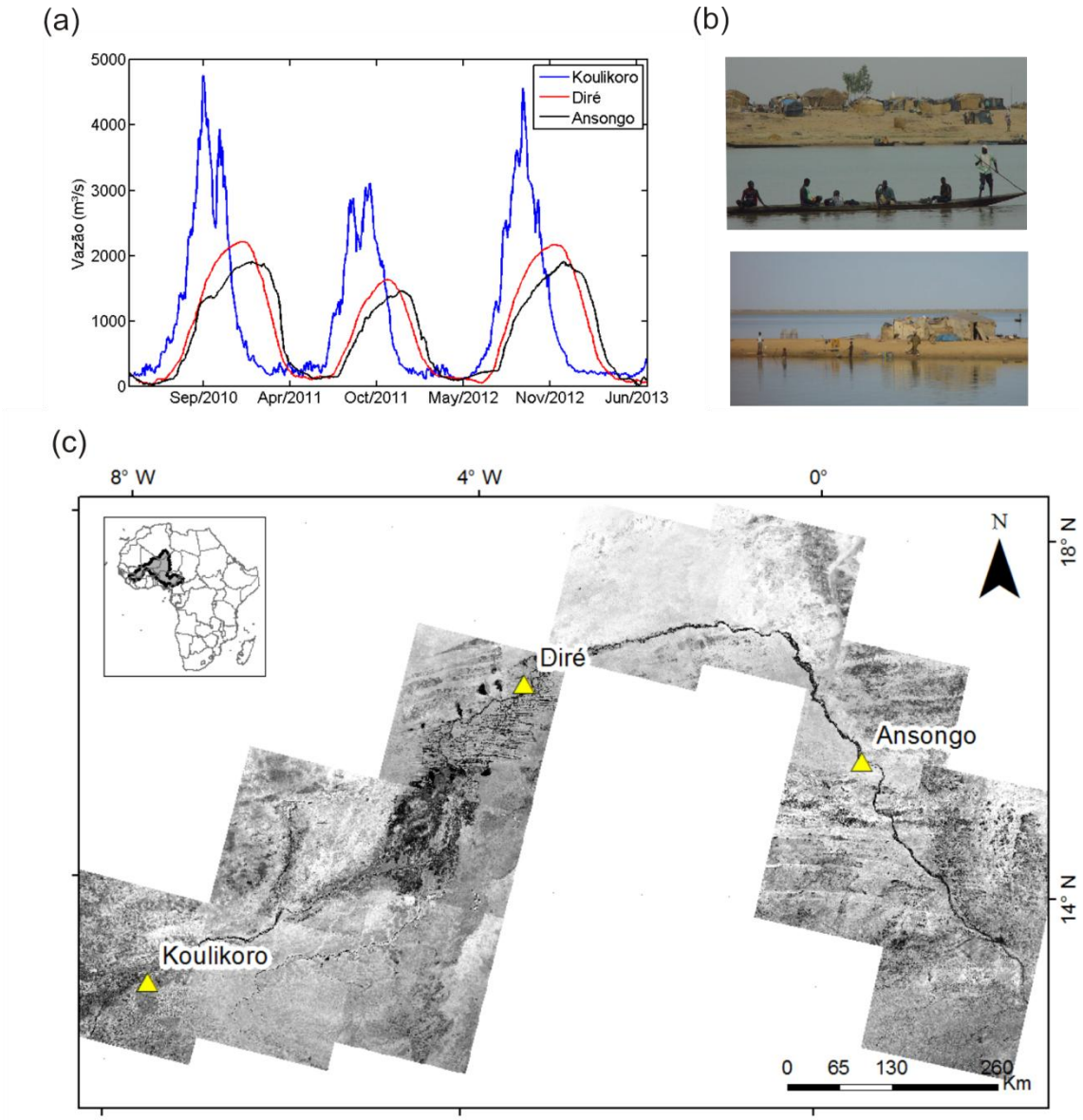

Figura 1.2. (a) Hidrogramas observados ao longo do Rio Níger, nas estações de Koulikoro, Diré e Ansongo. (b) Imagens do Delta Interno do Rio Níger. Fonte: Zwarts et al., 2005. (c) Localização da Bacia do Níger na África e imagens LANDSAT 8 da Banda 5 (disponíveis em <https://earthexplorer.usgs.gov/>) do período de águas altas (Dezembro/Janeiro), mostrando o arco realizado pelo rio Níger na região do Deserto do Sahel.

1.3 Objetivos

Objetivo geral

Compreender a interação entre processos hidrológicos e hidráulicos de grandes rios com extensas áreas inundáveis.

Objetivos específicos

- Compreender a relação entre rios e planícies de inundação e os efeitos desta nos hidrogramas observados, com ênfase na assimetria de hidrogramas;
- Aprimorar e validar um modelo hidrológico-hidrodinâmico de grande escala da bacia do Alto Rio Níger (África), que permita representar fluxos unidimensionais ao longo do rio, bem como fluxos difusos e bidimensionais ao longo da planície inundáveis;
- Compreender, através de simulação matemática, as interações entre planícies de inundação e processos hidrológicos verticais (infiltração, evapotranspiração) e a dinâmica de inundação da bacia do Alto Rio Níger (África);

1.4 Organização do trabalho

Neste trabalho são discutidos diversos processos hidrológicos e hidráulicos que ocorrem e interagem entre si em grandes áreas inundáveis. Inicialmente, no Capítulo 2 é apresentada uma revisão bibliográfica sobre as ferramentas de estudo disponíveis para compreensão destas áreas, bem como sobre o estado da arte de nossa compreensão da relação entre estes processos nos complexos sistemas rio-planície.

A metodologia do trabalho e os resultados estão descritos na forma de dois artigos científicos, escritos em inglês e apresentados nos capítulos 3 e 4. O Capítulo 3 apresenta um estudo detalhado da influência das planícies de inundação na relação entre velocidade de ondas de cheia e vazão observada em rios, e sobre os efeitos desta relação na assimetria dos hidrogramas observados em grandes sistemas rio-planície. O estudo apresenta experimentos numéricos e uma análise teórica deste fenômeno, além de um estudo de caso na Bacia Amazônica, avaliando a relação entre tipos de áreas inundáveis e assimetria observada em hidrogramas. Este capítulo encontra-se publicado na revista Water Resources Research.

O Capítulo 4 apresenta o desenvolvimento e validação de um modelo hidrológico-hidrodinâmico para a bacia do Alto Rio Níger, que envolve o Delta Interno do Niger, apresentado na Figura 1.2. O modelo desenvolvido é, então, utilizado para fornecer novas compreensões sobre os processos existentes nesta grande área inundável, em termos da interação entre evaporação e infiltração nas áreas inundáveis e hidrodinâmica dos canais da planície.

Por fim, o Capítulo 5 apresenta as conclusões, considerações finais e possibilidades de trabalhos futuros para a pesquisa aqui apresentada.

2 Processos hidrológicos e hidráulicos em grandes áreas inundáveis: compreensão e ferramentas de estudo

Este capítulo é dividido em duas partes: ferramentas de estudo e compreensão de grandes áreas inundáveis.

2.1 Ferramentas de estudo de grandes áreas inundáveis

Nesta parte, alguns métodos e técnicas utilizados na compreensão da hidrologia de grandes áreas inundáveis são descritos: dados observados in situ, sensoriamento remoto e modelagem matemática.

2.1.1 Dados observados *in situ*

A primeira etapa para a maior compreensão de grandes áreas inundáveis está relacionada ao melhor monitoramento in situ destas. Dados desta natureza são indispensáveis, como nível e vazão dos rios, concentração e carga de sedimentos, volumes de precipitação e nível das águas. Naturalmente, estes dados auxiliam diretamente na compreensão de processos hidrológicos, como as medições de perfis de velocidade e vazão em diferentes seções dos rios (Filizola et al., 2014), topobatimetria para o conhecimento da geometria de seções transversais e planícies, e perfil longitudinal dos rios e canais que formam a planície de inundação (Trigg et al., 2012). A composição isotópica de oxigênio na água pode auxiliar na identificação das fontes de água predominantes, como chuva local e água da calha fluvial (Richey et al., 1989). Além disso, técnicas de monitoramento in situ são de difícil aplicação em grandes regiões, como as áreas inundáveis abordadas neste trabalho. Por isso, outras ferramentas como sensoriamento remoto e modelagem matemática são bastante relevantes, as quais, por sua vez, utilizam dados in situ para sua calibração e validação.

2.1.2 Sensoriamento Remoto

Sensoriamento remoto (SR) pode ser entendido como o conjunto de dados sobre um objeto obtido a partir de certa distância (Pidwirny, 2013). As técnicas envolvidas baseiam-se na energia emitida ou refletida por objetos alvos na superfície terrestre, que é medida por sensores a bordo de balões, aeronaves ou satélites.

A maioria das grandes áreas inundáveis abordadas neste trabalho se enquadra na definição de regiões mal monitoradas, onde fatores como inacessibilidade, extensão da área, conflitos civis e um geral esparso monitoramento de variáveis hidrometeorológicas fazem com que o uso de métodos de SR seja fundamental para estudos relacionados a estas.

Neste contexto, recentes avanços em técnicas de SR têm permitido a criação de um grande número de bases de dados úteis no mapeamento de áreas inundáveis, permitindo a quantificação de muitos processos e fluxos do ciclo hidrológico terrestre (Alsdorf et al., 2003, 2007b, Rast et al., 2014). Existem bases de dados desenvolvidas/medidas a partir de um satélite específico, a partir da combinação e intenso processamento de dados de vários satélites, ou mesmo pela combinação de dados in-situ com dados de SR. Um aspecto importante destes produtos é a resolução espacial e temporal associada, que varia de poucos metros a centenas de quilômetros, e de horas a meses, respectivamente. A escolha de um determinado produto de SR deve ser realizada levando em consideração os objetivos do estudo e as resoluções requeridas. Além disso, é importante notar que dados de SR são baseados em hipóteses nem sempre aplicáveis. Por exemplo, um dos sensores utilizados no produto TMPA de precipitação (TRMM Multisatellite Precipitation Analyses, Huffman et al., 2007) baseia-se nas ondas do infra-vermelho e no princípio associado de que uma nuvem mais fria gera mais precipitação. Entretanto, em regiões montanhosas como a cordilheira dos Andes, esta hipótese nem sempre é aplicável, de tal forma que, além de outras causas como uma grande variabilidade espacial da chuva, nesta região o produto tem baixo desempenho (Zulkafli et al., 2014).

Dados de SR são baseados nas diferentes respostas de objetos na superfície terrestre em termos de absorção, emissão, transmissão e reflexão de radiação eletromagnética. Assim, cada um dos componentes do ciclo hidrológico terrestre (precipitação, evapotranspiração, volumes de rios e lagos, etc.) possui uma característica peculiar que permite a sua medição a partir de técnicas de SR. Então, partindo da equação da continuidade de uma dada bacia hidrográfica, nos próximos tópicos são abordados alguns dos principais produtos e técnicas de SR hoje utilizados em estudos hidrológicos de grande escala:

$$\Delta V/_{\Delta t} = Q + P - E \pm G \qquad (2.1)$$

Onde $\Delta V/_{\Delta t}$ é a variação de volume armazenado em cada intervalo de tempo (podendo estar na superfície, no solo ou nas águas subterrâneas), Q é a vazão, P a precipitação, E a evapotranspiração e G a água infiltrada ou recebida do solo.

*<u>*Armazenamento total de água terrestre*</u>. A principal forma de estimar a variação de volume de água em uma dada região é através dos dados da missão GRACE (Gravity Recovery and Climate Experiment, associação entre agências espaciais dos EUA e Alemanha, Tapley et al., 2004), que utiliza o impacto das massas de água na alteração do campo gravitacional terrestre para estimar o volume de água em uma dada região.

Este volume está relacionado ao volume total armazenado na superfície, solos e águas subterrâneas.

*_Extensão de áreas inundadas_. Este componente pode ser dividido entre rios, lagos e reservatórios (discutidos na seção "_Vazão e Níveis de Rios e Lagos_") e áreas inundáveis. Em estudos destas últimas, recentes esforços têm focado no uso de sensores de micro-ondas ativos, especialmente na banda L, devido a sua penetração na vegetação e nas nuvens. Por exemplo, dados da banda L da missão JERS (Agência Espacial Japonesa) foram usados por Hess et al. (2003) para desenvolver o primeiro mapeamento em larga escala das áreas inundáveis da bacia Amazônica. Produtos do sucessor do JERS, ALOS-PALSAR, foram recentemente disponibilizados gratuitamente e têm resolução espacial variando entre 12.5 e 100 m, abrindo um grande potencial para o mapeamento de áreas inundáveis com grande qualidade. A Figura 2.1 apresenta um exemplo deste último produto na região da Ilha do Bananal, no Rio Araguaia, para as estações seca e úmida. Os valores da imagem indicam o coeficiente de retroespalhamento do radar, onde valores baixos (altos) são referentes a água aberta (vegetação inundada). Imagens de micro-ondas passivos podem ser utilizados, como nos trabalhos de Hamilton et al. (2002) e Papa et al. (2008) para compreensão de inundações na América do Sul e no mundo inteiro, respectivamente. Por fim, produtos de sensores ópticos (e.g. LANDSAT e MODIS) são úteis para mapear a extensão de áreas inundáveis, através de classificação automática de imagem ou do uso de índices como o NDWI (Gao et al., 1996). As principais limitações destes estão relacionadas à não penetração de dosséis de vegetação e à indisponibilidade de imagens durante períodos chuvosos, quando normalmente ocorrem inundações (devido à cobertura de nuvens).

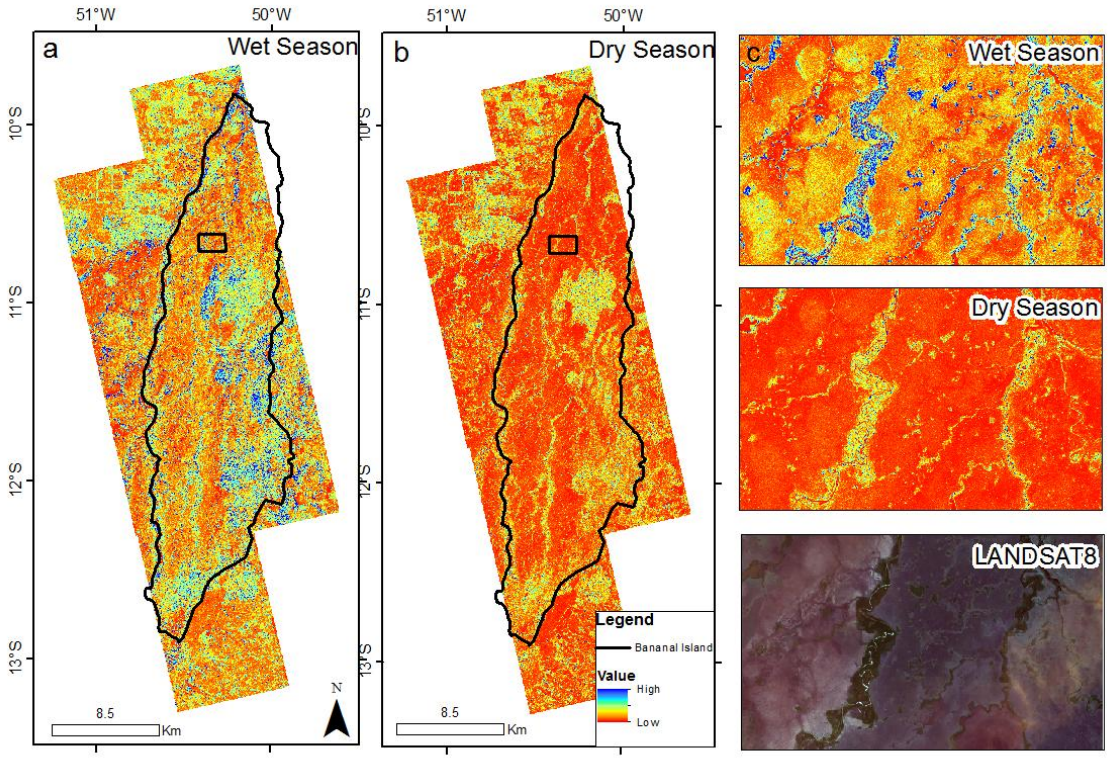

Figura 2.1. (a) Mosaico de imagens ALOS PALSAR (produto RTC do Alaska Satellite Facility) de 15/Jan/2011 e 13/Fev/2011 (estação úmida) para a Ilha do Bananal (contorno preto), em uma resolução especial de 12.5 m (b) Mosaico de imagens de 28/Set/2010 e 24/Ago/2008 (estação seca) para a mesma área. (c) Detalhe da Ilha do Bananal (destacada como uma caixa preta nas figuras a e b), mostrando a inundação existente na região ao redor dos tributários locais e a vegetação de cerrado através da comparação de imagens da estação úmida (wet) e seca (dry). Uma composição RGB (4,3,2) de imagens LANDSAT 8 também está apresentada para identificação da vegetação ripária e outras formas de vegetação. Os valores das imagens RTC são referentes ao coeficiente de retroespalhamento do radar, onde valores muito baixos indicam água aberta, e valores muito altos, vegetação inundada. Fonte: Pontes et al., 2017.

*<u>*Armazenamento de água no solo*</u>. Este componente se refere à umidade do solo. Existem alguns produtos de SR que foram desenvolvidos com o fim de medir umidade do solo, como as missões SMOS (Soil Moisture Ocean Salinity – European Space Agency) e SMAP (Soil Moisture Active and Passive), que medem umidade do solo a partir da banda L do micro-ondas e permitem um mapeamento desta variável para as primeiras camadas de solo (~0-5 cm) (Entekhabi et al., 2010; NASA-JPL, 2015).

***<u>*Armazenamento de águas subterrâneas*</u>. É difícil para satélites medir diretamente os volumes de águas subterrâneas separadamente dos demais componentes de águas superficiais. Os principais estudos têm utilizado produtos do GRACE para obter flutuações dos níveis freáticos. Por exemplo, Richey et al. (2015) utilizaram dados GRACE em conjunto com resultados de modelos matemáticos para identificar o número de aquíferos no mundo que têm sido deplecionados pela ação humana.

*****_Precipitação_. Existem hoje muitas técnicas disponíveis para a medição de chuva, sendo as principais relacionadas a sensores passivos de micro-ondas (identificando partículas de gelo dentro de nuvens), infravermelho (relacionado à temperatura de nuvens) e radar (retorno de sinais emitidos quando estes encontram massas de precipitação). A missão TRMM (Tropical Rainfall Measurement Mission – parceria das agências espaciais de EUA e Japão) foi a primeira desenvolvida para medir precipitação em uma cobertura quase global, e o seu principal produto (TMPA - Multisatellite Precipitation Analyses; Huffman et al., 2007) utiliza um conjunto de cinco diferentes sensores, combinando algumas da técnicas descritas acima. A missão terminou em 2015, e a sucessora Global Precipitation Measurement (GPM) começou há pouco a gerar dados. Outro produto disponível é o CMORPH (CPC MORPHing technique, do Serviço Meteorológico dos EUA), que combina dados de microondas e infravermelho para produzir dados de precipitação em alta resolução (Joyce et al., 2004). Por fim, alguns produtos combinam dados de satélite com dados observados por pluviômetros para aumentar a qualidade dos dados. Como exemplo, existe o MERGE (desenvolvido pelo Instituto Nacional de Pesquisas do Brasil, INPE), que combina dados de precipitação do TRMM com dados in situ para toda a América do Sul (Rozante et al., 2010).

*****_Evapotranspiração_. Não existe uma técnica que meça diretamente evapotranspiração. No entanto, esta pode ser obtida a partir de metodologias que utilizam balanços de energia, onde algoritmos usam parâmetros derivados de produtos de satélites (como cobertura de vegetação e temperatura da superfície terrestre obtidos pela missão MODIS) junto com observações in situ para calcular a evapotranspiração (e.g. Bastiaanssen et al., 1998).

*****_Vazão e Níveis de Rios e Lagos_. Dados de níveis podem ser obtidos diretamente a partir de SR, enquanto vazão é uma variável derivável, usando fórmulas como a equação de Manning. Para lagos, níveis d'água são normalmente convertidos em armazenamento a partir de uma relação do tipo nível-volume (Alsdorf et al., 2003). As principais técnicas de medição de nível envolvem uso de altimetria por radar, onde satélites emitem ondas de radar na direção vertical (nadir), que são refletidas quando encontram a superfície (e.g. missões TOPEX-POSEIDON, JASON, ENVISAT), e uso de laser (missão ICESAT e dados LiDAR). Rios, lagos e áreas inundáveis que cruzem o percurso destes satélites podem ser assim monitorados (Figura 2.2). A partir de passagens frequentes destes produtos são geradas as chamadas "estações virtuais", que reúnem dados sequenciais para uma mesma localidade a fim de se criar séries temporais de níveis. Modelos digitais de elevação (como os gerados pela missão SRTM – Shuttle Radar Topography Mission, Farr et al., 2007) também podem ser úteis na estimativa de níveis d'água no momento da passagem do satélite (Fevereiro de 2000), mas é restrito a regiões não florestadas. Outras fontes de dados são produtos de radar, que podem ser utilizados com a técnica de interferometria para estimar variações temporais de nível d'água (e.g. Alsdorf et al., 2007a). Por fim, a futura missão SWOT (Biancamaria, 2016) providenciará dados de altimetria em alta resolução para os principais rios do mundo

(larguras maiores que 100 m), podendo ser utilizado até mesmo para estimativa de declividade de linhas d'água. O seu lançamento está previsto para 2021 (CNES, 2017).

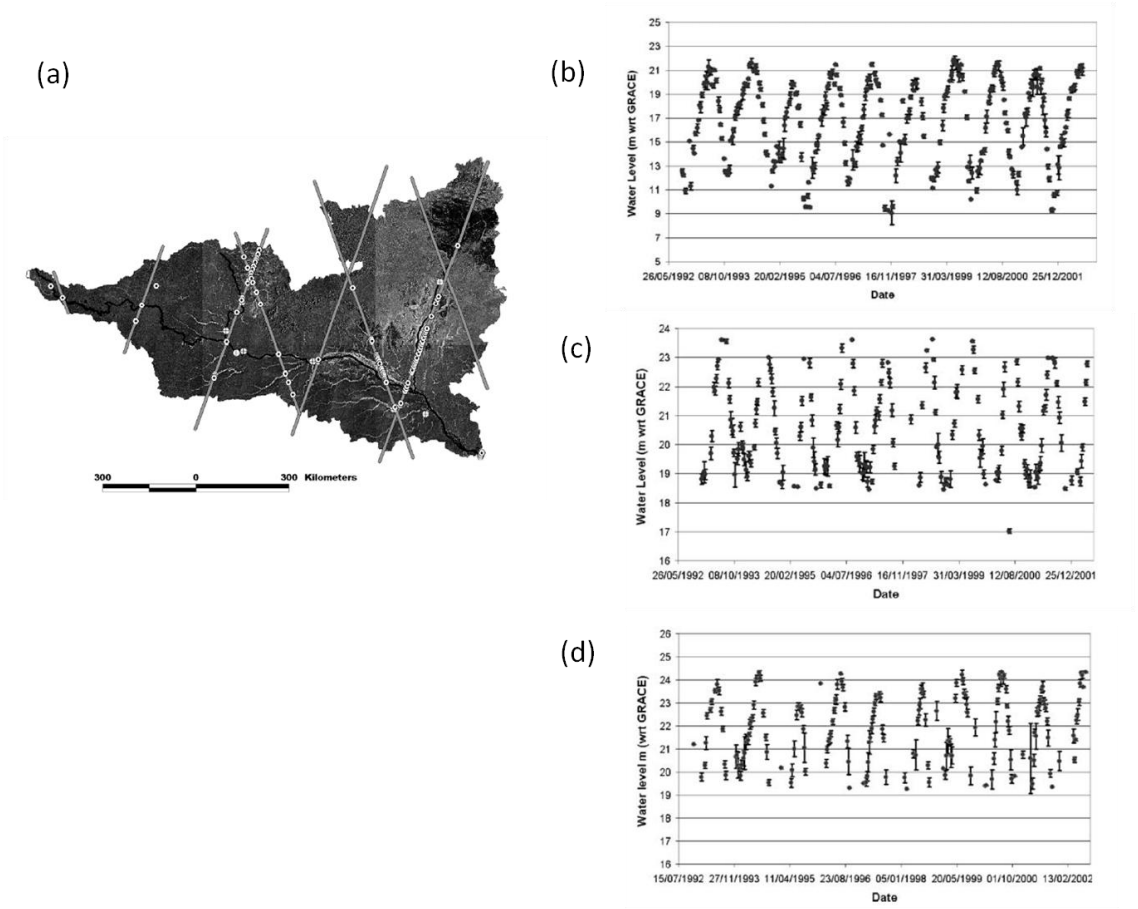

Figura 2.2. Estações virtuais de altimetria espacial da missão TOPEX/POSEIDON para a bacia do Rio Negro na Amazônia. (b) Série de altimetria de um trecho de rio com único canal, (b) múltiplos canais, e (c) de uma planície inundada. Fonte: Frappart et al., 2005.

***Outros componentes**. Além dos componentes do ciclo hidrológico mencionados anteriormente, outras características da superfície terrestre são importantes para estudos hidrológicos, como cobertura de uso do solo, tipo de vegetação e elevação do terreno. Típicas fontes de dados são imagens LANDSAT e outros produtos que utilizem radiação na faixa do visível (e.g. MODIS) para identificação de uso de solo e tipo de vegetação. Para informações de elevação do terreno, são normalmente utilizados modelos digitais de elevação, como a missão SRTM ("Shuttle Radar Topography Mission", Farr et al. (2007)), que forneceu um modelo digital para toda a superfície terrestre em uma resolução espacial de 30 m.

Estudos de grandes áreas inundáveis normalmente utilizam diversos tipos de produtos de SR para buscar compreender os processos que ocorrem nestes. Por exemplo, a integração de dados de altimetria por radar com estimativa de áreas inundadas por imageamento SAR (Synthetic Aperture Radar) permitiu que Frappart et al. (2005) estimassem os volumes armazenados nas planícies da bacia do rio Negro na Amazônia. Lee et al. (2011) utilizaram dados de altimetria e da missão GRACE para caracterizar a dinâmica das áreas inundáveis do Rio Congo. Dados de SR têm sido utilizados amplamente para a estimativa de variações espaço-temporais da extensão de grandes áreas inundáveis (e.g. Hamilton et al. (2002) para principais planícies da América do Sul; Aires et al., (2014) para o Delta Interno do Rio Niger; Lehner & Döll (2004) para um mapa global de áreas inundáveis, lagos e reservatórios). Por fim, dados de altimetria espacial também têm tido relevância em estudos de validação e calibração de modelos hidrológicos e hidrodinâmicos destas áreas inundáveis (e.g., Getirana et al., 2010; Paiva et al., 2013; Tourian et al., 2017), além de estimativas de curvas-chave para uso em regiões mal monitoradas (Paris et al., 2016). Assim, dados de SR surgem como uma poderosa ferramenta na compreensão de processos hidrológicos e hidráulicos de grandes áreas inundáveis.

2.1.3 Modelagem matemática

Diversas estratégias de modelagem matemática de grandes rios e áreas inundáveis têm sido desenvolvidas. Inicialmente, faz-se a distinção entre a representação de processos hidrológicos e processos hidráulicos. O primeiro está relacionado ao balanço de água no solo entre precipitação, interceptação vegetal, evapotranspiração e infiltração e à geração de escoamentos superficial, sub-superficial e subterrâneo. Processos hidráulicos referem-se à dinâmica dos fluxos de água no rio, nas áreas inundadas e na interface entre estes. A propagação de vazões no rio, a troca de água rio-planície, e os fluxos quase sempre bidimensionais nas áreas inundadas são exemplos de processos hidráulicos. Estas duas categorias estão explicadas com mais detalhes a seguir.

Processos hidrológicos verticais

Por processos hidrológicos verticais entende-se o balanço entre variáveis meteorológicas (e.g. precipitação, vento, insolação solar) e a infiltração de água nas colunas de solo, após serem parcialmente interceptadas pelo dossel da vegetação, existindo intensa interação com a vegetação. Parte do volume que infiltra atinge os reservatórios subterrâneos, e se propaga lateralmente através do aquífero, etc. até desaguar em um corpo d'água próximo. Fluxos sub-superficiais também ocorrem no solo, e quando há acúmulo de água na superfície, escoamentos difusos ou canalizados passam a existir, convergindo para a rede de drenagem próxima. A Figura 2.3 apresenta um esquema destes processos, na forma implementada no modelo MGB-IPH

(Collischonn et al., 2007). A geração de escoamento superficial de excesso de saturação do solo (processo Dunniano) e excesso de infiltração (processo Hortoniano) está inserida no contexto dos processos verticais. Os volumes de água gerados nesta etapa são então propagados nos canais dos rios, no terreno em forma difusa, e eventualmente nas planícies de inundação, através dos aqui chamados processos hidráulicos (Collischonn, 2001; Collischonn et al., 2007).

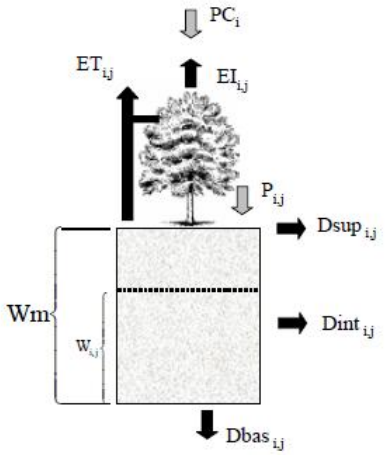

Figura 2.3. Esquematização de processos hidrológicos verticais. PC: precipitação; ET: evapotranspiração; EI: Evapotranspiração da lâmina interceptada pelo dossel; P: precipitação que passa pelo dossel; Dsup: escoamento superficial; Dint: escoamento sub-superficial; Dbas: escoamento subterrâneo; Wm: máximo armazenamento de água no solo; W: armazenamento de água no solo. Fonte: Collischonn et al., 2007.

Processos hidráulicos

Nos estudos de modelagem hidráulica de grandes bacias, rios são tipicamente representados como unidimensionais na direção longitudinal (1D), ou seja, integrando a profundidade e a direção lateral, enquanto as planícies de inundação adjacentes são tratadas desde formas simplificadas como zonas de armazenamento até formas mais realísticas, com fluxos bidimensionais (2D).

O fluxo 1D nos rios é modelado através das equações de Saint-Venant, que englobam a equação da conservação de massa e a equação de quantidade de movimento aplicados a um determinado trecho de rio:

$$\frac{\partial A}{\partial t} + \frac{\partial Q}{\partial x} = q \tag{2.2}$$

$$\frac{\partial Q}{\partial t} + \frac{\partial}{\partial x}\left(\frac{Q^2}{A}\right) + gA\frac{\partial h}{\partial x} = gA(S_0 - S_f) \tag{2.3}$$

Onde A é a área da seção transversal do trecho, t é o tempo, Q é a vazão, x é a direção longitudinal, q é a contribuição lateral no trecho (e.g. vazão gerada na área de

contribuição do trecho), g é a aceleração da gravidade, h é a profundidade, S_0 a declividade do fundo do rio e S_f a declividade da linha de energia (perdas por atrito).

Cada termo das equações de Saint-Venant representa processos/forças que atuam na hidrodinâmica do trecho de rio. Em ordem da esquerda para direita dos termos da Equação 3, encontra-se: (i) aceleração local, (ii) aceleração advectiva, (iii) forças de pressão, (iv) forças da gravidade, e (v) forças de atrito. Dependendo da relevância de cada processo, simplificações das equações podem ser feitas para facilitar a resolução do problema. Em muitos casos encontrados na natureza, os dois últimos termos são preponderantes, sendo possível negligenciar os primeiros três termos. Esta é a chamada aproximação cinemática, em que forças de atrito e de gravidade são utilizadas em conjunto com a variação de volume do trecho de rio (equação da continuidade) para estimar a propagação de fluxos no rio. Para casos mais complexos, como rios bastante planos, a utilização de todos os termos da equação de momento pode ser necessária (e.g. Amazônia, Getirana & Paiva, 2013).

Para a modelagem de fluxos em áreas inundadas, Paiva (2009) e Paz (2010) destacam quatro principais tipos de representação das planícies:

(i) Zona de armazenamento (Figura 2.4a): neste caso, considera-se que a velocidade é nula nas planícies de inundação, ou seja, elas funcionam como zonas de armazenamento de água (a rugosidade é infinita). A zona ativa de fluxo é a calha fluvial. O nível é assumido o mesmo entre o canal do rio e a planície, e o fluxo de água entre rio e planície é modelado como um termo adicional na equação da continuidade: $q_{fl} = \frac{A_{fl}}{dx}\frac{\partial h}{\partial t}$, onde q_{fl} é a vazão por unidade de largura de troca entre rio e planície, A_{fl} é a área inundada da planície (obtida através de uma relação cota do rio x área inundada) e dx é o comprimento da planície na direção longitudinal.

(ii) Seção composta (Figura 2.4b): neste caso, considera-se que há fluxo na planície. A seção transversal do rio é representada em dois estágios, o canal principal e a planície. A diferença nos fluxos é calculada considerando diferentes condutâncias hidráulicas para cada estágio, e valores de rugosidade diferentes para cada um (e.g., coeficiente de Manning na faixa de 0.02-0.04 para canal principal e na faixa de 0.1 para planície).

(iii) Lagoas interconectadas (Figura 2.4c): cada "unidade" de planície é considerada como uma lagoa, com relação cota x área x volume própria para cada uma, e o fluxo entre as unidades é modelado como se fossem canais de conexão, os quais dependem do volume armazenado em cada unidade. Pode também ser interpretado como um conjunto de reservatórios interconectados.

(iv) Modelo Bidimensional (Figura 2.4d): nesta aproximação, o domínio rio + planície é considerado tipicamente como uma grade regular de pixels, em que o fluxo entre cada pixel é modelado através de equações bidimensionais das equações de quantidade de movimento e continuidade:

$$\frac{\partial h}{\partial t} + \nabla.(h\boldsymbol{v}) = 0 \tag{2.4}$$

$$\frac{\partial v}{\partial t} + \boldsymbol{v}.\nabla\boldsymbol{v} + g\nabla(z_0 + h) + \frac{n^2 g\boldsymbol{v}|\boldsymbol{v}|}{h^{4/3}} = 0 \tag{2.5}$$

Onde v é o vetor de velocidade média nas dimensões x e y, z_0 o nível de fundo e n o número de Manning.

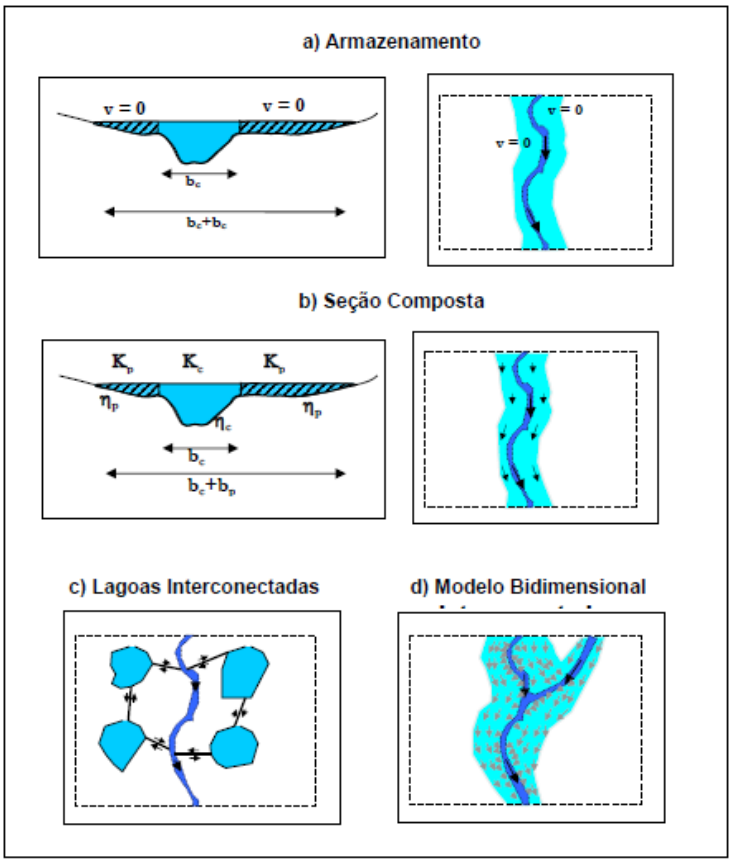

Figura 2.4. Diferentes esquemas de representação matemática de planícies de inundação. Fonte: Paiva, 2009.

Modelagem hidrológica e hidráulica de grandes sistemas rio-planície

Recentes avanços computacionais têm permitido o desenvolvimento de técnicas de modelagem que agreguem uma representação coerente dos processos hidrológicos verticais, bem como da hidrodinâmica existente tanto nos rios quanto nas áreas inundadas. Assim, alguns trabalhos de modelagem de grandes áreas inundáveis focaram em simular o fluxo 1D no rio com as equações completas de Saint-Venant, as planícies como zonas de armazenamento, e a geração de escoamento através de modelos

conceituais hidrológicos (e.g. Yamazaki et al., 2011 em aplicação global; Paiva et al., 2013 na Amazônia). Outros, mais complexos, acoplaram modelos 1D de propagação no rio a modelos 2D de fluxo na planície, aqui abreviados por modelos 1D/2D (e.g. Wilson et al. (2007) na Amazônia; Biancamaria et al., (2009) no rio Ob; Paz et al. (2011) no rio Paraguai). Modelos recentes têm aplicado métodos bidimensionais com estimativas "sub-grid" dos canais de planícies, onde canais que ocorram dentro da escala da célula são computados a parte com fluxos próprios; neste caso, redes de drenagem difusas, normalmente existentes em áreas muito planas e onde canais não seguem uma direção 1D do tipo montante-jusante pré-estabelecia, podem ser simuladas com relativa eficiência computacional (e.g., Paz et al. (2011) na região do Pantanal; Neal et al. (2012a) no rio Níger; Fernández et al. (2016) na planície de Logone, na bacia do Lago Chade). Todos estes últimos trabalhos 1D/2D aplicaram uma formulação semelhante à implementada no modelo LISFLOOD-FP (Bates & De Roo, 2000; Neal et al., 2012a), em que a planície é representada como uma grade retangular de células de armazenamento, e o fluxo entre estas é computado por equações desacopladas nas direções x e y, sendo estas equações difusivas (baseadas na equação de Manning, Bates & De Roo, 2000), inerciais (Bates et al., 2010) ou hidrodinâmicas completas (Villanueva & Wright, 2006; Neal et al., 2012b), e o nível relativo entre duas células adjacentes a força motriz do movimento. Por outro lado, a principal diferença entre as diversas aplicações 1D-2D está na forma com que os modelos representam os processos hidrológicos verticais ao longo da planície, sendo que alguns sequer os representam. Sobre este aspecto, Paz et al., (2014) realizaram alguns testes do modelo aplicado por Paz et al. (2011) para a região do Pantanal, considerando ou não o balanço vertical de água no solo (infiltração de água no solo e diferença entre precipitação e evapotranspiração real). De modo geral, os resultados indicaram a necessidade de se considerar tais processos; em especial, em rios que recebem grande aporte de água de planícies adjacentes, que são bastante influenciadas pela chuva local. Este é o caso das grandes áreas interfluviais existentes no Pantanal. Além disso, o modelo de Paz et al. (2011) representa de forma simplificada o balanço hidrológico, e outros aspectos como uma modelagem mais detalhada da evapotranspiração e dos fluxos subterrâneos podem ser bastante importantes a se considerar (Fan & Miguez-Macho, 2011). Do ponto de vista da modelagem hidrodinâmica, diversos trabalhos têm apontado a necessidade de se simular áreas inundadas com modelos 2D, a fim de representar as variações de nível existentes ao longo destas, a histerese de secagem e molhagem da planície, entre outros processos (Alsdorf, 2003; Alsdorf et al., 2005; Rudorff et al., 2014a). Por sua vez, resultados indicam que simulações 1D de complexos trechos de rio como o Amazonas devem utilizar modelos hidrodinâmicos (Trigg et al., 2009, Paiva et al., 2013).

A representação de trechos de rio com equações hidrodinâmicas permite a representação de redes difusas, onde não existe uma única direção de fluxo (e.g. defluências e fluxo difuso em canais e planícies) (Serra, 2006; Neal et al., 2012a; Yamazaki et al., 2014; Pontes et al,. 2015). Muitos rios com vastas planícies apresentam padrões geomorfológicos complexos, anastomosados, com diversas defluências intercaladas. Interessante definição foi dada por Serra (2006) para as áreas planas do

Pampa e Patagônia argentinos, onde redes onde o fluxo se comporta de forma unidimensional do tipo montante-jusante foram definidas como "típicas", enquanto aquelas regiões planas (regiões de "mesetas") foram chamadas de "não-típicas", e apresentando inclusive intensa variação sazonal e anual de seus caminhos preferenciais.

Outra parte fundamental no desenvolvimento de modelos matemáticos é a calibração e validação destes. Considerando que as grandes áreas inundáveis são geralmente mal monitoradas, além de apresentaram uma extensão de impraticável cobertura por redes de monitoramento, faz-se necessário o uso de dados de sensoriamento remoto. Assim, dados in situ (quando houverem) são complementados por séries de altimetria, estimativas de áreas inundadas e armazenamento de água (GRACE) (e.g. Paiva et al. 2013 com ampla validação de um modelo com dados de SR). Para os dados de entrada, uso de dados de precipitação por satélite (e.g. TRMM) são fundamentais em muitas destas regiões. Em termos de calibração de regiões mal monitoradas, uma interessante alternativa é avaliar a possibilidade de calibrar modelos com dados observados por sensoriamento remoto (e.g. nível dos rios, umidade do solo), e verificar a qualidade da vazão calculada. Neal et al. (2012a) mostraram em simulação do Delta Interno do rio Níger que esta alternativa fornece bons resultados, encorajando o uso de apenas dados de SR para calibrar modelos e gerar séries de vazões confiáveis.

Além disso, deve-se manter em conta que todo modelo é uma simplificação da realidade (Beven, 2012). Em modelagem de grande escala, estas simplificações são ainda mais necessárias, dada a impossibilidade de se representar fisicamente e na escala adequada todos os processos existentes na bacia hidrográfica. Assim, por exemplo, em modelos de grandes áreas inundáveis, busca-se uma representação coletiva dos canais e fluxos que ocorrem nas planícies da melhor forma possível. Parâmetros "efetivos" são também utilizados (e.g. único valor de condutividade hidráulica aplicado para toda uma região), como valores de rugosidade para rios e terrenos adjacentes. Calhas de rios são muitas vezes representadas como retangulares, e de fato alguns trabalhos indicam que esta representação é precisa o suficiente para grande regiões como o baixo Rio Amazonas (Trigg et al., 2009), apesar de ainda não ser consensual a capacidade de modelos de grande escala representarem os efeitos de planícies sem considerarem microcontroles na topografia do terreno (Neal et al., 2012a). Nesta representação de calha retangular, a largura do rio passa também a ser um parâmetro efetivo.

A topografia da planície deve ser bem representada (Neal et al., 2012a), e informações extraídas de Modelos Digitais de Elevação (MDE) como o SRTM têm sido fundamentais em aplicações e estudos em grandes áreas inundáveis (Wilson et al,. 2007; Paiva et al., 2011; Rudorff et al., 2014a). Entretanto, entre outros erros na representação do terreno, estes MDEs não conseguem penetrar alvos como o dossel das florestas, e precisam muitas vezes ser corrigidos para tal, a fim de evitar custos bastantes danosos nas simulações hidrodinâmicas de planícies (e.g. Neal et al., 2012a). Um recente produto de sensoriamento útil para estas simulações é o SRTM BareEarth (O'loughlin et al., 2016), onde o SRTM original foi corrigido globalmente através de mapas de altura e densidade de vegetação e medições altimétricas da cota do terreno.

Por fim, um aspecto importante na modelagem está associado ao custo computacional destas, visto que na maioria das aplicações é necessária a resolução de equações numéricas sujeitas a instabilidades e, portanto, a reduzidos intervalo de cálculo para estabilidade e convergência das simulações. Para aliviar estes custos, estratégias que podem ser adotadas envolvem códigos computacionalmente mais eficientes, que vão desde a linguagem de programação adotada até a forma com que *"loops"* são definidos, e programação paralela (e.g., uso da interface de programação "*Open MultiProcesing*" - Open MP, Neal et al., 2009), onde a memória é compartilhada simultaneamente entre diferentes plataformas para realização de cálculos, como, por exemplo, entre diferentes linhas de execução (*"threads")* do processador do computador. Além disso, o passo de tempo de cálculo adotado em soluções numéricas das equações de Saint-Venant é sujeito à condição de Courant-Freidrichs-Levy para estabilidade, a qual depende do comprimento de intervalo espacial (Δx) em que a rede de drenagem é discretizada (isto é, a distância entre elementos de cálculo). Assim, discretizações espaciais mais eficientes, que evitem trechos de rede muito curtos, podem ser empregados (Yamazaki et al., 2013; Siqueira et al., *submitted paper*).

2.2 Processos hidrológicos e hidráulicos em grandes áreas inundáveis

A compreensão dos processos hidrológicos e hidráulicos em grandes áreas inundáveis pode ser baseada na análise da equação da continuidade para estas áreas, considerando um volume de controle representativo da planície de inundação:

$$\Delta V/\Delta t = Q_{upland} \pm Q_{overbank} + P - E \pm G \qquad (2.6)$$

Onde $\Delta V/\Delta t$ é a variação de volume armazenado em cada intervalo de tempo, Q_{upland} é a vazão das áreas contribuintes a montante, de terra firme, $Q_{overbank}$ é a água extravasada do rio, P a precipitação, E a evapotranspiração e G a água infiltrada ou recebida do solo.

Assim, a variação do volume armazenado na planície depende de diversos componentes do ciclo hidrológico, relacionados por sua vez a fatores como cobertura vegetal, nível do lençol freático, declividade, topografia e demais controles geomorfológicos do terreno, proximidade a grandes rios, existência de canais dentro da planície e possível conectividade entre áreas da planície, características do solo (profundidade, condutividade hidráulica, porosidade, granulometria) e clima (sazonalidade, regime pluviométrico, temperatura). Nas próximas seções, estes aspectos são abordados no contexto de sua relação com a dinâmica das águas nas grandes áreas inundáveis.

2.2.1 Inundação via extravasamento da calha fluvial

Após o extravasamento da calha fluvial, que muitas vezes ocorre em vazões menores que a de calha cheia, através de aberturas nas margens e canais preferenciais, a água flui de modo complexo pelas planícies, com caminhos preferenciais variando entre os diferentes estágios do ano, e alternando entre canais já existentes na planície, ou na forma de fluxo difuso, superficial ou sub-superficialmente. A direção do fluxo de água na planície pode ocorrer tanto paralela ao rio quanto em um padrão complexo e difuso (Figura 2.5) (Mertes, 1997; Alsdorf et al., 2007a; Paz, 2010; Trigg et al., 2013). Diferentes processos hidráulicos interagem com as diversas redes de drenagem – dos relativamente pequenos canais nas planícies aos grandes rios circundantes. Em regiões muito planas, como o baixo Amazonas, a densidade de canais é extremamente elevada (Alsdorf, 2003; Trigg et al., 2012). Além disso, na transição entre calha fluvial e planície de inundação, diferentes características são encontradas, como uma maior rugosidade e complexidade na última (Paz, 2010; Trigg et al., 2012). Trocas de momento lateral entre os fluxos lentos na planície e os rápidos na calha do rio acarretam fluxos secundários (Knight & Shiono, 1996), os quais acabam sendo pouco importantes quando se trata de grandes áreas inundáveis, dada a complexidade dos canais e fluxos existentes.

A água que avança a partir dos grandes rios pode encontrar planícies secas ou inundadas por tributários internos a estas (Mertes et al., 1995). Em muitos casos, existe uma histerese na relação nível-área inundada durante os processos de inundação e secagem da planície de inundação (Mertes et al., 1995; Hamilton et al., 2002), onde a planície tende a secar mais lentamente do que inundar (permanece inundada por mais tempo durante a recessão). Relações como estas são também observadas em lagos existentes nas planícies (e.g. Lago Grande de Curuai no Baixo Amazonas, Rudorff et al. (2014a)). Além disso, o tempo entre a subida e descida do rio pode ser um importante fator na definição do tamanho da planície de inundação, já que rápidas variações de níveis podem fazer com que a água não consiga avançar muito na planície, retornando rapidamente para a calha fluvial (Mertes et al., 1995). Baseado em análises interferométricas a partir de imagens de radar da missão SIR-C (NASA) dos dias 9 e 10 de Outubro de 1994, Alsdorf (2003) e Alsdorf et al. (2005) demonstraram que, durante a recessão das vazões dos rios Negro e Amazonas (trecho principal), a taxa de diminuição do nível de água nas planícies é maior nas regiões próximas à calha do rio que nas áreas mais distantes. Entre outras implicações, esta análise indica que o nível da água nas planícies não é o mesmo que na calha fluvial. Avaliando a variação de níveis ao longo do rio Negro, observa-se que estes variam sazonalmente cerca de 10 metros no Baixo Negro devido ao efeito de remanso do Rio Solimões-Amazonas, e bem menos nos de montante. Este efeito é bastante influente no tamanho (e.g., largura) observado da planície.

Outro aspecto importante na compreensão das áreas inundáveis está relacionado ao tempo de residência da água, que dita o tempo com que processos de transformação biogeoquímicos (transformações de carbono e outros nutrientes) podem atuar nos volumes de água presentes nestas áreas. Por exemplo, Richey et al. (1989) estimaram que 30% do volume que passa por Óbidos no Rio Amazonas passam pelas suas planícies de inundação, enquanto Bonnet et al. (2008) estimaram um tempo de residência de cerca de três meses para a água do Lago Grande de Curuai, sendo que a água extravasada pela calha do rio permanece cerca de 5 meses neste lago. Alsdorf et al. (2005) mostraram que existe uma tendência de maior residência em trechos da planície mais distantes do rio.

2.2.2 Evaporação e infiltração

Como estas grandes áreas inundáveis são bastante planas, parte da água fica armazenada em lagos e depressões do terreno, de onde às vezes ela sai apenas por evaporação ou infiltração (Paz, 2010; Mahé et al., 2009). Este fenômeno é particularmente importante em grandes bacias endorreicas de regiões áridas e semi-áridas, como o delta do rio Okavango no sul da África, onde apenas 1.5 % do volume anual que chega à região sai na forma de água superficial. Grande parte do volume é perdido na forma de evapotranspiração. Além disso, durante a chegada anual da onda de

cheia, o solo está relativamente seco, ocorrendo taxas relevantes de infiltração de água da planície (McCarthy et al., 1998; Milzow et al., 2009). Outro exemplo é o Delta Interno do Rio Niger, na África Ocidental (Figura 2.6), uma região muito plana e seca que drena grandes áreas úmidas do oeste africano e que apresenta dezenas de lagos sazonal ou permanentemente inundados devido aos fluxos oriundos de montante. No Delta, cerca de 30-40% do volume anual que chega é perdido por evaporação ao longo dos 73.000 km² da região (Mahé et al., 2009), e estudos com produtos de sensoriamento remoto indicam que infiltração no solo pode ser um processo influente na área (Ogilvie et al., 2015). Em regiões áridas, importantes perdas por infiltração para aquíferos profundos podem também ocorrer (Pedinotti et al., 2012), além de perdas distribuídas ("*transmission losses*") ao longo dos canais para a zona hiporreica circundante (Costa et al., 2012). Por sua vez, nas planícies do rio Amazonas existem cerca de oito mil lagos (Alsdorf, 2003), que variam de tamanho entre menos de 1 ha e mais de 600 km² (Forsberg et al., 1998). Diferentes processos geomorfológicos levaram à formação destes lagos, que foram distinguidos por Latrubesse (2012) em duas classes: (i) lagos relacionados a migração lateral de canais e (ii) lagos formados por processos de acreção vertical (deposição de sedimentos) por inundações nas planícies. Migrações laterais são presentes em tributários bastante sinuosos como os rios Purus e Jurua, e geram os chamados "*oxbow lakes*" em meandros abandonados e "*scroll bars lakes*" (Figura 2.7a). Por sua vez, a segunda categoria é formada pelos intensos processos fluviais de inundação e formação de padrões geomorforlógicos anastomosados, onde lagos estão presentes nas margens dos rios ("*levee lakes*"), em ilhas ("*island lakes*") e nos chamados vales bloqueados ("*blocked valleys*"). Estes últimos são conhecidos na região amazônica como "*Ria Lakes*", e são caracterizados pela presença de rios com grande transporte de sedimentos criando extensas e estáveis margens ("*levees*") que impedem a drenagem de tributários. Importante exemplo destes é a foz do rio Tapajós, cujo desaguar é impedido pelo depósito de sedimentos do Rio Amazonas e acaba sendo realizado através de uma pequena ligação entre os rios (Figura 2.7b).

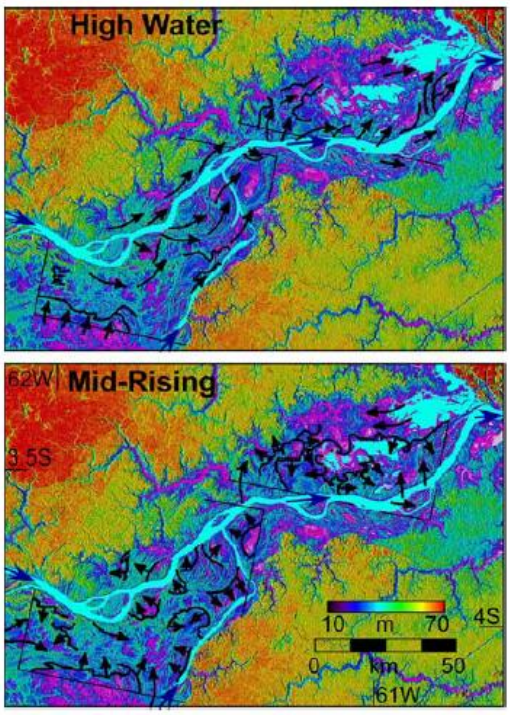

Figura 2.5. Diferenças entre os fluxos preferências de água na planície de inundação da confluência entre Rio Amazonas e Rio Purus durante período de águas altas (*high water*) e de subida de nível (*mid-rising*). Fonte: Alsdorf et al. (2007a).

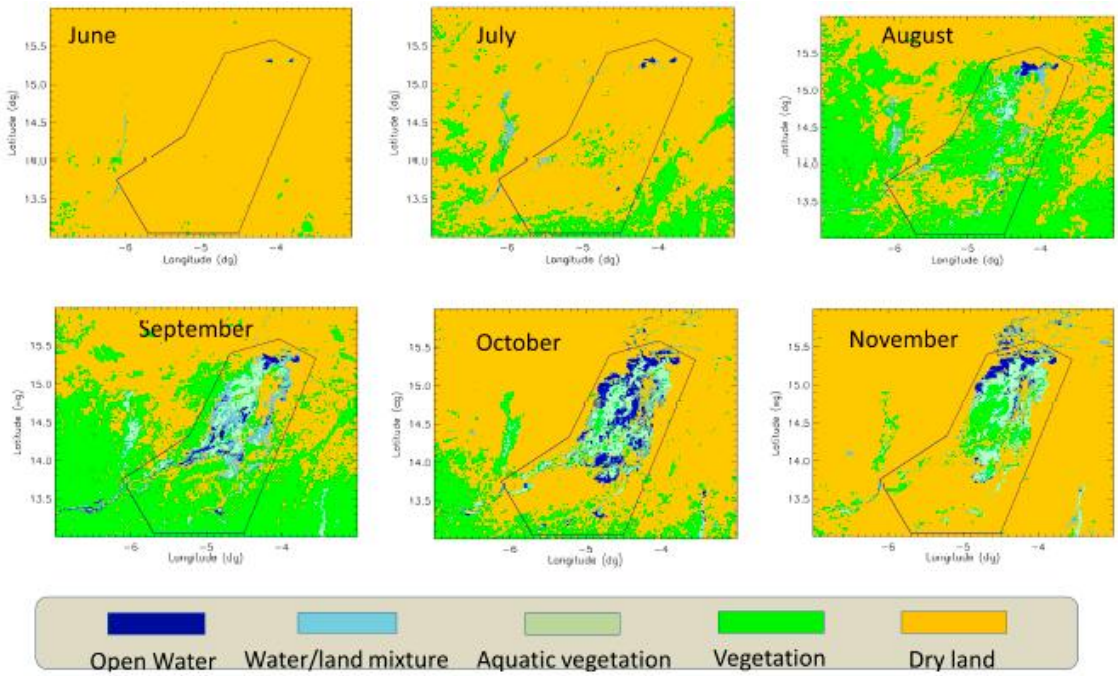

Figura 2.6. Variação sazonal das áreas inundadas na árida e plana região do Delta Interno do Rio Niger, na África Ocidental. A inundação ocorre devido a volumes transportados das regiões de savanas de montante. Nos meses de inundação, cerca de 30-40% da volume que chega é evaporado. Classificação da imagem: águas abertas (*open water*), mistura entre água e terra (*water/land mixture*), vegetação aquática (*aquatic vegetation*), vegetação (*vegetation*), e terra seca (*dry land*). Fonte: Bergé-Nguyen & Crétaux (2015).

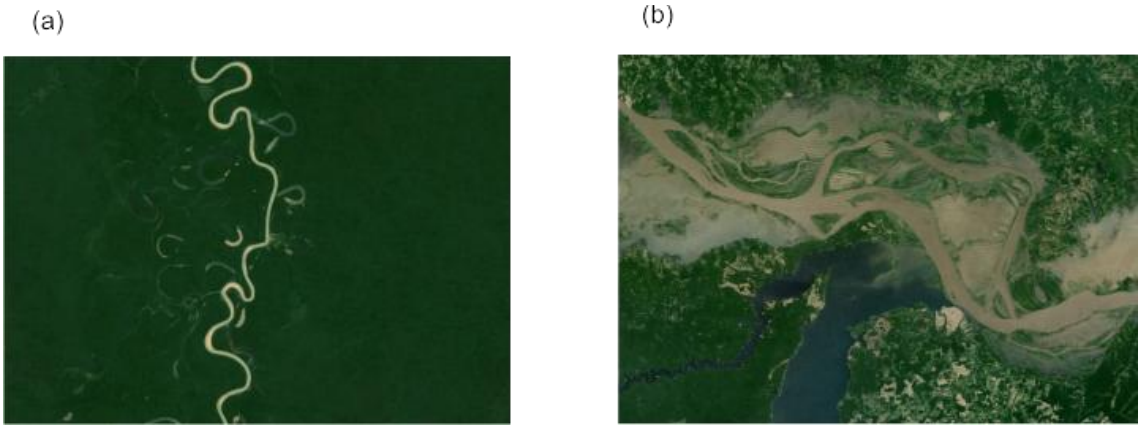

Figura 2.7. Padrões de lagos na Amazônia. (a) Lagos existentes em meandros abandonados do Rio Purus ("*oxbow lakes*"). (b) Foz do rio Tapajós, apresentando típico padrão de drenagem impedida dos lagos chamados "*Ria Lakes*". Fonte: Imagens Google Earth.

2.2.3 Conectividade, lagos e canais em planícies

Pesquisas na Amazônia indicam que lagos com uma grande área de contribuição (assim como grande distância do rio principal e incidência de chuva local) podem garantir uma carga de pressão grande o suficiente para evitar a intrusão de água oriunda do extravasamento do rio. Nestes casos, a razão entre área inundada e área de contribuição dos lagos é utilizada para avaliar o grau de influência do rio no lago (Lesack & Melack, 1995; Mertes, 1997; Forsberg et al., 1998; Bonnet et al., 2008; Rudorff et al., 2014a). Outros fatores como distância do rio principal e incidência de chuva local também podem ser considerados. Esta região de fronteira e mistura entre água de origem local e proveniente do extravasamento dos rios principais foi chamada de "zona perirréica" por Mertes (1997), sendo uma zona de ecótone, com importantes implicações biogeoquímicas. Em trabalho no Lago Grande de Curuai, localizado na planície do Rio Amazonas próxima a Óbidos, Bonnet et al. (2008) mostraram que durante o início do período de cheia (Janeiro), basicamente o rio alimenta o lago por canais, enquanto de meados de Janeiro a Maio, ocorre tanto alimentação quanto liberação de vazão entre o lago e o rio, dependendo da ocorrência de chuva local sobre o lago. Até Outubro, a maior parte dos canais passam a alimentar o rio principal, e a partir deste mês existe apenas perda por evaporação e infiltração de água no lago. Esta dinâmica sazonal depende de variações climáticas, sendo que em anos mais úmidos que a média, água fornecida pelo rio tende a ser preponderante, enquanto em anos abaixo, chuva local e fluxos oriundos da área de contribuição local são mais importantes. Rudorff et al. (2014a) mostraram para o mesmo lago a importância relativa entre fluxos via canais na planície e fluxos difusos: de Fevereiro a Agosto o mecanismo principal seria o fluxo difuso acima das margens que contornam o lago, e no início das águas altas e fim da recessão, a inundação (ou secagem) seria controlada pelos canais. Além

disso, fluxos entre rio e planície aumentam em uma relação exponencial com a vazão no rio principal. A partir do período de águas altas, existe um fluxo líquido da planície para o rio, pois saídas pelos canais do Leste passam a superar todas as entradas de água do rio. No período seco, a principal alimentação da planície é via água armazenada nos solos e sedimentos adjacentes nas margens. Assim, um complexo padrão de fluxos existe nestes lagos, que interagem constantemente com os rios adjacentes.

Outro papel destes lagos reside na conectividade entre as áreas inundáveis e o rio principal. Em termos de hidrologia, conectividade pode ser definida pela existência de macro conexões entre diferentes unidades da bacia hidrográfica, como planícies de inundação e canais de rios, ou ainda pelo grau de acoplamento entre diferentes componentes do ciclo hidrológico (e.g. fluxos superficiais e subterrâneos) (Michaelides & Chappell, 2009). Pringle (2001) usa o termo para se referir à transferência, através da água, de matéria, energia e/ou organismos entre diferentes elementos do ciclo hidrológico.

Trigg et al. (2012) analisaram a conectividade das planícies de inundação da região central do Amazonas por meio de canais que ligam o rio principal a canais coletores. Durante o período de águas altas, escoamento difuso tende a ocorrer, gerando um padrão mais homogêneo devido à conectividade via canais ao longo da planície de inundação, enquanto durante a estação seca os canais coletores e mais profundos geram fluxos em direções menos organizadas (Alsdorf et al., 2007a; Figura 2.5). Os canais na planície aparentemente têm um mecanismo de manutenção em que as reversões de fluxo entre enchimento e esvaziamento da planície de inundação permitem a deposição de sedimentos durante o enchimento, com a sucessiva erosão durante o esvaziamento (Rowland et al., 2009). Trigg et al., (2012) mostraram que os canais com área geradora de escoamento ("*local runoff*") possuem profundidade consideravelmente maior que aqueles que apenas carregam água durante as cheias (Figura 2.8). Além disso, os diferentes tipos de canais levam a diferentes características físico-químicas da água, e consequentes diferentes ecossistemas associados. Por fim, o conceito de conectividade pode ser também aplicado à compreensão das grandes áreas interfluviais inundadas por processos hidrológicos locais, cuja drenagem para o rio principal ocorre lentamente através das redes de drenagem internas a estas. Nestes casos, a conexão rio-área inundável é mais fraca que nas regiões diretamente influenciadas pelo extravasamento do rio.

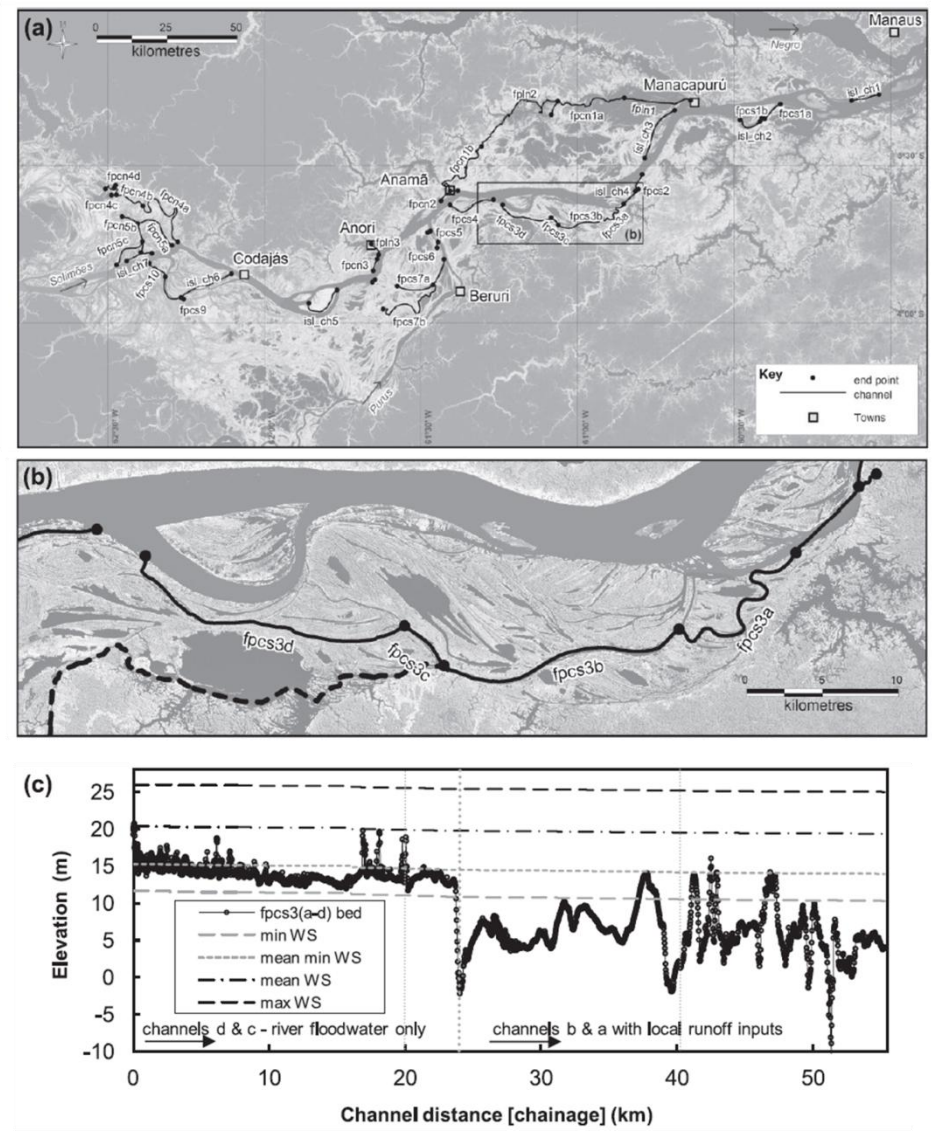

Figura 2.8. Trecho do Rio Amazonas próximo à confluência com o Rio Purus. Os dois quadros de destaque (b e c) mostram os canais fpcs3a e fpcs3b que conectam o Rio Purus ao Amazonas. Os canais fpcs3c e fpcs3d existem apenas durante o período de cheias, e sua profundidade está relacionada com a amplitude anual do nível do rio Amazonas (Fonte: Trigg et al., 2012).

2.2.4 Papel da água subterrânea e do armazenamento em zona hiporréica

Rudorff et al. (2014) mostraram para o Lago Grande de Curuai que, durante as águas baixas, há uma grande quantidade de pequenos canais e lagos que permanecem desconectados dos grandes rios e lagos, o que muda durante as águas altas. Muitos destes canais, lagos e áreas inundadas estão conectados sub-superficialmente pelos níveis e fluxos da água subterrânea, os quais mantêm a conectividade entre as diversas regiões (Winter & LaBaugh, 2003; Fan & Miguez-Macho, 2011; Miguez-Macho & Fan, 2012a; Pfeffer et al., 2014). Pfeffer et al. (2014) estimaram a distribuição espaço-temporal dos níveis subterrâneos na Amazônia central durante o período de águas

baixas, partindo da observação de que nesta fase o nível da água coincide com o dos rios adjacentes. Fatores como condutividade hidráulica, geologia, gradiente hidráulico e configuração dos fluxos subterrâneos definem estas conexões sub-superficiais. Rudorff et al. (2014a) e Lesack (1995) ressaltaram a relevância de infiltração de água entre o rio e a planície e o armazenamento de água nas margens (zona hiporréica) em lagos da Amazônia central. Outro exemplo da conectividade em planícies de inundação é dado pelas chamadas "ipucas" na Ilha do Bananal, que são depressões no terreno que permitem a ligação entre inúmeros canais e lagos no meio da planície durante a época de chuvas (Martins, 2004; Brasil, 2001). Em áreas como a Ilha do Bananal, o aumento dos níveis freáticos também contribui expressivamente para as dinâmicas das áreas inundadas, garantindo a manutenção da extensão e de altas taxas de evapotranspiração mesmo durante as épocas secas (Borma et al., 2009; Miguez-Macho & Fan, 2012b).

2.2.5 Processos hidrológicos verticais: geração de escoamento e chuva local

Além das águas oriundas do extravasamento dos rios, existe uma interação da área inundável com os volumes gerados nas partes mais altas do terreno (chamadas de "*uplands*" na literatura, e "terra firme" na região amazônica) (Lesack & Melack, 1995; Bonnet et al., 2008; Rudorff et al., 2014a, 2014b). Trigg et al. (2012), por exemplo, diferenciaram geomorfologicamente os canais na planície de inundação central do Amazonas entre aqueles que possuem ou não uma área de captação, capaz de gerar escoamento e sustentar vazões em períodos em que não há inundação do rio principal. Os que apresentam profundidade maior e podem agir como caminhos preferenciais para a água durante as cheias.

A chuva incidente na área inundável, aqui chamada de chuva local, é a causa de extensas áreas inundadas, estando muitas vezes associada a uma baixa capacidade do terreno de drenar a água acumulada (seja por impedimento devido a níveis altos da rede de drenagem próxima ou por solo já saturado, com capacidade de infiltração reduzida) ou a níveis altos do lençol freático (Bourrel et al., 2009; Borma et al., 2009; Trigg et al., 2012; Valente et al., 2013; Ovando et al., 2015). Um exemplo deste tipo de área inundável ocorre nos chamados Llanos de Moxos, Bolívia, localizado entre os rios Mamoré e Beni, no alto rio Madeira, na Amazônia. Estes possuem uma combinação de processos endógenos (chuva local associada ao alto nível freático, que alimenta redes de drenagem internas à planície) e exógenos (extravasamento da calha fluvial do rio Mamoré) (Bourrel et al., 2009; Ovando et al., 2015). Para esta região, Bourrel et al. (2009) propuseram três classes para as cheias endógenas: (i) strictu-sensu, onde apenas a chuva local gera inundação; (ii) controlada, onde o controle hidrodinâmico do rio Mamoré sobre canais internos à planície faz com que estes extravasem, sem ocorrer extravasamento do rio Mamoré; e (iii) combinada, onde há o extravasamento de canais internos à planície devido à entrada de água do rio Mamoré e a alta incidência de chuva local (Figura 2.9a). A importância relativa destes processos varia ao longo dos anos. Na

Amazônia, Junk et al., (2015) argumentam que o efeito da chuva local é quem domina a dinâmica de rios e córregos de pequena ordem.

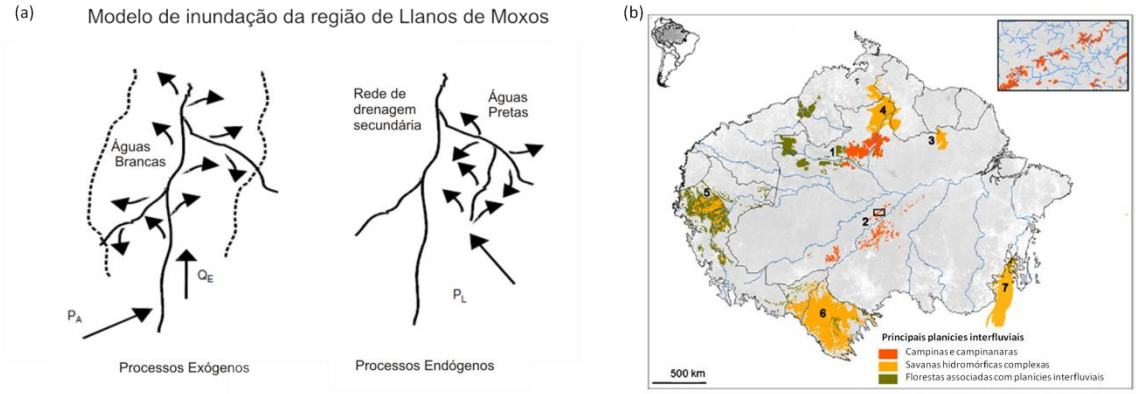

Figura 2.9. (a) Modelo de inundação da região de Llanos de Moxos na Amazônia Boliviana. Os processos exógenos estão relacionados ao extravasamento de água do rio Mamoré carregado de sedimentos (águas brancas), enquanto os endógenos ocorrem devido a inundação de tributários internos por chuva local. Fonte: Adaptado de Bourrel et al., 2009. (b) Localização das principais áreas inundáveis interfluviais na Bacia Amazônica. Fonte: adaptado de Junk et al., 2011.

Em estudo de modelagem hidrológica-hidráulica no Pantanal, Paz et al., (2014) mostraram, para afluentes do Rio Paraguai, que, enquanto a dinâmica do Rio São Lourenço é definida basicamente pelo extravasamento da calha fluvial para as planícies adjacentes, a água que deixa este rio é transportada via planície de inundação até o Rio Piquiri. Neste caminho, os processos de chuva local, evapotranspiração e infiltração de água no solo são bastante influentes nos volumes que atingem o rio. Os autores mostraram que o impacto destes processos hidrológicos verticais na vazão do rio é diretamente relacionado ao volume de água recebido por este das planícies adjacentes. Por outro lado, em outros trechos do Rio Paraguai a importância destes processos verticais nas áreas inundadas reside basicamente na evapotranspiração durante períodos de águas baixas, que atuam na diminuição das vazões. O modelo desenvolvido permitiu aos autores classificar os trechos de rio do sistema do Pantanal em termos de predominância de ganho ou perda de água das planícies (Figura 2.10).

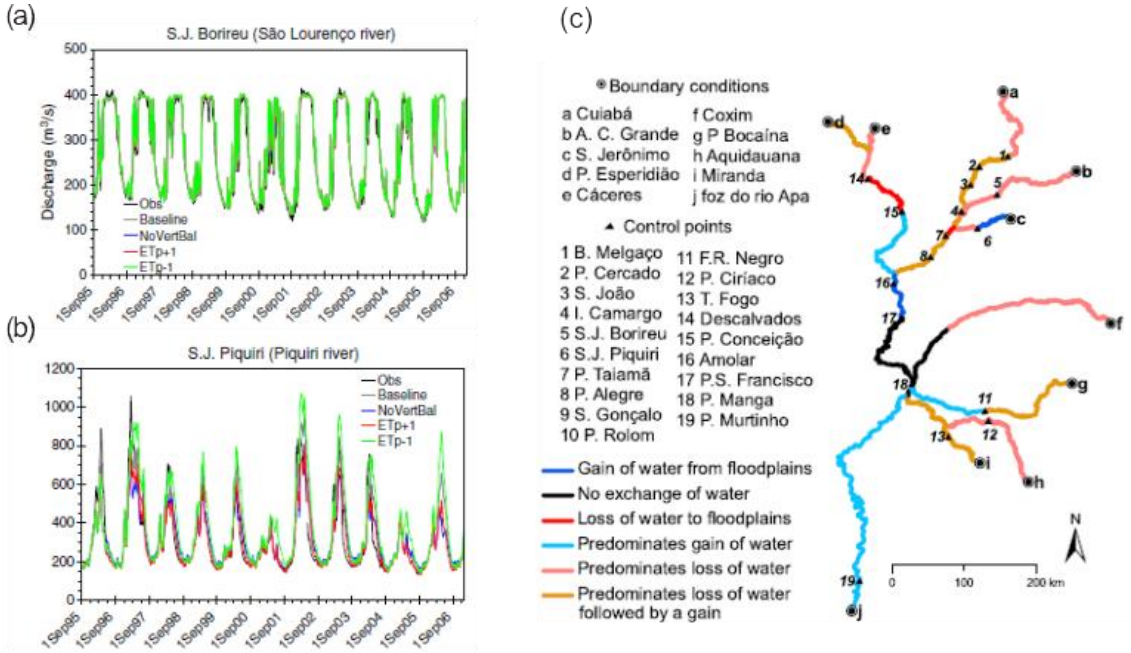

Figura 2.10. Resultados do estudo de Paz et al., (2014). (a) Resultados das simulações com (verde) e sem balanço hidrológico vertical (cinza) para o rio São Lourenço, mostrando pouca variação entre os cenários. (b) Resultados para o Rio Piquiri. Como este rio recebe água da planície, as vazões observadas neste rio são bastante sensíveis aos processos verticais (chuva local, evapotranspiração). (c) Classificação dos principais rios da região do Pantanal em termos de perda ou ganho de água para as planícies de inundação adjacentes. Fonte: Paz et al., 2014.

2.2.6 Planícies interfluviais

Na América do Sul, importantes savanas estão relacionadas a grandes áreas de inundação por chuva local (definidas anteriormente como áreas interfluviais). Estas áreas de savana estão relacionadas a regiões com inundação sazonal e pequena variação de níveis entre as estações (Junk et al., 2011; Junk et al., 2015), apesar de a intervenção humana muitas vezes auxiliar na manutenção destes biomas (e.g. savanas de Roraima e Llanos de Moxos; Hamilton et al., 2002). Os principais exemplos são a Ilha do Bananal, a maior ilha fluvial do mundo, formada pelos rios Araguaia e Braço Menor do Araguaia ou Javaés (Aquino et al., 2008; Borma et al., 2009; Valente et al., 2013); o Llanos de Moxos, localizado entre os rios Mamoré e Beni, afluentes do rio Madeira na região norte da Bolívia (Bourrel et al., 2009; Ovando et al., 2015); o alto Rio Branco, no estado de Roraima, Brasil; os Llanos na bacia do Rio Orinoco na Venezuela; e o Pantanal na bacia do Rio Paraguai. Hamilton et al., (2002) apresentaram, através de observacoes de microondas passivo, a dinâmica e evolução temporal destas áreas, e Junk et al. (2011) apresentaram uma classificação qualitativa destas na região Amazônica (2.9b). De fato, estas áreas possuem muitas características morfológicas e biológicas em comum, estando todas envolvidas pela densa floresta amazônica (Cardoso & Bates, 2002). Deve-se refletir, então, sobre qual a importância de distinguir entre zonas interfluviais e planícies de inundação devido ao extravasamento de grandes

rios? Basicamente, as águas presentes nestas diferentes regiões possuem distintas origens, influenciando diretamente os ciclos biogeoquímicos e ecossistemas associados. Nas planícies do Alto Madeira, por exemplo, os processos endógenos geram águas pretas (substâncias orgânicas), enquanto os exógenos extravasam águas brancas, carregadas de sedimentos em suspensão (Bourrel et al., 2009).

2.2.7 Processos geomorfológicos e hidrossedimentológicos

A geomorfologia das grandes áreas inundáveis depende em larga escala de controles geológicos e da evolução da geomorfologia de modo geral (Figura 2.11 e 2.12). Eventos neotectônicos são bastante atuantes na Amazônia (Latrubesse & Rancy, 2000; Latrubesse & Franzinelli, 2002; Latrubesse & Franzinelli, 2005), como uma mega captura fluvial que alterou a direção do Rio Negro, criando condições para a formação do gigante arquipélago de Anavilhanas (Almeida-Filho & Miranda, 2007; Latrubesse & Stevaux, 2008). Mudanças de direção dos canais ao longo de todo o rio Amazonas são comandadas por feições geológicas, e o tamanho das planícies de inundação depende das falhas tectônicas existentes na região (Trigg et al., 2012). Além disso, muitas destas grandes áreas inundáveis são bacias sedimentares ainda em formação, como a planície amazônica e a Ilha do Bananal, onde sedimentos são constantemente depositados.

Os processos atuais de erosão e sedimentação, altamente dependentes da hidráulica destes sistemas, são outros fatores fundamentais na definição da geomorfologia dos rios e áreas inundáveis. Na Amazônia, os diferentes tipos de rios são caracterizados de acordo com a sua concentração de sedimentos (rios de águas brancas ou pretas). Nestas áreas, o aporte de sedimentos através de fluxos preferenciais garante a manutenção dos canais das planícies (Mertes, 1997), que por sua vez geram padrões característicos de deposição (e.g. "*crevasse splays*") onde diversos lagos são formados (Latrubesse, 2012). Constantes avulsões (migração de canais) e cortes de meandros são muito frequentes nos rios planos que alimentam essas áreas inundáveis, e comandam direções de fluxos dos canais preferenciais e a existência de lagos. Além disso, os rios com as planícies de inundação mais bem desenvolvidas na Bacia Amazônica (e.g. em termos da relação largura de planície/largura do rio), como Purus e Juruá, apresentam um regime aluvial com grande concentração de sedimentos em suspensão associado à existência de bacias sedimentares recentes (Latrubesse, 2012).

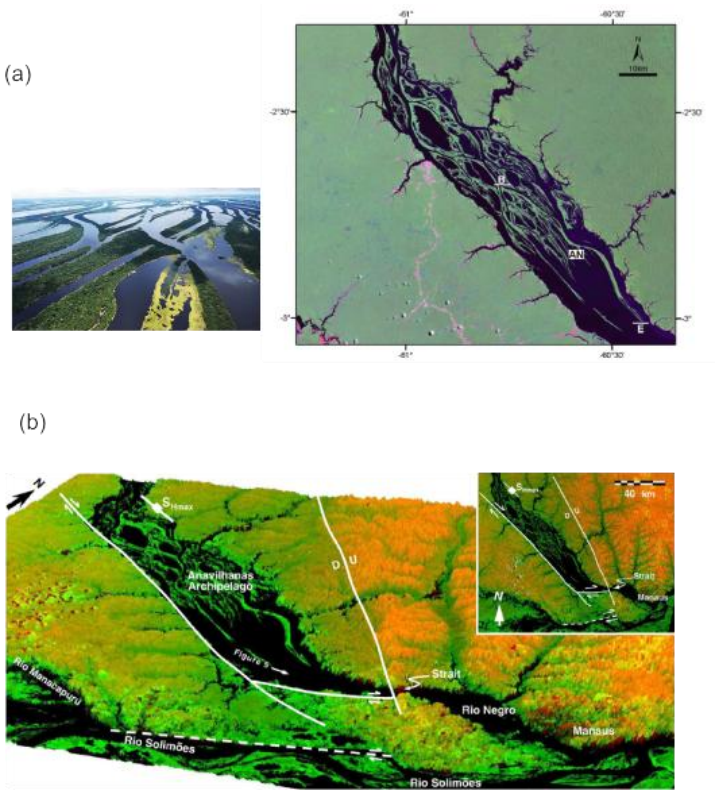

Figura 2.11. Controles geológicos no arquipélago de Anavilhanas, no Baixo Rio Negro, bacia Amazônica. (a). Arquipélago de Anavilhanas. Fonte: Latrubesse & Stevaux (2008). (b) Controles geológicos e falhas neotectônicas no arquipélago. Fonte: Almeida-Filho & Miranda (2002).

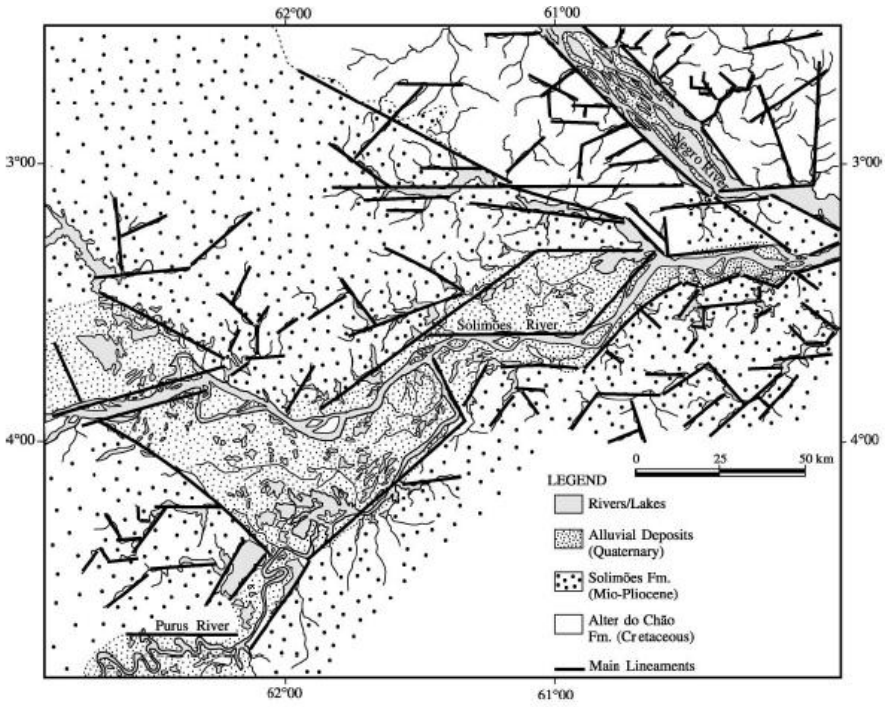

Figura 2.12. Principais controles geológicos no trecho principal do Rio Amazonas. Fonte: Latrubesse & Franzinelli, 2002.

2.2.8 Interação planície-biosfera-atmosfera

Naturalmente, o clima e suas mudanças são controles fundamentais na dinâmica das grandes áreas inundáveis, com regimes de precipitação e demais variáveis meteorológicas atuando diretamente. Eventos atípicos impactam sobremaneira tais regiões. Por exemplo, anos de El Niño costumam gerar secas na Amazônia e cheias no sul do Brasil, e alteram significativamente o regime hidrológico continental e o desenvolvimento dos ecossistemas associados (Schöngart et al., 2004; Schöngart & Junk, 2007). Chuvas convectivas extremas e migrações anômalas da Zona de Convergência do Atlântico Sul, associadas a anomalias positivas da temperatura da superfície do Oceano Atlântico, podem ter ocasionado uma das maiores cheias já registradas na região amazônica (Filizola et al., 2014). Diferentes padrões de chuva e sazonalidade geram comportamentos complexos e muitas vezes imprevisíveis das dinâmicas das grandes áreas inundáveis. Além disso, variações interanuais ocorrem na Amazônia (Espinoza et al., 2009a, 2009b), e os efeitos de mudanças climáticas têm sido bastante debatidos na comunidade científica recentemente (Malhi et al., 2008; Cochrane & Barber, 2008; Sorribas et al., 2016).

É possível também relacionar aspectos hidrológicos e geomorfologia fluvial a tipos de vegetação nos distintitos tipos de áreas inundáveis (Mertes et al., 1995; Valente et al., 2013), e a teoria do Flood Pulse Concept (Junk et al., 1989) defende o papel fundamental da dinâmica de cheias no desenvolvimento e manutenção dos ecossistemas e vegetação associados às áreas inundáveis. Hess et al. (2003) mapearam esta interação planície e vegetação para toda a Amazônia central com imagens radar de sensoriamento remoto (Figura 2.13). Na floresta amazônica, rios com grandes planícies tendem a ter bastante concentração de sedimentos, e são associados às planícies do tipo várzea, enquanto rios de águas escuras, como o Rio Negro, possuem áreas inundáveis associadas às matas de igapós. A vegetação associada a cada tipo de planície é bastante distinta, sendo que as várzeas possuem mais nutrientes e árvores mais desenvolvidas. Em regiões sazonais como o cerrado (e.g. Ilha do Bananal), a vegetação decídua nas áreas inundáveis responde diretamente ao ciclo anual: durante a época de chuva, os solos hidromórficos, com lençol freático aflorante, controlam o fornecimento de água para as plantas, gerando as maiores taxas mensais de evapotranspiração na região. Durante a época seca, a ausência de água disponível para as plantas associada à senescência das folhas diminui drasticamente a taxa de evapotranspiração, mesmo havendo maior radiação incidente (Borma et al., 2009; Da Rocha et al., 2009). Além disso, a profundidade das raízes é maior na Amazônia que em muitas regiões do cerrado, permitindo um maior acesso à água armazenada no solo por parte das primeiras (Da Rocha et al., 2009). De fato, na Amazônia a maior evapotranspiração ocorre nos meses de menor volume de chuva, devido à menor cobertura de nuvens (maior radiação disponível), e ao fato de que a estação seca não é tão seca e que as raízes são profundas, de modo que a disponibilidade de água no solo não seja um fator limitante.

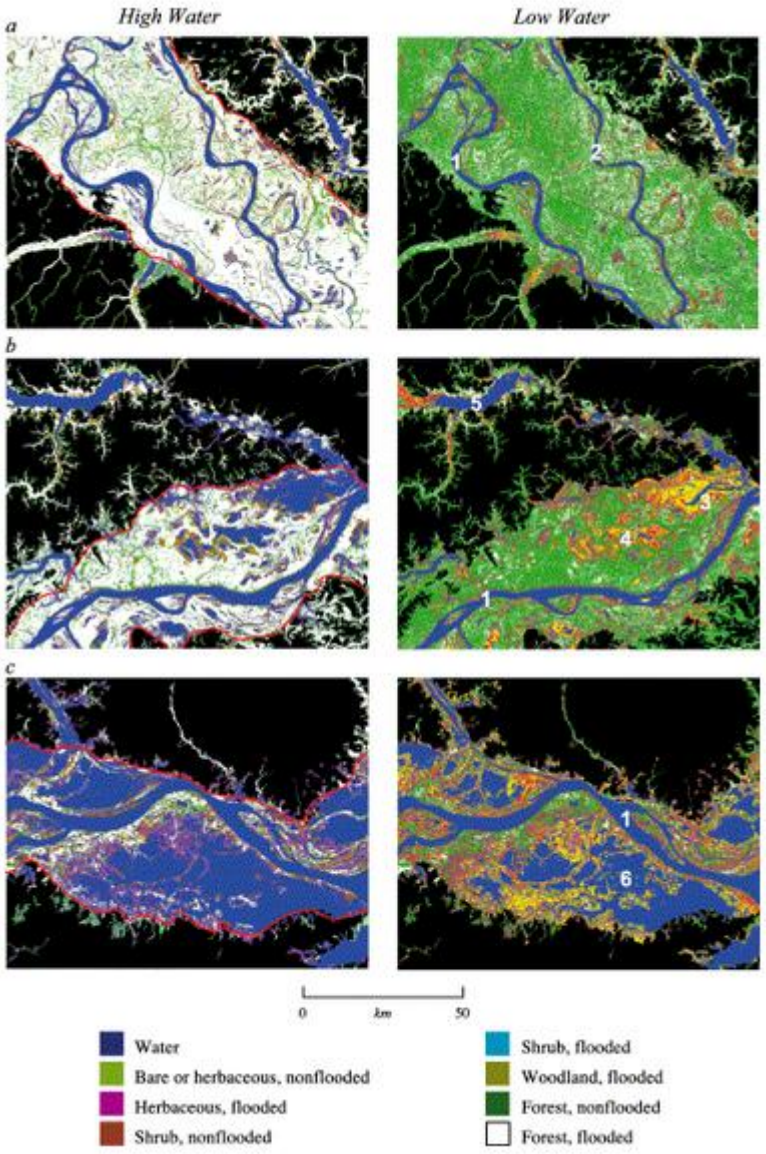

Figura 2.13. Mapeamento das diferentes formações de vegetação da Amazônia central, para águas altas (high water) e baixas (low water). Fonte: Hess et al. (2003).

2.2.9 Considerações finais sobre processos hidrológicos e hidráulicos em grandes áreas inundáveis

Finalmente, considerando o tamanho das bacias hidrográficas às quais pertencem estas grandes áreas inundáveis, que variam entre dezenas de milhares a milhões de quilômetros quadrados, surge a seguinte questão: quais são os efeitos destas grandes áreas inundáveis na escala das grandes bacias hidrográficas? Distintos efeitos podem existir. Ainda não é conhecida a distinção entre o papel hidrológico das grandes planícies interfluviais e das áreas de extravasamento de grandes rios: uma possível hipótese é de que as águas das áreas interfluviais demorem mais para atingir os rios principais, podendo ser responsáveis por grande parcela de evapotranspiração e

interações com fluxos de carbono e emissão de gases. As grandes taxas de evapotranspiração nas áreas inundáveis alteram diretamente os fluxos sazonais de água. Por outro lado, sabe-se que planícies de inundação têm influência direta na propagação de ondas de cheia, através do armazenamento temporário de água, que pode gerar atenuação considerável dos picos de vazão e retardamento de fluxos devido às grandes perdas por atrito com vegetações ripárias (Wong & Laurenson, 1983; Knight & Shiono, 1996), alterando enormemente a resposta da bacia nos trechos a jusante (Paiva et al., 2013), e mesmo a forma dos hidrogramas, como apresentado no próximo capítulo.

Os diversos processos hidrológicos e hidráulicos explanados neste capítulo existem e interagem simultaneamente nas grandes áreas inundáveis. Existe uma compreensão qualitativa significativa destes processos, mas a sua quantificação e distribuição espaço-temporal permanecem temas maiores na comunidade científica. Além disso, bastante esforço tem sido posto em áreas de estudo particulares (e.g. bacia Amazônica, com destaque para o trecho central do Rio Amazonas), fazendo-se necessária uma compreensão mais ampla sobre os processos que atuam nas diversas áreas inundáveis. Neste contexto, diversas questões científicas podem ser elencadas a fim de nortear futuras pesquisas sobre o tema, como sobre a origem das águas (chuva local, extravasamento da calha fluvial, pequenos tributários com relativa área de contribuição), a interação entre processos de evaporação, infiltração e inundação, o papel das águas subterrâneas na manutenção das áreas inundáveis, o tempo de residência da água nas planícies, e as direções preferenciais de fluxos ao longo destas. Ferramentas ainda devem ser desenvolvidas que permitam estudá-las com maior qualidade.

3 Interação rio-planície de inundação e assimetria de hidrogramas

Este capítulo aborda a relação hidráulica entre rio e planície de inundação e o efeito que esta pode causar em hidrogramas observados nestes sistemas. A motivação deste trabalho surgiu a partir da observação de certas particularidades em comum a hidrogramas de diversos rios com forte influência de planícies de inundação: a presença de uma assimetria negativa no hidrograma observado, onde a ascensão deste é notadamente mais lenta que a recessão, ao contrário do hidrograma típico observado em tantos estudos e livros de hidrologia. Assim, o capítulo aborda de forma detalhada o papel do armazenamento de água e das diferentes geometrias de seções transversais em sistemas rio-planície na relação entre os hidrogramas observados e a propagação de ondas de cheia.

Hidrogramas podem ser considerados assinaturas hidrológicas de uma bacia hidrográfica, refletindo e integrando os diversos processos que ocorrem dentro dela (Hannah et al., 2000; Sivapalan et al., 2003; Hrachowitz et al., 2013). Além disso, compreender processos hidrológicos a partir de características fornecidas pelos hidrogramas pode ser bastante interessante em regiões mal monitoradas. Por exemplo, o tempo de pico pode ser relacionado ao tempo de concentração, ao tamanho da bacia e à declividade; a relação Q90/Q50 utilizada para estimar a importância das águas subterrâneas na vazão dos rios; e o número de picos um indicativo da aleatoriedade da série histórica (NERC, 1975). Neste contexto, este capítulo apresenta uma série de estudos sobre a influência de planícies de inundação na alteração da dinâmica hidráulica de rios, e os possíveis efeitos desta nos hidrogramas observadas em regiões com grandes planícies de inundação. É destacada a mudança na assimetria típica de hidrogramas influenciados por planícies.

Inicialmente, é apresentada uma revisão da literatura sobre a forma dos hidrogramas e as possíveis causas de alteração desta. Observou-se que em hidrogramas de rios com grandes planícies de inundação existe uma assimetria negativa, com uma ascensão mais lenta que a recessão, contrária à assimetria "típica" de hidrogramas (recessão mais lenta que ascensão). A seguir, a partir de testes numéricos com diferentes seções transversais, é mostrado como diferentes geometrias de canais podem levar a diferentes relações entre celeridade da onda de cheia e vazão observada. Este efeito pode ocasionar uma mudança na assimetria dos hidrogramas, o que é então corroborado por uma análise teórica sobre a relação entre celeridade e vazão e a assimetria dos hidrogramas.

Por fim, é realizado um estudo de caso na Bacia Amazônica, onde diversos rios estão associados a grandes planícies de inundação. São utilizados dados observados in situ de vazão e nível para estimar a assimetria dos hidrogramas, mostrando que rios com maiores planícies de inundação tendem a apresentar maior assimetria negativa. Explora-se então o potencial da teoria apresentada para diferenciar tipos de áreas inundáveis. Regiões com grandes planícies de inundação tendem a apresentar uma assimetria

negativa nos hidrogramas observados, ao passo que regiões com extensas áreas inundáveis interfluviais tendem a apresentar hidrogramas com um formato mais típico. Os resultados deste trabalho indicam um potencial interessante do uso da métrica desenvolvida na compreensão de processos de grandes áreas mal monitoradas. Por exemplo, poderia-se utilizar dados de altimetria de satélite para estimar a assimetria de cotagramas de um determinado rio e fazer inferências sobre as planícies de inundação ali presentes.

Este capítulo é apresentado na forma de um artigo científico em língua inglesa. Estes resultados foram publicados recentemente na revista Water Resources Research:

Fleischmann, A., Paiva, R., Collischonn, W., Sorribas, M., Pontes, P. On river-floodplain interaction and hydrograph skewness. Water Resources Research 52(10), 2016.

Abstract

Understanding hydrological processes occurring within a basin by looking at its outlet hydrograph can improve and foster comprehension of ungauged regions. In this context, we present an extensive examination of the roles that floodplains play on driving hydrograph shapes. Observations of many river hydrographs with large floodplain influence are carried out and indicate that a negative skewness of the hydrographs is present among many of them. Through a series of numerical experiments and analytical reasoning, we show how the relationship between flood wave celerity and discharge in such systems is responsible for determining the hydrograph shapes. The more water inundates the floodplains upstream of the observed point, the more negatively skewed is the observed hydrograph. A case study is performed in the Amazon River Basin, where major rivers with large floodplain attenuation (e.g. Purus, Madeira and Juruá) are identified with higher negative skewness in the respective hydrographs. Finally, different wetland types could be distinguished by using this feature, e.g., wetlands maintained by endogenous processes, from wetlands governed by overbank flow (along river floodplains). A metric of hydrograph skewness was developed to quantify this effect, based on the time derivative of discharge. Together with the skewness concept, it may be used in other studies concerning the relevance of floodplain attenuation in large, ungauged rivers, where remote sensing data (e.g., satellite altimetry) can be very useful.

3.1 Introduction

The hydrograph of river discharge at a particular location results from the integration of processes that occur within a catchment, and include water and energy inputs and outputs, storage and transport. This strong relation between processes and river basin output can be useful in two major ways, one predictive and the other interpretative. First, one can be interested in predicting the hydrograph of a basin based

on knowledge of its physical characteristics (Parajka et al., 2013). Second, one can be interested in inferring what are the relevant hydrological processes occurring in the river basin by examination of the output hydrograph (Rinaldo et al., 1995; Hannah et al., 2000).

Most of the studies concerning hydrograph shape during the last decades have been concentrated on the first objective, while a some of them have focused on the role played by the river network physical characteristics, in the context of the theory of the Instantaneous Response Function (IRF) and the Geomorphological Instantaneous Unit Hydrograph (GIUH) (Rodriguez-Iturbe and Valdes, 1979; Rinaldo and Rodriguez-Iturbe, 1996). Several of those studies analyzed the relative importance of hillslope processes, hydrodynamic dispersion and geomorphological dispersion on the catchment response and hydrograph shape (Rinaldo et al., 1991; Robinson et al., 1995, Botter and Rinaldo, 2003). However, most of those researchers considered river hydraulics in a rather simplified manner. Initial studies were based on the hypothesis of constant wave celerity both in space and in time (Gupta et al., 1980, Rinaldo et al., 1991), and subsequent efforts included flow speed variation in space, according to the river reach physical characteristics such as the slope and the cross section shape, but not in time (Sako and Kumar, 2002; Grimaldi et al. 2010; White et al., 2004; Olivera and Koka, 2004; Li and Sivapalan, 2011). It was only recently that the influence of river hydraulics, including floodplains, on the shape of the resulting hydrograph started to be considered (Snell et al. 2004; Mejia and Reed, 2011; Akesson et al., 2015).

In the river hydraulics field, separately from the work done using the IRF and GIUH frameworks, a lot of experimental research effort has been dedicated to study the hydraulic interactions between flow in the main channel and floodplain (Knight and Demetriou, 1983; Stephenson and Kolovopoulos, 1990; Knight and Shiono, 1996; Cao et al., 2006). However, most of these studies concentrated on channels with smooth beds and margins with a rather simplified geometry, generally referred to as "two-stage channels", or "compound channels". Those studies contributed to the understanding of the interchange of water and energy between the river and its floodplains but were mostly based on steady streamflow.

On the other hand, field data analyses of time variable discharge during floods revealed significant effects of floodplains on river flow dynamics and resulting hydrographs. Wong and Laurenson (1983) identified systematic effects of floodplains on the speed of flood waves (celerity) along rivers in Australia, while McCartney and Naden (1995) explored a flattening deformation of the rising limb of the hydrograph, which they called "shoulder", due to floodplain inundation along the river Severn. The same "shoulder", or deformation on hydrographs caused by floodplain inundation was shown in modeling studies by several authors (Wolff and Burges, 1994; Tang et al.; 1999; Garbrecht and Brunner, 1991; Cao et al., 2006; Costabile and Macchione, 2012; and Price, 2009). Other studies were concerned with the attenuation of hydrographs due to floodplain inundation and water storage, and the impacts of floodplains on peak flows, but had no information about hydrograph shape (Sholtes and Doyle, 2011;

McCartney and Naden, 1995; Moussa and Bocquillon, 2009; Jothityangkoon and Sivapalan, 2003; Di Baldassarre et al. 2009).

On a larger scale context, many works have focused on understanding complex floodplain river and wetland systems dynamics (Biancamaria et al., 2009; Bourrel et al., 2009; Hung et al., 2012; Kuppel et al., 2015) and the associated complex flow patterns, which relate floodplain hydraulics and hydrological processes (Alsdorf et al., 2007; Trigg et al., 2009; Fan and Miguez-Macho, 2011; Neal et al., 2012; Trigg et al., 2013; Paiva et al., 2013; Paz et al., 2014; Pontes et al., 2015) and ultimately affect ecosystem development (Junk et al., 1989, Melack et al., 2009) and global environmental cycles (Richey et al., 2002; Melack et al., 2004). In such regions, where data scarcity is frequently a strong limitation, the usage of hydrological signatures such as hydrographs to infer hydrological behaviors can be very relevant (McDonnell and Woods, 2004; Wagener et al., 2007; Sawicz et al., 2011; Wagener et al., 2013). For instance, the time to peak can be a surrogate for time of concentration, catchment size and topographical characteristics such as slope and catchment form, the baseflow index can be used to estimate the importance of groundwater on the river discharge, and the number of peaks used to indicate the randomness of a series (NERC, 1975). However, to our knowledge, no consistent hydrograph feature has yet been described to address the interaction between extensive floodplains and river hydraulics.

In this context, an interesting feature of hydrograph shape that we observed in a number of recent studies in rivers with floodplains in South America (e.g. Bravo et al., 2012; Paiva et al., 2013; Paz et al., 2014) is that of slower rising than falling hydrograph limbs, herein called a negatively skewed shape. Figure 3.1 presents examples of such hydrographs for large river systems in South America, with different spatio-temporal scales, climatology and catchment sizes. This is in contrast with "typical" hydrographs, which tend to be positively skewed, with fast rising and slow falling limbs. Negatively skewed hydrographs are also shown in observed discharge of rivers with floodplains by Ovando et al. (2015), Perumal et al. (2001), Turner-Gillespie et al. (2003), Moussa and Bocquillon (2009) and Casse et al. (2015), and in modeling results of rivers with floodplains by Turner-Gillespie et al. (2003), Moussa and Bocquillon (2009), Yamazaki et al., (2011) and Miguez-Macho et al. (2015), although these authors do not highlight this common feature.

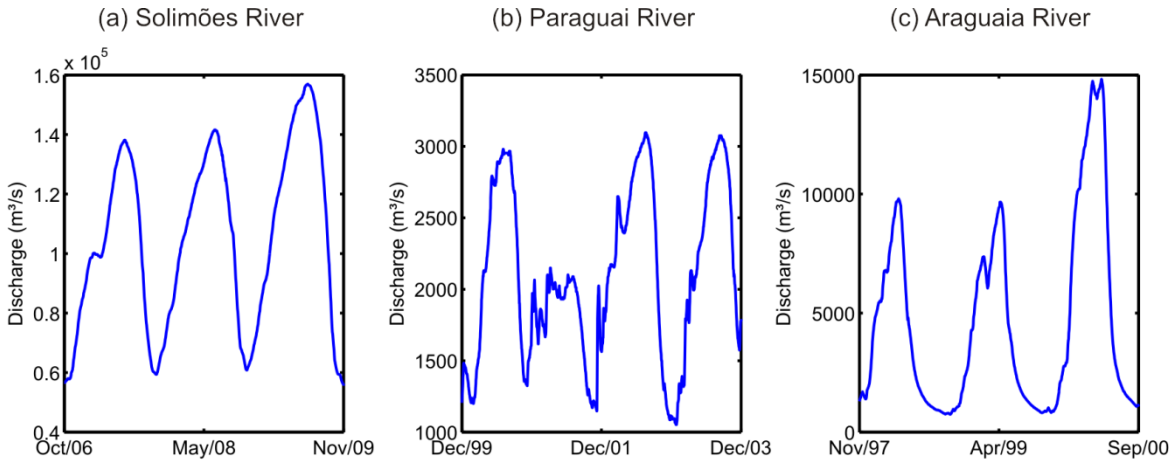

Figure 3.1. Observed hydrographs at rivers with extensive floodplain attenuation in South America. (a) Manacapuru gauge at Solimões River (Amazon basin), with a drainage area of 2,200,000 km²; (b) Porto Murtinho gauge at Paraguai River, 576,000 km²; and (c) Conceição do Araguaia gauge at Araguaia River, 332,000 km². Data obtained from Brazilian National Water Agency (ANA, available at < http://hidroweb.ana.gov.br/>).

More interestingly, we noted that one river may present the two types of hydrograph skewness depending on the hydrologic conditions such as it is observed in the river Piquiri, a tributary of the Parana river in South Brazil (Figure 3.2a, 3.2b), where small (large) floods present positive (negative) skewness. While the hydrograph of Figure 3.2a has a peak of 630 m³/s, and is positively skewed, the hydrograph shown in Figure 3.2b has a peak of 5760 m³/s and is clearly negatively skewed. By computing the travel times of flood wave hydrographs in a 110 km reach of this river, we derived the relationship between flood wave speed (celerity) and discharge for the reach (Figure 3.2c). This curve is in accordance with observations from NERC (1975) and Wong and Laurenson (1983) for other natural rivers, and shows that depending on the river discharge, a different relationship between celerity and discharge may exist, which in turn may be important in defining basin response time, and ultimately, hydrograph skewness.

From the above arguments, we developed the hypothesis that negatively skewed hydrographs may be characteristic of rivers with floodplains, and may be useful as a signature of the presence of river-floodplain interactions upstream of a particular location. Then, the aim of this paper is to show that the presence of floodplains adjacent to rivers potentially affects hydrograph shape, specifically the hydrograph skewness, and to investigate the involved mechanisms. We used analytical reasoning, numerical experiments, and examination of empirical data. Due to the effect of floodplains on hydrograph skewness, we suggest that there is potential to infer the relative importance of river-floodplain connections from a stage or discharge hydrograph at a single location.

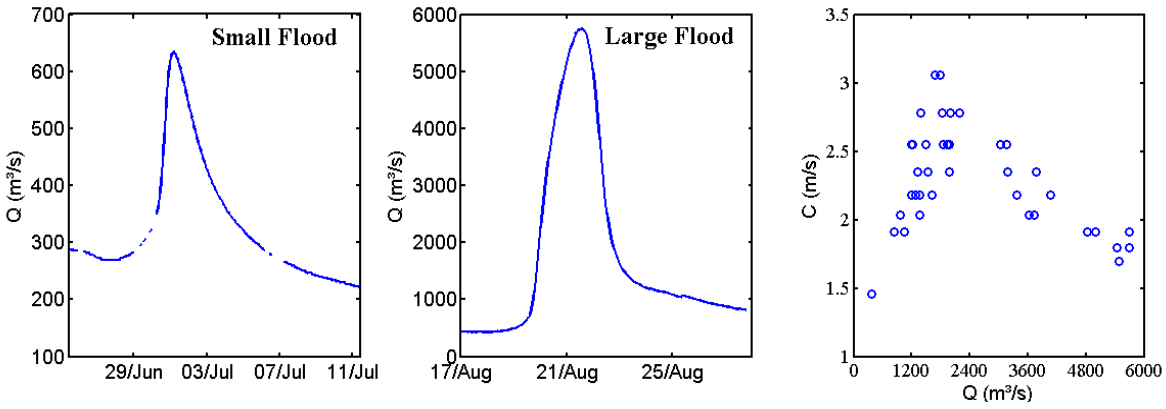

Figure 3.2. Observed hourly discharge data for the Piquiri River at Balsa Santa Maria (20,900 km²). (a) A typical streamflow hydrograph with faster rising limb than the falling one, resulting in a positive skewness, can be observed in small floods in the Piquiri river. (b) Large floods presenting a negatively skewed hydrograph. (c) Relationship between observed flood wave celerity (C) and discharge (Q). Flood wave celerity was computed by the travel time of discharge peaks between upstream Novo Porto 2 gauge station and downstream Balsa Santa Maria, separated by a reach length of 110 km. Data obtained from Brazilian National Water Agency (ANA, available at < *www.snirh.gov.br/telemetria/*>).

3.2 Methodology

The following three complementary approaches were adopted to address how the hydrograph skewness can be related to the presence of floodplains, each one explored in a different section:

- **Section 3.3. Numerical modeling experiments**: a series of HEC-RAS flood wave routing simulations to explore the effects of different channel cross sections in the outflow hydrograph shape and check if river-floodplain interactions can cause negative skewed hydrographs
- **Section 3.4. Theoretical analysis**: mathematical analyses of 1-D continuity equation to understand how river-floodplain interactions cause changes in hydrograph skewness as flood wave travels downstream, and to derive analytical criteria to predict when one can expect such behavior.
- **Section 3.5. Empirical analysis**: a case study in the Amazon River Basin to show from observation data that negatively skewed hydrographs occur in rivers with large floodplains and to assess how hydrograph skewness can be used to infer about the presence of floodplains and different wetland types.

Since each approach has its particular method, the methods and results are presented within each section. This paper is organized as follows. Section 3.3 presents the methods (3.3.1) and results (3.3.2) for the HEC-RAS numerical experiments, while section 3.4 is related to the theoretical analysis and sections 3.5.1 and 3.5.2 to the Amazon basin case study. Finally, in section 3.6, we present a discussion of how the

different approaches explored here contribute to the understanding of hydrograph shape in floodplain regulated river systems.

3.3 Numerical modeling experiments

3.3.1 Methods

The speed of natural flood waves occurring along rivers can be estimated by the kinematic wave celerity (c) given by Equation 3.1 (Chow et al., 1988; Lighthill and Witham, 1955):

$$c = \frac{dQ}{dA} \qquad (3.1)$$

where Q is discharge and A is the cross section area.

During floods that do not inundate overbank, celerity rises with river discharge, and larger floods move faster than smaller ones, resulting in positively skewed hydrographs (Chow et al., 1988; Ponce, 1989). Channels with floodplain geometry present a different behavior, where at overbank stages an inverse celerity-discharge relationship is present (Wong and Laurenson, 1983; Knight and Shiono, 1996). The overall result for large flows is a lower celerity and slower peak travel times, which potentially affect the hydrograph shape.

The impact of different cross sections shapes and flood wave celerity-discharge relationships on hydrograph shape can be illustrated by numerical modeling experiments. We conducted flood routing experiments using HEC-RAS (USACE, 2010) and three different river-floodplain channel geometries (Figure 3.3a).

The first geometry is a rectangular channel with no floodplains. The second is a two-stage channel with floodplains that are flooded when discharge is roughly 310 m³/s. The third geometry is similar to the second one for the main channel, but instead it has a floodplain with a mild slope. Because of this, for the third geometry, bankfull discharge also starts at ~310 m³/s, but floodplain inundation increases gradually. Typical values of Manning's roughness coefficient for natural rivers were selected based on USACE (2010) – 0.030 for the main channel and 0.10 for the floodplain. For each channel geometry, celerity-discharge curves were computed as a steady state dQ/dA relationship.We applied HEC-RAS for the three channel and floodplain geometries using the same upstream and downstream boundary conditions, in a 175 km long river channel, with a bed slope of 10 cm/km. The upstream boundary condition was a hydrograph based on *NERC* (1975):$Q(t) = Q_{base} + \left(Q_{peak} - Q_{base}\right)(\frac{t}{Tp}\exp\left(1 - \frac{t}{Tp}\right))^{\beta}$, where Q is the discharge, t is time, Q_{base} is the baseflow, Q_{peak} is the peak

discharge, Tp is the time to peak and β is a constant. The following parameters were adopted Q_{base}=200 m³/s, Q_{peak}=2,000 m³/s, Tp=24 h and β=8. The downstream boundary condition was set to normal depth, based on the assumed slope of the channel.

3.3.2 Results

Celerity-discharge curves for the three channel geometries are presented in Figure 3.3b, while Figure 3.3c shows the routed outflow hydrographs, together with the inflow hydrograph for the three cross section geometries. In the case without floodplains, it can be seen that the hydrograph is slightly positively skewed, and at the same time flood wave celerity increases with discharge. In the two-stage channel simulation, the outflow hydrograph clearly shows the "shoulder" or nearly constant discharge at bankfull conditions, which has been previously described in the literature (Garbrecht and Brunner, 1991; Wolff and Burges, 1994; McCartney and Naden, 1995; Tang et al.; 1999; Cao et al., 2006; Costabile and Macchione, 2012; and Price, 2009). A pronounced discontinuity in the celerity-discharge curve is presented in this case, which explains the hydrograph shape: at bankfull discharge, a sudden decrease in flood celerity slows down the hydrograph, creating the observed displacement.

The third cross-section geometry, with a mild slope floodplain bottom that is slowly and progressively inundated while river stage and discharge increases, leads to an outflow hydrograph with an almost imperceptible "shoulder". The most important feature of the outflow hydrograph in this case is that the hydrograph rise is slower than its recession, leading to a negative skewness. It occurs because celerity decreases continually with discharge for high flows, as can be seen in the celerity-discharge relation. The changes in the celerity with increasing discharge for a river with floodplains were also presented for the Piquiri river in the "Introduction" section (see Figure 3.2). Using data from two gauge stations in a reach of 110 km and by computing the peak travel time between them, we developed the celerity-discharge relation shown in Figure 3.2c. For the small flood, the peak discharge of 600 m^3/s is in the rising part of the celerity-discharge curve, and the hydrograph exhibits a positive skewness. In contrast, the large flood is found to be negatively skewed, and its peak discharge (more than 5000 m^3/s) is in the decreasing part of the celerity-discharge curve. Finally, Figure 3.2c indicates that for discharges about 1800-2200 m^3/s the celerity is expected to begin to decrease, and this threshold is related to bankfull discharge. This case study corroborates our numerical experiments by showing that small floods are located within the range of increasing discharge with celerity and are positively skewed (Figure 3.3, single channel), while large floods tend to be negatively skewed due a inverse relationship between celerity and discharge (Figure 3.3, mild floodplain).

Finally, the HEC-RAS modeling experiment indicates that river channel and floodplain geometry influence the development of hydrographs that are both skewed to

the left and to the right. A symmetric inflow hydrograph can be transformed into a positive asymmetric outflow hydrograph when celerity increases with discharge, or it can be transformed into a negative asymmetric one when celerity decreases with discharge.

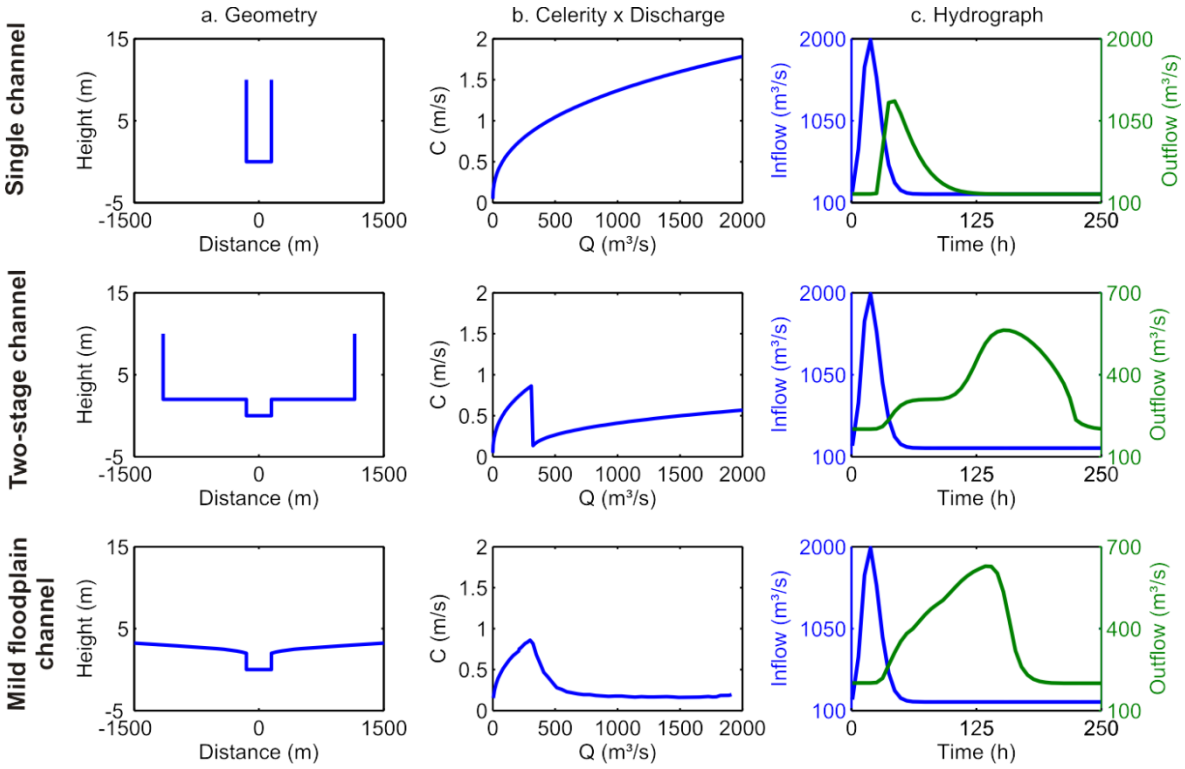

Figure 3.3. Results of HEC-RAS modeling experiments of flood routing in a 175 km river reach considering three different cross section/floodplain geometries. (a) Channel cross section geometries. (b) Relationship between flood wave celerity and discharge. Celerity was computed as dQ/dA. (c) Hydrograph calculated at channel inflow (blue) and outflow (green). Please note that the scales of Y-axes in column (c) are different between inflow (blue) and outflow (green) for the two bottom scenarios to allow a better visualization of the hydrograph shape.

3.4 Theoretical analysis

The HEC-RAS modeling analysis of a river reach shows that floodplains can change river hydrograph shape, and symmetric inflow hydrographs may be transformed into negatively skewed ones depending on the river and floodplain cross section geometry. We examine next from an analytical point of view what governs changes in hydrographs skewness as a flood wave travels downstream. The hydrograph at a given point can be described by the rate of change in discharge $\frac{\partial Q}{\partial t}$, where the quantity $\left|\frac{\partial Q}{\partial t}\right|$ shows how fast or slow is the rising limb (when $\frac{\partial \mathrm{Q}}{\partial \mathrm{t}} > 0$) or the recession ($\frac{\partial \mathrm{Q}}{\partial \mathrm{t}} < 0$). As a

flood wave travels downstream, the hydrograph is modified and the change in space of the rising limb or recession slope can be expressed as $\frac{\partial\frac{\partial Q}{\partial t}}{\partial x}$. If this quantity is positive (negative), the downstream hydrograph presents a faster (slower) rising limb and a slower (faster) recession. The factors that govern these changes can be studied by applying the $\frac{\partial}{\partial t}$ operator to the 1 D river continuity equation:

$$\frac{\partial}{\partial t}\left(\frac{\partial Q}{\partial x}+\frac{\partial A}{\partial t}\right)=0 \quad (3.2)$$

Using the chain rule ($\frac{\partial A}{\partial t}=\frac{\partial A}{\partial Q}\frac{\partial Q}{\partial t}=\frac{1}{c}\frac{\partial Q}{\partial t}$), after some operations and assuming $\frac{\partial^2 Q}{\partial t^2}$ is small, then:

$$\frac{\partial\frac{\partial Q}{\partial t}}{\partial x} = -\frac{1}{c}\frac{\partial^2 Q}{\partial t^2}+\frac{1}{c^2}\frac{\partial c}{\partial Q}\frac{\partial Q}{\partial t}\frac{\partial Q}{\partial t} \approx \frac{1}{c^2}\frac{\partial c}{\partial Q}\left(\frac{\partial Q}{\partial t}\right)^2 \quad (3.3)$$

where $c=\frac{\partial Q}{\partial A}$ is the kinematic celerity of the flood wave, i.e. the velocity of propagation of a flood wave in the river. In Eq. 3, the terms $\frac{1}{c^2}$ and $\left(\frac{\partial Q}{\partial t}\right)^2$ are necessarily positive, so the signal of $\frac{\partial\frac{\partial Q}{\partial t}}{\partial x}$ depends on the signal of $\frac{\partial c}{\partial Q}$. This result explicitly shows that the changes in the downstream hydrograph are governed by how the flood wave celerity changes with discharge:

$$\frac{\partial\frac{\partial Q}{\partial t}}{\partial x}\propto\frac{\partial c}{\partial Q} \quad (3.4)$$

Then, Eq. 4 shows that:

- If celerity increases with discharge ($\frac{\partial c}{\partial Q}>0$), then the downstream hydrographs will accelerate, presenting faster rising limb and slower recession, as $\frac{\partial\frac{\partial Q}{\partial t}}{\partial x}>0$.
- If the celerity decreases with discharge ($\frac{\partial c}{\partial Q}<0$), the downstream hydrograph will present slower rising limb and faster recession ($\frac{\partial\frac{\partial Q}{\partial t}}{\partial x}<0$).

The example of Piquiri river in Figure 3.2, other previous empirical studies (NERC, 1975; Wong and Laurenson 1983; Knight and Shiono, 1996) and HEC-RAS simulations show that rivers with floodplains have parts of their celerity-discharge curve where celerity decreases with discharge ($\frac{\partial c}{\partial Q}<0$). From Eq. 4 one can conclude that this affects flood hydrographs by reducing the slope of the rising limb.

The condition to predict how flood wave celerity changes with discharge (or water height h), and consequently how hydrographs may change downstream, can be derived by applying the operator $\frac{\partial}{\partial h}$ to $c = \frac{\partial Q}{\partial A} = \frac{\partial Q}{\partial h} / \frac{\partial A}{\partial h}$, and assuming river top width as $W = \frac{\partial A}{\partial h}$:

$$\frac{\partial c}{\partial h} = \frac{\frac{\partial^2 Q}{\partial h^2} W - \frac{\partial Q}{\partial h}\frac{\partial W}{\partial h}}{W^2} \quad (3.5)$$

In equation 3.5 the signal depends on the relative values of $\frac{\partial^2 Q}{\partial h^2} W$ and $\frac{\partial Q}{\partial h}\frac{\partial W}{\partial h}$. This analysis shows that celerity increases or decreases with water height depending on variations in discharge and river width. Table 3.1 summarizes these criteria and presents particular cases.

Table 3.1. Summary of analytical criteria to characterize the effect of river-floodplain characteristics on flood wave celerity and downstream river hydrograph with some particular cases.

Hydrograph changes	Rising limb	Falling limb	Flood wave celerity	Criteria	Particular cases
$\partial \frac{\partial Q}{\partial t} / \partial x > 0$ Rising limb becomes steeper	Faster	Slower	$\frac{\partial c}{\partial h}, \frac{\partial c}{\partial Q} > 0$ Celerity increases with discharge	$\frac{\partial Q}{\partial h}\frac{\partial W}{\partial h} < \frac{\partial^2 Q}{\partial h^2} W$	$\frac{\partial W}{\partial h}$ is small or null. River width (W) is relatively constant
					Large $\frac{\partial^2 Q}{\partial h^2}$. Fast increase of discharge with height (e.g. flash floods)
$\partial \frac{\partial Q}{\partial t} / \partial x < 0$ Rising limb becomes less steep	Slower	Faster	$\frac{\partial c}{\partial h}, \frac{\partial c}{\partial Q} < 0$ Celerity decreases with discharge	$\frac{\partial Q}{\partial h}\frac{\partial W}{\partial h} > \frac{\partial^2 Q}{\partial h^2} W$	Large $\frac{\partial W}{\partial h}$ and small $\frac{\partial^2 Q}{\partial h^2}$. Width increases fast with height. Rivers with large floodplains.
					Negative $\frac{\partial^2 Q}{\partial h^2}$. e.g. reservoirs regulated by bottom orifice $Q=ah^b$ and $b<1$

According to these relations, it is the balance of how storage ($\frac{\partial Q}{\partial h}\frac{\partial W}{\partial h}$) and discharge ($\frac{\partial^2 Q}{\partial h^2}W$) capacities change with height that regulates celerity and how downstream hydrographs evolve. If changes in river width are small and river width is relatively constant ($\frac{\partial W}{\partial h} \approx 0$), then $\frac{\partial Q}{\partial h}\frac{\partial W}{\partial h} < \frac{\partial^2 Q}{\partial h^2}W$. As a consequence, celerity increases with discharge and the rising limb of the downstream hydrograph becomes steeper than the inflow hydrograph. This is the case of the HEC-RAS simulation of the single channel case in Figure 3. An enhanced acceleration occurs if the increase in discharge with water height is large ($\frac{\partial^2 Q}{\partial h^2} \gg 0$), as in the case of flash floods on relatively dry rivers, where effects of bed friction are much higher at small heights.

The opposite occurs when river width increases fast with height ($\frac{\partial W}{\partial h} \gg 0$), as in the case of river with large floodplains. For those cases celerity decreases with discharge and the rising limb of the downstream hydrograph becomes less steep than the upstream hydrograph. The resulting hydrograph may have a negative skewness, as shown in the case of the river with mild floodplain in Figure 3.3. A similar behavior is found when $\frac{\partial^2 Q}{\partial h^2}$ is negative, which means that as height increase, the storage always increases more than discharge terms. Such mechanism is found in reservoirs regulated by typical bottom orifices, where $Q=ah^b$ and $b<1$.

3.5 Empirical analysis: Amazon River Basin case study

In sections 3.3 and 3.4 we have shown that the skewness of the hydrograph flowing out of a river reach depends on the relation between flood wave celerity and discharge in the river. Both the analytical approach and the numerical experiments show that the shape of the hydrograph may be changed to become more positively or negatively skewed depending on the cross section and the associated celerity-discharge curve. It is expected that rivers with extensive upstream floodable areas will generate flood hydrographs with a clear negative skewness, while rivers with no will floodplains generate flood hydrographs with positive skewness. To evaluate these ideas, in this section we propose a metric for skewness evaluation and analyze data from rivers in the Amazon basin.

The Amazon River basin (Figure 3.4) is the largest in the world (~6 x 10^6 km^2) with an average discharge of 2 x 10^5 m^3/s, which represents ~17% of global freshwater arriving to the oceans (Callede et al., 2002). Hydrographs of the main river and its larger tributaries present monomodal flood pulses in response to dry and wet seasons. River stage amplitude between minimum and maximum annual values can reach up to 15 m, and large lowland areas are seasonally flooded. Mapping of the Amazon wetlands using Synthetic Aperture Radar imagery from JERS-1 satellite at ~100 m spatial resolution for low and high water seasons in 1995-96 indicates that the seasonally inundated

floodplains covers about 17% of the lowland Amazon (extent ranging from 300 to 600 $\times 10^3$ km^2) (Melack and Hess, 2010). The extension of floodplains regulates the magnitude and timing of the annual flood wave and acts as an important driver for ecological processes and sediment and carbon fluxes (Junk, 1997; Dunne et al. 1998; Melack et al. 2009). Furthermore, different types of wetlands exist along the basin, where different inundation processes occur, e.g. interfluvial wetlands (local rainfall and runoff generating floods) and river floodplains (overbanking flow) (Junk et al., 2011). Previous studies on this region show that river hydraulics plays an important role. It has been shown that (i) low river slopes causes backwater effects to control part of the river dynamics and (ii) storage of water in floodplains is important for regulation of the annual flood (Meade, 1991; Trigg et al. 2012; Paiva et al. 2013). In this study, we analyze how floodplains may affect runoff hydrographs in terms of skewness.

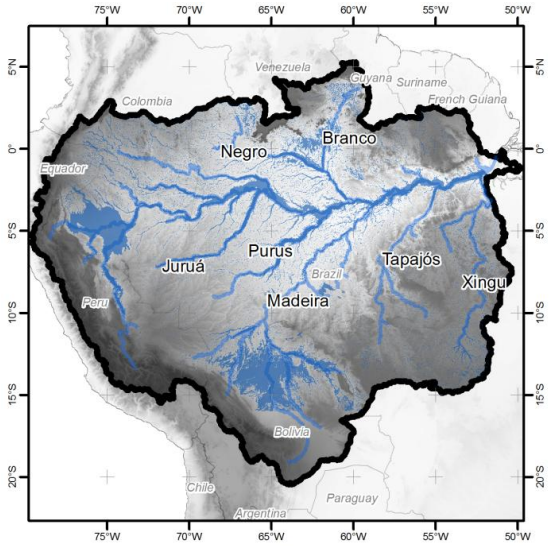

Figure 3.4. (a) Amazon River Basin, its main tributaries, relief from SRTM Digital Elevation Model (Farr et al., 2007) (gray) and floodable areas (blue) from Amazon wetlands map product of Melack and Hess (2010).

3.5.1 Methods

In this empirical analysis we use observed discharge and water stage data to explore the skewness of hydrographs from river gauges along the Amazon river and its main tributaries. To quantify the hydrograph skewness we propose a metric, termed the Skewness Index (S), obtained by taking daily discharge time series and computing the derivative of discharge for each day ($(Q_t - Q_{t-1})/\Delta t$) and separately averaging positive derivatives (rising limb) and negative derivatives (falling limb). The metric is the ratio between the averages of negative and positive derivatives, as shown by Equation 3.6.

$$S = 1 - \frac{falling\ limb\ \left|\frac{dQ}{dt}\right|}{rising\ limb\ \left|\frac{dQ}{dt}\right|} = 1 - \frac{\frac{1}{n_{neg}}\sum_{i=1}^{n_{neg}}\frac{|\Delta Q_{neg,i}|}{\Delta t}}{\frac{1}{n_{pos}}\sum_{i=1}^{n_{pos}}\frac{|\Delta Q_{pos,i}|}{\Delta t}} \quad (3.6)$$

where ΔQ is the increment of discharge between two consecutive days, n is the number of time intervals (days) and the subscripts neg and pos denotes the time intervals where ΔQ is negative (falling limb) or positive (rising limb), respectively. Low flows (below 20% percentile) were removed from the computation to focus on medium to high flows of flood hydrographs. If S is negative ($S < 0$), then the rising limb is slower than the recession and the hydrograph is negatively asymmetric; if S equals zero, the hydrograph is symmetric; and if $S>0$ the rising limb is faster than the recession, as in typical stream hydrographs with positive skewness.

We used daily discharge (stage) time series from 119 (379) gauges to derive *S* values for the Amazon river basin. Data were obtained from the Brazilian Agency for Water Resources (ANA, available at < http://hidroweb.ana.gov.br/>), the Peruvian and Bolivian National Meteorology and Hydrology Services (Servicio Nacional de Meteorologia e Hidrologia, available at < http://www.senamhi.gob.pe/>), and the Hydrology, Biogeochemistry and Geodynamic of the Amazon Basin program (HYBAM, available at < http://www.ore-hybam.org/>).

Finally, we analyze the hypothesis that different types of wetlands could be distinguished through a hydrograph skewness analysis. Based on our numerical modeling experiments and literature on floodplain/wetland hydrology, we expect a negative skewness to be higher (in absolute values) where floodplains are inundated by river water coming from upstream. In regions with no floodplains or floodplains that are mainly maintained by local rainfall, we expect less impact on hydrograph skewness. We investigate how changes in hydrograph shape relate to the size and type of wetlands by studying the correlation between the fraction of floodable areas in the drainage area at each river gauge (*%FA*) and the hydrograph skewness (S) at the same location. An Amazon wetland map developed from JERS Synthetic Aperture Radar data at ~100 m spatial resolution (Melack & Hess, 2010, available at <https://daac.ornl.gov/LBA/guides/LC07_SAR_Wetlands_Mask.html>) was used to extract the floodable area upstream of each Amazon River Basin gauge. To exclude large river channels from the analysis, we used the difference between high and low water wetland maps. Analyses were performed for the main tributaries of the Amazon River basin - Juruá, Purus, Madeira, Negro (before confluence with Branco river), Branco, Tapajós and Amazon main stem (Figure 3.4).

3.5.2 Results

Hydrograph skewness from gauge data

A striking feature of hydrographs at some places in the Amazon is the hydrograph shape, which can be clearly negatively skewed, as in Solimões river at the Manacapuru gauge station in Figure 3.1a. We hypothesize that the negative skewness of the hydrograph in the Amazon is caused, at least in part, by river hydraulics in general, and particularly by changes in flood wave celerity that occur due to floodplain inundation. For instance, Figure 3.5 shows observed hydrographs at different reaches of the Purus and Negro rivers, which are main tributaries of the Amazon basin. Purus has extensive floodplains in its lowlands, with large floodplain width compared to the main channel width, while the Negro river has a different pattern, with a wide valley with alternating islands and interfluvial wetlands (Alsdorf et al., 2005; Latrubesse, 2008; Junk et al., 2011). In Figure 3.5 it can be seen that Purus hydrographs become more negatively skewed when travelling downstream, while the Negro ones remain almost unchanged.

In Figure 3.5, the skewness metric *S* is presented for each gauge to highlight these differences. Purus' values for the *S* metric decreased from 0.29 to -0.05 in the downstream direction, while Negro's ones remain almost constant along the channel, possibly indicating the effects of floodplains.

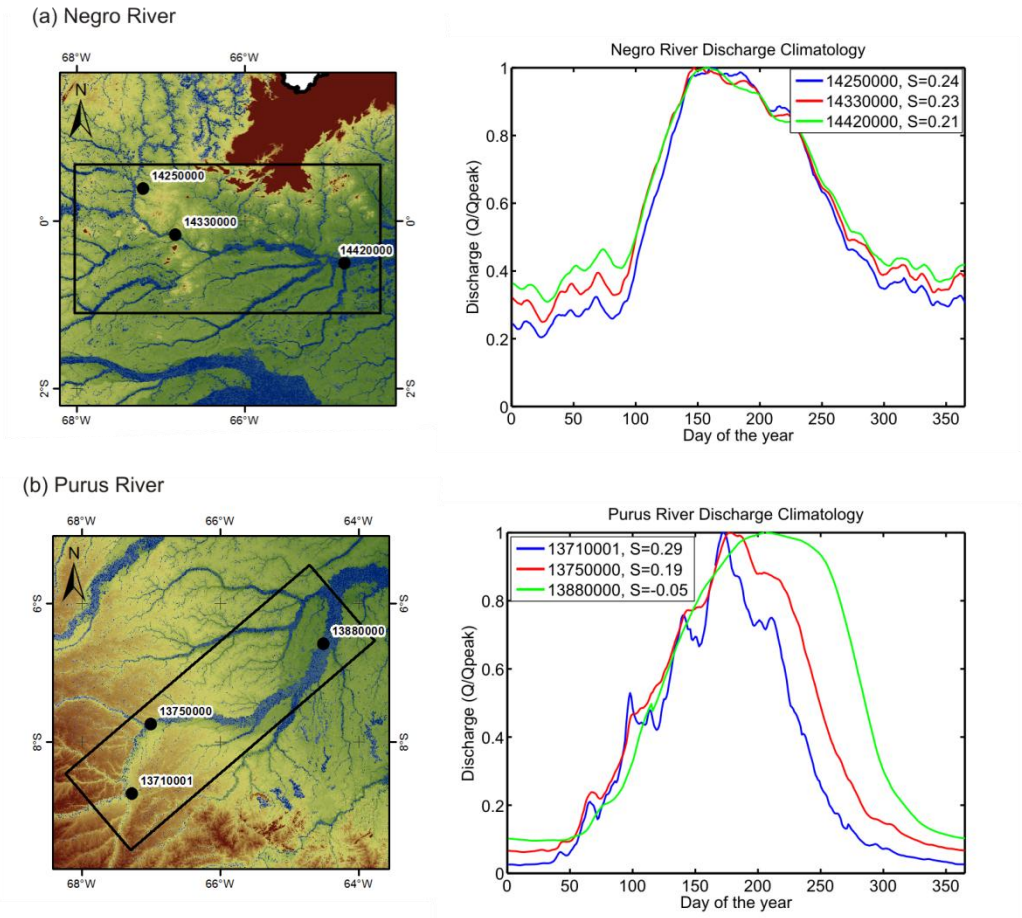

Figure 3.5. Observed hydrographs from upstream to downstream direction for (a) Negro river at São Felipe (gauge number 14250000; drainage area 124,000 km²), Curicuriari (14330000; 194,000 km²) and Serrinha (14420000; 293,000 km²); and (b) Purus river at Valparaiso (13710001; 105,000 km²), Seringal Fortaleza (13750000; 154,000 km²) and Canutama (13880000; 236,000 km²). Hydrographs are displayed according to the hydrological year, and refer to an average from multiple years rescaled by the maximum discharge. S values relate to the skewness metrics described in Section 3.5.1. SRTM DEM and flooded area maps from Melack & Hess (2010) are used in the maps for visualization of the wetlands.

Figure 3.6 shows the location of the gauges and the calculated skewness *S* values. As the skewness derived from the stage and discharge data were strongly, linearly correlated (R=0.909, P<0.05), stage and discharge data were analyzed together. In general, low or negative *S* values occur mainly in the Amazon main stem and at some tributaries (lower Purus, lower Juruá and Madeira rivers) that have large floodplains. Also, *S* values tend to decrease in the downstream direction, indicating that the hydrograph is changing as the floodwave travels along the river.

Figure 3.7 shows the relationship between the skewness *S* values and drainage area for discharge gauges along the Amazon main stem and its main tributaries basins, namely Juruá, Purus, Madeira, Branco, Negro and Tapajós rivers. According to Figures

3.6 and 3.7, there is a general trend of high, positive *S* values for the headwaters and decreasing *S* in the downstream direction. Such behavior is in accordance with the analyses from Section 3.3, indicating that the existence of large floodplains in the lowland Amazon basin may cause such evolution on the hydrographs shapes, due to the storage effects from floodplains and changes in celerity as the flood waves travel downstream. For rivers such as Purus and Juruá, extensive floodplains exist in the downstream reaches, explaining the observed behavior. Also, the lowest *S* values were obtained for rivers with larger floodplains, i.e. Amazon main stem, Purus, Juruá and Madeira.

Furthermore, we recognize that river hydraulics is not the only factor that can result in negatively skewed hydrographs. The characteristics of the drainage network and climatic heterogeneities may also play important roles. For instance, contrasting rainfall regimes are found in the northern and southern parts of the basin with the rainy season occurring in June to August and December to February, respectively (Espinoza et al. 2009). Therefore, the spatial and temporal rainfall distributions contribute to lagged tributaries' discharges to the main stem. In this context, the positive correlation between drainage area and skewness for Tapajós river, which does not feature large floodplains, may be the timing of the response of tributaries. On the other hand, Negro river does not present a significant correlation, as expected from the hydrographs presented in Figure 3.5.

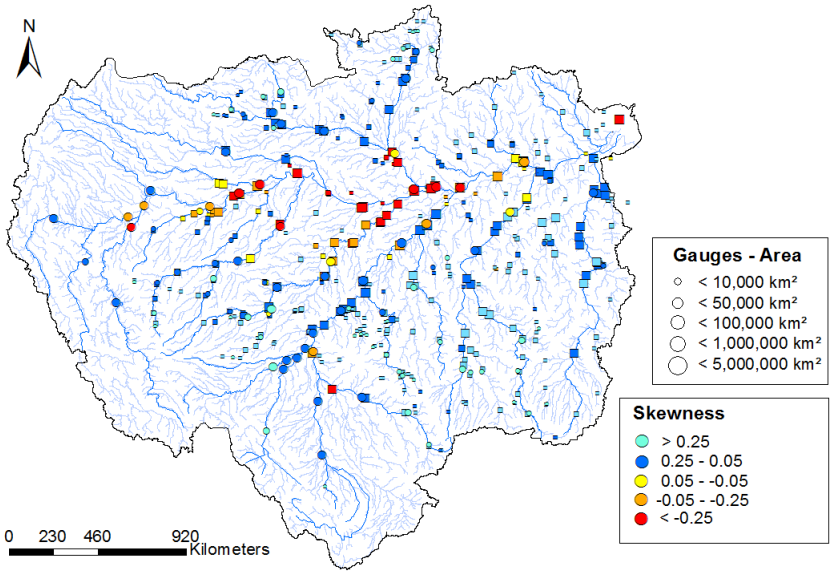

Figure 3.6. Spatial distribution of hydrograph skewness metric S computed for discharge (circles) and stage (squares) time series from gauges.

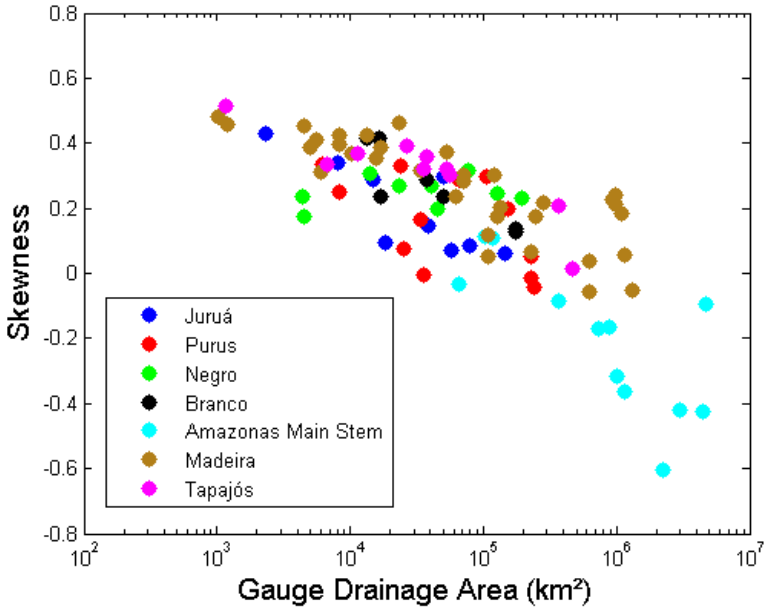

Figure 3.7. Relationship between hydrograph skewness S and drainage area (log km²) for discharge gauges at different Amazon tributaries basins.

Wetland extent and hydrograph skewness

In the Amazon basin, the largest wetlands can be distinguished between river floodplains, which have high flood amplitudes (e.g., 11 m in the Madeira river floodplain at Porto Velho), and interfluvial wetlands, which have small ones (1-3 m) (Junk et al., 2011; Keddy et al., 2009). These interfluvial regions occur due to local precipitation and the presence of flat areas in the basin, so that it takes long for the river network to drain the excess rainfall. The main large interfluvial wetlands occur in the Upper and Middle Negro, Branco (Roraima wetlands) and Upper Madeira rivers (Llanos de Moxos wetlands) (Melack and Hess, 2010; Junk et al., 2011; Junk, 2012). The importance of understanding these areas lies in the fact that they are poor in nutrients and sustain different ecological systems in comparison to other types of Amazonian wetlands (Junk, 1993). While floodplains receive most of their water and biogeochemical material from its parent rivers, interfluvial areas receive most of the water from direct rainfall. In addition, recent studies identified that both floodplain and interfluvial wetland characteristics may occur simultaneously in some regions, such as in the Llanos de Moxos (Bourrel et al., 2009; Junk et al., 2011; Ovando et al., 2015). Although evaluation of the wetland extent still does not account for these differences, Junk et al. (2011) argued that in very flat interfluvial regions, areas influenced by local rainfall can be much larger than the areas affected by overbank flow.

Figure 3.8 presents the correlation between fraction of floodable area (*%FA*) and *S* values for gauges of the seven selected tributaries. A high correlation between floodable area and negative skewness is expected in rivers with floodplains fed by river

water, while interfluvial wetlands systems fed by local runoff or rivers basins with small wetlands should not reveal such pattern. Furthermore, skewness in rivers not regulated by floodplains should be smaller than in regulated ones. Figure 8 results show that a positive and significant correlation was found for the Juruá, Purus, Madeira and Amazon main stem rivers ($p<0.05$), while no correlation was found for the other three rivers (Negro, Branco and Tapajós). Negative S values were only found for the Juruá, Purus, Madeira and the Amazon main stem. Although a direct interpretation of these results is not straightforward, it is interesting to notice how the spatial distribution of the skewness could relate to types of wetland systems. In Juruá, Purus and Madeira rivers are all classified as white water rivers with their origins in the Andes, and transport nutrient-rich sediments. In all of them, large floodplains (large floodplain to channel width ratios) exist along the rivers, justifying the positive correlation obtained here.

The three other rivers (Negro, Branco and Tapajós) have particular characteristics that could explain the lower skewness values and the low correlation with *%FA*. While the Tapajós river does not have a large developed floodplain, the Branco river presents large, interfluvial floodable savannas (Junk et al. 2011). In turn, although the Negro river comprises extensive floodplains areas (Melack & Hess, 2010), near the confluence with Branco river the flat terrain presents large connection between interfluvial and forested wetlands. High ratios of *%FA* (up to 0.05) were then obtained for Negro and Branco rivers due to these extensive interfluvial areas, and hence a significant correlation was not achieved. Finally, in the cases where both floodplain and interfluvial wetlands are present, negative skewness can also occur, as in the Upper Madeira river, where Llanos de Moxos interfluvial wetlands are very large, but floodplain effects also exist and attenuate the flood wave (Junk et al., 2011). In this case, a positive correlation was found between *S* and *%FA*.

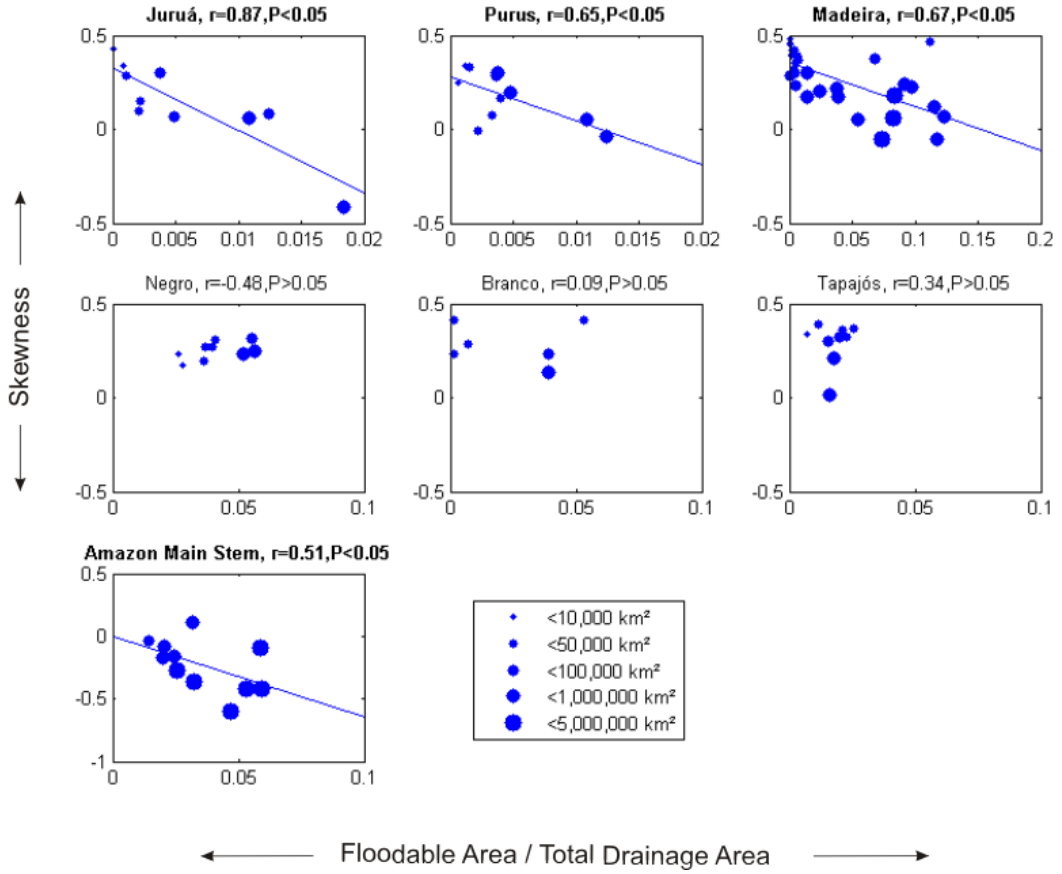

Figure 3.8. Relationship between discharge gauge skewness and flooded area/drainage area ratio (%FA) for main tributaries of the Amazon Basin (see Figure 4 for location of rivers). Size of the circles are related to gauge drainage area. Flooded areas were derived from Melack & Hess (2010) product. Significant relationships are highlighted in bold.

3.6 Discussion

Although the shape of runoff hydrographs has been extensively debated in the hydrology literature, to our knowledge, no previous work has shown that floodplains can generate negatively skewed hydrographs. HEC-RAS numerical experiments, together with theoretical and empirical analyses in the Amazon basin, corroborate our hypothesis that floodplain water storage and its impact on flood wave celerity are important factors to define the hydrograph skewness in floodplain regulated rivers.

Many studies have observed a "shoulder" at near bankfull discharge in hydrographs of rivers with floodplains, although most of them were derived from numerical experiments. Through HEC-RAS simulations we have shown that this displacement is a result of a sudden decrease of celerity at bankfull stage. On the other hand, strong hydrograph deformation, as the one related to "shoulders", are not always evident, due to a less marked transition between the main channel cross section and

floodplain. As noted by Wong and Laurenson (1983), localized floodplain storage occurs below bankfull discharge because there are connections between river channel and floodplain that are activated before water stage is above the general bank level of the river reach. This gradual inundation of floodplain results in a smooth curve relating celerity and discharge, as shown in Figure 3.3b. The overall result is a negatively skewed hydrograph, and examples from South American rivers' hydrographs show it (Figures 3.1, 3.2 and 3.5). Although most of our case studies here concerned large rivers, the analysis criteria presented in section 3.4 suggest that the negative skewness from river-floodplain interaction may arise wherever large floodplain storage exists relatively to river discharge.

Furthermore, previous studies in headwater catchments that analyzed hydrograph dispersion (Rinaldo et al., 1991) suggested that hydrograph skewness depends on the relative influences of hillslope processes and channel routing (Robinson et al., 1995; Botter and Rinaldo, 2003; Li and Sivapalan, 2011). According to those studies, positively skewed hydrographs reflect the dominance of hillslope dispersion over geomorphological dispersion and are typical for small river basins, while negative skewness is a reflection of the dominance of geomorphologic dispersion, being more common in larger basins. However, as noted by Snell et al. (2004), when examining discharge data, even relatively large river basins with negatively skewed width-functions tend to show hydrographs with positive skewness. Nevertheless, our study showed that negatively skewed hydrographs occur in large rivers with floodplains.

Different reasons can be considered for the appearance of negatively skewed hydrographs in these systems, such as the above-mentioned geomorphological dispersion and structure of the river network, the timing of flood arrival from different tributaries (e.g. the Amazon main stem hydrograph being formed by the different contribution from many large tributaries inflows), and the long duration of the rainfall "event" (e.g. in the Amazon basin the rainfall event duration would be the whole length of the rainy season). However, based on our study, we propose a new mechanism that is important for the definition of hydrograph skewness in such rivers, which is related to floodplain water storage.

Our results are encouraging for the understanding of floodplain dynamics and its effects on the basin hydrograph response in floodplain regulated systems. Possible applications of our hydrograph skewness concept relate to (i) understanding the role of floodplains in a given basin from the shape of hydrograph or stage time series; (ii) predicting types of wetlands from hydrograph skewness, distinguishing river floodplains from interfluvial wetlands; and (iii) providing new insights for the improvement of hydrological models, which should represent floodwave hydraulics (e.g. celerity varying with discharge) in order to correctly represent the response of basins with large floodplain influence.

3.7 Conclusions

We investigate the effect of river-floodplain interactions on the shape of discharge hydrographs, with an emphasis on hydrograph skewness. The work was motivated by a common characteristic that was observed over several rivers with floodplains (e.g. Amazon, Paraguai and Piquiri rivers): asymmetric hydrographs with a rising limb slower than the recession one and a characteristic negative skewness, which is the opposite behavior that one expects from typical river hydrographs in headwater catchments.

The results suggest that hydrograph skewness is strongly controlled by the relation between river discharge and flood wave celerity, reflecting an important component of transport processes in defining such hydrological signatures. In rivers with no floodplains, the relationship between celerity and discharge generally leads to positively skewed hydrographs, while in rivers with floodplains this can lead to negatively skewed ones as shown here. Previous studies have shown that the processes of floodplain inundation result in a flattening deformation of the rising limb of the hydrograph, sometimes called "shoulders". In a modeling exercise, we showed here that those "shoulders" occur in rivers with "two-stage channels", i.e. river reaches with relatively simple channel and floodplain geometry, and with a sharp transition between main river and floodplain, for which the floodplain inundation is sudden. Because of this sudden floodplain inundation, there is a discontinuity in the relation between river discharge and speed or celerity of the flood wave and this discontinuity is the cause of the so-called "shoulder". In several natural channels, however, the transition between main river and floodplain is gradual, as observed previously by *Wong and Laurenson* (1983). As a result, there is no discontinuity in the celerity-discharge relation, and after bankfull discharge, celerity gradually decreases with discharge. The effects of floodplain inundation on the hydrographs of those rivers is less marked than the "shoulders" observed in simplified river geometries, and the flattening deformation of the rising limb of the hydrograph can be only observed as a slower rising limb. Depending on the dimensions of floodplains the outflow hydrograph can show slower ascending than descending limbs. Analyses of the 1-D river continuity equation corroborate this and show that changes on the downstream hydrograph are directly related to how flood wave celerity changes with discharge or water level.

Finally, a case study in the Amazon basin using in situ discharge and stage data from several gauges and a wetland map derived from remote sensing reinforce the theoretical results, indicating that high negative skewness occurs in hydrographs of Amazon rivers with extensive floodplains (e.g., Amazon main stem and Purus river). Also, floodplain regulated rivers present a significant correlation between the size of floodable areas and negative skewness, demonstrating the strong control of floodplains on hydrograph shapes, while basins with no relevant wetlands or dominated by interfluvial wetlands do not show such relationship.

Understanding seasonal timing, predictability and interannual variability of flood pulses is fundamental for studies about the ecology of wetlands and floodplain processes in general (Hamilton et al., 2002). We believe that future research can give new insights on the use of the negative skewness of hydrographs to foster scientific knowledge of floodplain systems. The skewness metric could be used in other basins in order to understand possible river-floodplain connections, while the possibility of identifying watersheds where floods are shaped by overbank flow and not by endogenous processes (e.g., local rainfall) seems to be an interesting way forward. Finally, to better use this hydrograph feature, observed data of stage or discharge are needed. In large, ungauged river-floodplain systems, the few available *in situ* hydrological information can be complemented with river height time series obtained from nadir altimetry satellites (e.g. ENVISAT, JASON, ICESAT, ICESAT2, Altika) or from the forthcoming Surface Water and Ocean Topography (SWOT) satellite mission (Durand et al., 2010; Biancamaria et al., 2015), which in turn could potentially be used to derive hydrograph skewness values and help in understanding the hydrologic dynamics of such regions.

4 Simulação acoplada de hidrologia e hidrodinâmica de grandes áreas inundáveis: estudo de caso no Delta Interno do Rio Níger, África

A bacia do Rio Níger compreende cerca de 1,5 x 10^6 km² de área hidrologicamente ativa (ou seja, áreas diretamente conectadas à bacia, não sendo endorreicas), onde cerca de um milhão de pessoas vivem. O rio nasce nas montanhas da Guinea, onde recebe grande parte do volume de água de seu trecho superior, passando então pela plana região do Delta Interno do Níger no Mali, já na área semi-árida do Deserto do Sahel, onde cerca de 40% do volume afluente é perdido por evaporação e infiltração nos mais de 10.000 km² de área sazonalmente inundada. A região abriga uma grande população, dependente do ciclo de inundação sazonal, onde atividades como pesca e cultivo de arroz são fundamentais para a economia local. Além disso, o Delta Interno do Níger é a maior área inundável do Oeste da África, sendo um dos grandes deltas internos do continente, junto com o Delta do Okawango e as planícies de Sudd no Rio Nilo, e responsável por importantes interações terra-atmosfera na escala local e regional.

Apesar de sua relevância global, são poucos os estudos desenvolvidos para esta região que envolvem modelos hidrológicos com uma boa capacidade preditiva dos processos de inundação. Mais especificamente, modelos distribuídos com um satisfatório acoplamento entre hidrologia e hidrodinâmica das planícies são ainda inexistentes, como os realizados em outras áreas como o Pantanal na América do Sul (Paz et al., 2011) e o Delta do Okawango na Botsuana, África (Bauer et al., 2006). Estes modelos trazem benefícios para a compreensão dos processos ocorrentes nestas áreas, permitindo avaliações sobre o papel relativo do armazenamento e dos canais em planícies de inundação e da interação entre áreas inundadas, evaporação e infiltração, por exemplo. Além disso, a capacidade destes em estimar áreas inundadas, vazões e níveis de rios de forma distribuída na bacia apresenta grandes potencialidades para a gestão de recursos hídricos, especialmente em áreas mal monitoradas e que sofram com conflitos civis, como é a região da bacia do Alto Rio Níger. Assim, este capítulo apresenta o desenvolvimento e validação de um modelo hidrológico-hidrodinâmico da bacia do Alto Rio Níger, capaz de representar a inundação do Delta Interno do Níger de forma satisfatória, e de trazer importantes contribuições para a compreensão dos processos de inundação desta região e, de forma geral, sobre o papel relativo de diversos processos na determinação da resposta da bacia em regiões complexas de planícies de inundação.

Este capítulo é apresentado na forma de um artigo científico, escrito em língua inglesa e a ser submetido para a revista Journal of Hydrology.

Abstract

The Upper Niger Basin is located in Western Africa, flowing from Guinea Highlands towards the Sahel region. In this area lies the seasonally inundated Niger Inner Delta, which supports important environmental services such as habitats for wildlife, climate and flood regulation, as well as large fishery and agricultural areas. Given its enormous impacts on regional and continental scale, the development of a large scale model that couples both hydrodynamic and hydrology processes becomes an important issue for studies related to basin alteration such as climate change and dam regulation, as well as to foster the comprehension of key processes driving the basin hydrological cycle. In this study, we present the application of MGB-IPH large scale hydrologic and hydrodynamic model for the Upper Niger Basin, totaling c.a. 650,000 km² and set up until the city of Niamey in Niger. The model couples hydrodynamic flood wave propagation across floodplain channels with hydrological vertical processes and streamflow generation, enabling representation of feedbacks between flooded areas and soil column, as well as computation of evapotranspiration from both soil-vegetation interface and open water areas. The model is forced with TRMM 3B42 daily precipitation for the period 1999-2015 and monthly mean climatology data from Climate Research Unit (CRU), and is calibrated against in-situ discharge gauges and validated with in-situ water level, remotely sensed estimations of flooded areas and satellite altimetry. Model outputs are in good agreements with daily discharge (used for calibrating the model) and with in-situ and satellite altimetry water levels at stations both upstream and downstream of the Inner Delta (Nash-Sutcliffe Efficiency (NSE)>0.6 for most discharge gauge stations), as well as for flooded areas within the delta region (NSE =0.6; r=0.85). It is able to simulate flooding of both perennial (e.g., Niger main stem) and ephemeral rivers (e.g., Niger Red Flood tributaries in Sahel). The model is then used to analyze driving hydrological processes along the Niger Inner Delta. Estimated annual water losses across the Delta varied between 20.1 and 30.6 km³/yr, and annual calculated evapotranspiration ranged between 760 mm/yr and 1130 mm/yr. Evaluation of model structure indicate that representation of both floodplain channels hydrodynamics (storage, backwater, bifurcations, lateral connections) and vertical hydrological processes (floodplain water infiltration into soil column; evapotranspiration from soil and vegetation and evaporation of open water) are necessary to correctly simulate flood wave attenuation and evapotranspiration along the basin. Finally, such coupled hydrologic and hydrodynamic modeling proves to be an important tool for integrated evaluation of hydrological processes in such poorly gauged, large scale basins. We hope that this model application provides new ways forward for large scale model development in such systems, involving semi-arid regions and complex floodplains. Possible uses of the model involve the assessment of different scenarios of anthropic alteration, e.g., the effects of reservoirs implementation and climate and land use changes.

4.1 Introduction

Niger River is the third longest in Africa, comprising nine countries across the West Africa, and about 100 million people (Andersen et al., 2005). With headwaters in the Guinean highlands, it flows northward through the seasonally flooded Niger Inner Delta and towards the Sahel desert, and then turns back flowing southward on the direction of Niger Delta and the Gulf of Guinea. Along its course, contrasting environments lead to a complex interaction between society and the river system, such as in the large floodplains of the Inner Delta surrounded by Sahel desert, where extensive fishery and rice production activities during flooding are replaced by livestock during receding flow and dry periods (Zwarts et al., 2005). Alterations in the basin hydrological response are related to already built and planned dams (Zwarts et al., 2005), past droughts (Descroix et al., 2009), land use and climate change (Cassé et al., 2015; Thompson et al., 2016). Such changing environment reveals the importance of improving our predictability methods at the basin scale, in order to foster our knowledge of the basin main hydrological processes.

In this context, large scale hydrological models arise as an important tool. Previous model applications in the basin include simplified water balance approaches (Sutcliffe & Parks, 1989; Conway & Mahé, 2009), off-line coupling between global rainfall-runoff conceptual models and simple (Dadson et al., 2010; Pedinotti et al., 2012) or 1D hydrodynamic flood routing (Yamazaki et al., 2011), and a 2D regional hydrodynamic model of the Niger Inner Delta (LISFLOOD-FP, Neal et al., 2012). Particular complexity is related to simulation of Inner Delta region, given its extensive flooding along a semi-arid area through both channelized and diffuse flows. Hydrodynamic simulation of floodplain channels and flow bifurcations has been shown necessary for a satisfactory representation of flood dynamics in the region (Neal et al., 2012), and similar modeling challenges involving multiple floodplain channels are found in other inner deltas such as the Okavango (Bauer et al., 2006), large wetlands as the Pantanal (Paz et al., 2011) and large delta systems as the Mekong (Yamazaki et al., 2014).

Although modeling efforts for complex, large scale systems such as the Upper Niger Basin have increased in the last years, there is still a lack of model development that takes into consideration important feedbacks between floodplain hydrodynamics and vertical hydrology (i.e., soil infiltration, evapotranspiration, etc.), since most models employ an offline coupling approach between hydrology and hydrodynamics. An interesting example of such coupled models is presented by Paz et al. (2014), who explored in a large scale 1D/2D model of Pantanal wetlands in South America how the vertical hydrological balance (evapotranspiration, precipitation and soil infiltration) interacts with flooded areas, showing that their representation is fundamental for the correct representation of wet and dry processes along the wetland, as well as channel-floodplain water exchange. In turn, Bauer et al. (2006) developed for the Okavango Delta in Botswana, a semi-arid area similar to Niger Inner Delta, a regional model

coupling surface and groundwater processes, highlighting the groundwater level control on flooding maintenance.

In semi-arid regions that are periodically flooded, specific model implementations may be necessary to realistically represent hydrological and hydrodynamic processes, including floodplain water infiltration into unsaturated soil and related feedbacks (Bauer et al., 2006; Milzow et al., 2009; Pedinotti et al., 2012); a thorough representation of open water evaporation, given high evaporation rates (Neal et al., 2012); and river and floodplain transmission losses from channel (Costa et al., 2012). Additionally, specific runoff generation mechanisms may occur (e.g., occurrence of Hortonian processes in contrast to tropical mostly dominant Dunnian processes; Esteves et al., 2003; Mamadou et al., 2015), while the existence of ephemeral reaches and associated dry beds, and changes of endorrheic basins into exorheic ones (and vice-versa) may alter the basin hydrological response (Mamadou et al., 2015).

Finally, the development of such coupled models in Niger basin would allow a better evaluation of which model structure (i.e., which hydrological and hydrodynamic processes) is necessary to better simulate and understand the Niger hydrological cycle. It would ultimately improve our prediction capabilities of the basin hydrologic response under current and future alterations (e.g., climate change and flow regulation). In this context, here we present the improvement, calibration and validation of a coupled hydrodynamic and hydrological model (MGB-IPH, Pontes et al., 2017) for the Upper Niger Basin, explicitly representing flood wave routing along multiple floodplain channels throughout the Inner Delta and feedbacks between the floodplain and unsaturated soil column, as well as evapotranspiration from soil and flooded areas. The model is then used to characterize and understand the role of different hydrological and hydraulic processes along the basin.

4.2 Materials and methods

4.2.1 Study area: Upper Niger River Basin

The Niger River basin is located in Western Africa and includes nine countries - Benin, Burkina Faso, Cameroon, Chad, Côte d'Ivoire, Guinea, Mali, Niger, and Nigeria (Andersen et al., 2005) (Figure 4.1). The river has around 4200 km from its headwaters in the Guinean Highlands until its mouth in the Gulf of Guinea in Nigeria, and its hydrologically active basin area is around 1.5 million km². In this study, the Upper Niger River Basin is defined as the drained area of the Niger River upstream Niamey city (657,000 km², which contains both hydrologically active and inactive areas). Along its course, the river receives most of its water from the tropical Guinean Highlands (precipitation ~1900 mm/yr), with steep and typical drainage network, and flows until the flat Niger Inner Delta in Mali, which is one of world's largest wetlands with over 73,000 km² in the middle of Sahel Desert (annual precipitation ~ 550 mm/yr, with most

precipitation in the months June to August). In the Inner Delta, large losses occur through mainly evapotranspiration (annual loss of about 40% of inflow, average inflow and outflow being 1490 and 900 m^3/s, Mahé et al., 2009), and intensive flood wave attenuation and delay occur due to extensive floodplains (Neal et al., 2012). At the Delta entrance, Niger main stem receives the contribution of Bani river (Figure 4.2d), which flow has been regulated by Talo reservoir since 2005. Downstream the Delta, after the historical city of Tombouctou, the river flows through hundreds of kilometers until Niamey city, receiving water mainly from its "Red Flood" tributaries, a set of three intermittent rivers in the Niger right bank that contribute to a hardly predictable flood in Niamey (Cassé et al., 2015; Figure 4.1). In the left bank, most channels (locally known as "koris") are not connected to the river system.

In the Niger Inner Delta, different hydrological processes occur in Southern and Northern areas (see Mahé et al. 2009 for definition of these areas; Figure 4.2): in the former, flow bifurcation mainly due to Diaka river (Figure 4.2d) drives large floods, where flood is basically delayed, while in the latter, three main distributaries (Figure 4.2b, three arrows) feed a vast field of dunes called Erg of Nianfunké (stationary sand dunes running from west to east; Davies et al., 1996), where dozens of channels meander and account for a similar water volume loss as in its southern counterpart, although the flooded area is considerably smaller (Mahé et al., 2009). The border between Southern and Northern Delta regions is defined by a region of lakes, with the large Lac Débo receiving most waters from Niger main stem before releasing it downstream (Figure 4.2a and b). The Inner Delta also provides important feedbacks on convection and generation of precipitation in a regional scale (Taylor et al., 2010). Potential Evapotranspiration in the Inner Delta region is around 2300 mm/year (Olivry, 1994), and is higher in the Northern than in Southern Delta areas (Mahé et al., 2009).

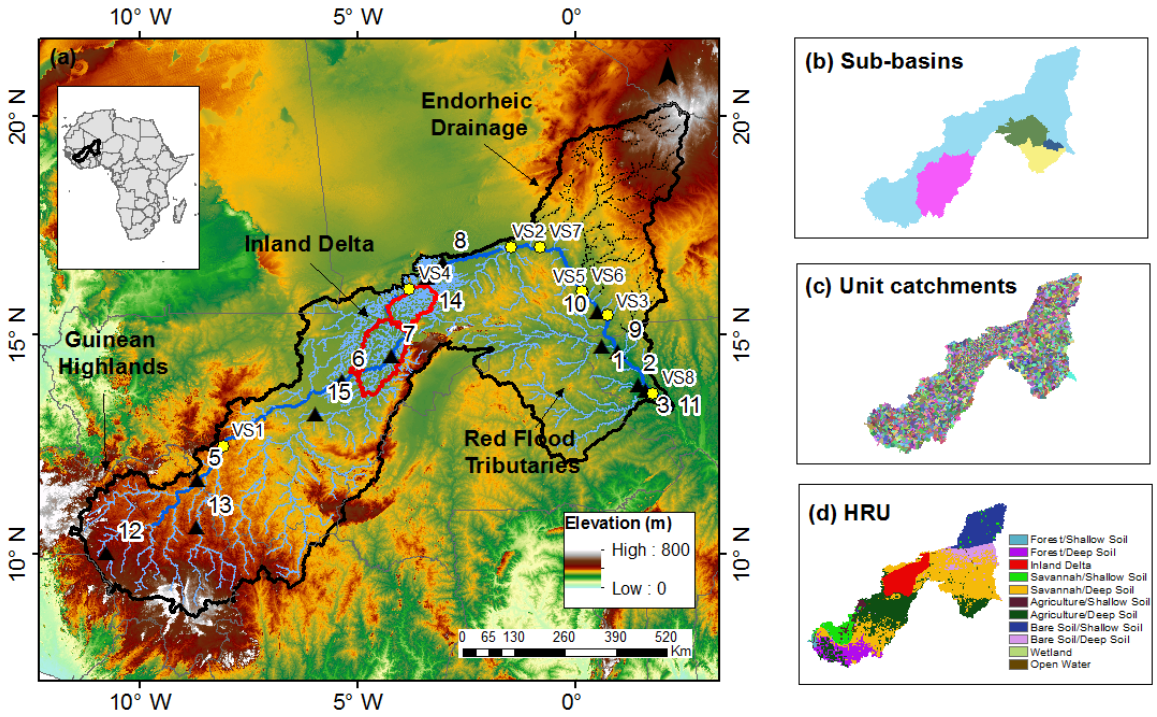

Figure 4.1. Upper Niger Basin. (a) In-situ gauges with discharge and/or water level data (numbered black triangles; see Table 4.1 for gauge description), altimetry virtual stations (yellow circles, VS1-8), extracted drainage network and SRTM 250 m Digital Elevation Model. Red polygons indicate Southern and Northern Inner Delta regions as described in Figure 4.2. Dark blue drainage refers to the Niger main stem and dashed black lines to endorheic drainage that was not included in the model. (b) Sub-basins used for definition of model parameters. (c) Basin discretization into 4307 unit-catchments. (d) Hydrological Response Units (HRU) map used for model parameterization.

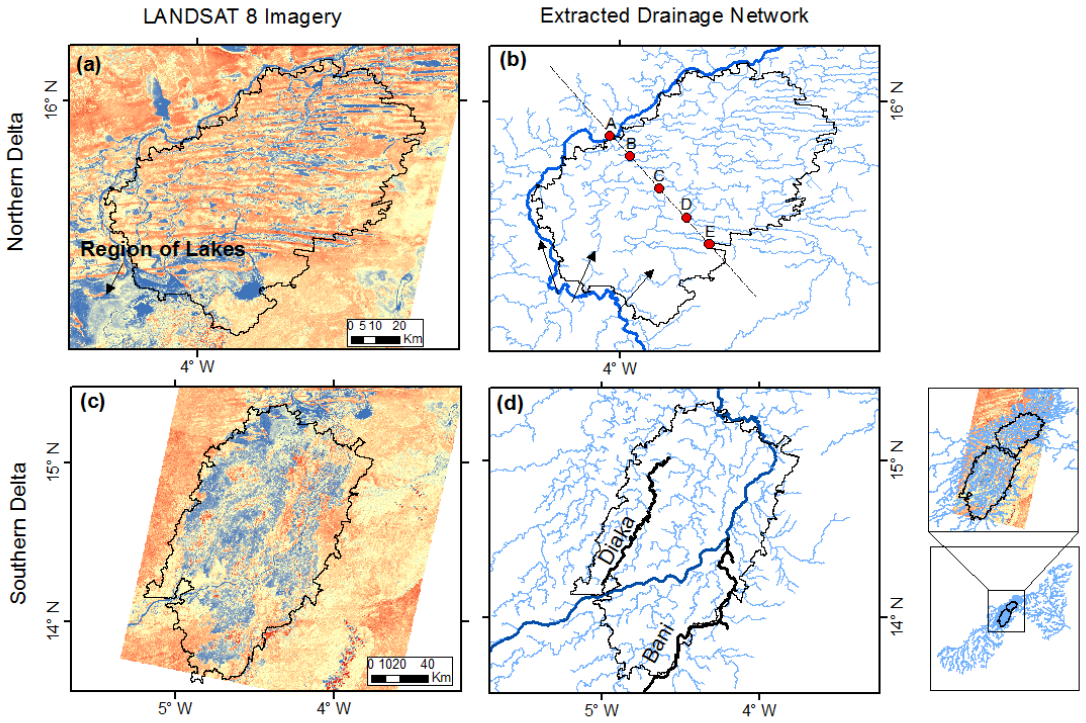

Figure 4.2. Northern and Southern regions of the Niger Inner Delta with a dense drainage network for representation of floodplain channels, as defined by Mahé et al., 2009. LANDSAT8 images LC81970502015304LGN00 and LC81970492015352LGN00 (available at http://earthexplorer.usgs.gov/) from 2015 high water period were used for visualization of Delta's channels and landscape. Dark blue lines in (b) and (d) indicate Niger main stem, as defined in Figure 4.1. The transect in Northern Delta region (dashed black line, figure (b)) is used for simulated water level analysis at locations A-E in Figure 4.11. Arrows in (b) indicate the direction of Niger distributaries in Northern Delta Region. Diaka distributary's direction and Bani river are presented in (d) as thick black lines.

4.2.2 The MGB-IPH model

The MGB-IPH model (Collischonn et al., 2007, Pontes et al., 2017; "*Modelo de Grandes Bacias*" or "Large Basins Model") is a semi-distributed rainfall-runoff model developed for simulation of large basins. In its most recent version, river maps are extracted from high resolution DEMs using a vector-based approach and the basin is divided into unit-catchments (Fig. 4.1c), each one containing a single river reach with associated floodplain and hydrological vertical water and energy balance. Within each unit-catchment, Hydrological Response Units (HRUs) are defined based on soil type and land use (Fig. 4.1d), and for each one the water and energy budget is computed through the soil-vegetation system. Surface, subsurface and groundwater outflows from water balance are routed to the main river of the unit catchment using linear reservoirs, while flow propagation through drainage networks is computed using the Muskingum-Cunge method or 1D hydrodynamic equations. Additionally, sub-basins are defined as

macro-regions unifying many unit-catchments with the same model parameter values (Fig. 4.1b).

Main model parameters are related to soil water budget for each HRU: maximum soil water storage (*Wm*, based on ARNO rainfall-runoff model,Todini, 1996), three equivalent hydraulic conductivities (*Kbas*, *Kint*, and *Kinf*), parameter from the variable contributing area model for runoff generation (*b*) and three parameters related to surface, subsurface, and base flow residence time (*Cs*, *Ci*, and *Cb*). Supplementary Material 4.A1 presents model calibrated parameters for the Upper Niger River Basin, and a detailed explanation of model parameters is provided by Collischonn et al. (2007). Additionally, the hydrodynamic module requires width, bankfull depth and bed elevation for each river reach (one per unit-catchment), as well as Manning' n roughness coefficient and floodplain topography (see description in section 4.2.4).

Model forcing data are precipitation and surface meteorological data for energy budget and evapotranspiration computation (wind speed, solar radiation, relative humidity, air pressure and air temperature). For each unit-catchment, observed precipitation is interpolated to the respective centroid using a squared inverse method, while surface meteorological data values are attributed by nearest neighbor interpolation. Details on datasets used in the Niger model application are presented in section 4.2.4

Evapotranspiration is calculated with Penman-Monteith equation following methodology by Wigmosta et al. (1994), where evaporative demand is first available for evaporation of vegetation interception water, and the remaining demand is used for soil evapotranspiration or open water evaporation from flooded areas. Limited plant evapotranspiration due to soil water deficit is considered by increasing surface resistance under water stress situation (Collischonn et al., 2007).

Flood wave routing is based on the 1D inertial formulation developed by Bates et al. (2010) which is a simplification of Saint Venant's equation by neglecting the local acceleration term and has been recently applied with success in many large scale models, including the Niger Inner Delta (Neal et al., 2012) and other areas across the globe (Fernández et al., 2016; Pontes et al., 2017). Time step is governed by Courant–Freidrichs–Levy condition (Bates et al., 2010). In MGB-IPH model, each unit-catchment has one river reach with rectangular cross section, with pre-defined width, bankfull depth and Manning's n coefficient. For each unit-catchment a stage-area-volume relationship is derived from DEM using the HAND model (Rennó et al, 2008) and following the approach described in Yamazaki et al. (2013) and Siqueira et al. (submitted paper), which is used for estimation of sub-grid floodplain topography (Paiva et al., 2011; Pontes et al., 2017). Also, bankfull level is automatically derived from the DEM as the average elevation pixels along channel pixels for each unit-catchment. Then, the bankfull depth (a model parameter, as defined in the section 4.2.4) is discounted from it to yield the unit-catchment channel bed elevation. At each time step, discharge is calculated between upstream-downstream adjacent unit-catchments, or

between neighbor unit-catchments with pre-defined lateral connection (see next section 4.2.3 for description of lateral connections), and then those calculated flows are computed in the unit-catchment water storage together with evaporation and precipitation over flooded areas and generated streamflow. The stage-volume relationship is used to convert the unit-catchment updated volume into water level (Yamazaki et al., 2011), while the stage-area relationship is used to estimate the flooded area within the unit-catchment, which is then used to calculate open water evaporation. If water level is below bankfull depth, flooded area equals the channel surface area.

4.2.3 Model improvement for arid regions and Niger river basin

Infiltration from floodplain

A new formulation was included in the model to account for infiltration from floodplains into unsaturated soil column. This process may be important in regions where flooding occurs from exogenous sources into areas where soils are relatively dry before flood arrival (e.g. Niger main stem channel flooding the Inner Delta). For each unit-catchment at each time interval, infiltration from floodplain into soil column is computed based on the degree of soil saturation and unit-catchment flooding area as $Dinf = \frac{A_{fl}}{A} Kinf(1 - \frac{w}{W_m})$, where A_{fl} is the flooded area at a given unit-catchment, A the unit-catchment area, $Kinf$ the infiltration rate that occurs when the whole unit-catchment is flooded and soil is totally dry (mm.Δt^{-1}), w the soil water content and W_m the maximum soil water storage. $Kinf$ value was calibrated together with other vertical hydrological balance parameters (see Supplementary Material 4.A1), and model sensitivity to it is discussed in section 4.3.4.

Then, the calculated infiltration volume is removed from the unit-catchment's flood control volume and inserted into unit-catchment's soil water storage.

To better represent the dense drainage network that exists within the Inner Delta, and to increase model calculation units in this area, a densification of the drainage network was applied by decreasing the area threshold (number of cells that defines the beginning of river drainage) in this area. The result was a much denser drainage within the Inner Delta (Figure 4.1a and Figure 4.2). Regarding endorheic reaches that were present in the extracted drainage network (Figure 4.1a, dashed black drainage), they were all removed from model simulation since they do not contribute to the basin hydrology (Autorité du Bassin du Niger (ABN), personal communication).

Inner Delta specific modeling

In order to represent channel bifurcation and diffuse flows along Niger Inner Delta floodplain, lateral connections (rectangular channels with pre-defined width and depth values) were set between all neighbor unit-catchments along the Inner Delta region, including main distributaries (Diaka river in Southern Delta and Issa Ber, Bara Issa and Kolikoli branches at the entrance of Northern Delta). Given the high density of unit-catchments defined throughout the Inner Delta, this approach leads to an unstructured 2D model in this region. This approach was applied by Pontes et al. (2017) to simulate flooding in the Bananal Island floodplain (Central Brazil), and is similar to the flow bifurcation scheme proposed by Yamazaki et al., (2014). Considering the unit-catchment area as a circle, the length of the connection channel is computed as the sum of the radiuses of two adjacent unit-catchments, $L = \sqrt{\frac{A_1}{\pi}} + \sqrt{\frac{A_2}{\pi}}$, where L is the channel length and A_1 and A_2 are the values for the area of the unit-catchments connected by the channel.

In Niger basin model application, a modification was applied for the condition where water level is below bankfull depth. Channel surface area is considered as zero when river channel is dry (ephemeral rivers) and increases linearly until bankfull depth, where flooded area equals the channel surface area (channel width times length). This implementation avoids unrealistic high open water evaporation rates during low flow periods.

4.2.4 Model input data and parameterization

The model was run from 1999 to 2014 using TRMM-3B42 daily precipitation product (available at https://pmm.nasa.gov/data-access/downloads/trmm; Huffman et al., 2007) as forcing data, together with CRU 10' long-term climatology data (monthly climate normals of wind speed, solar radiation, relative humidity, air pressure and air temperature were used; New et al., 2002) for computation of model evapotranspiration. The first year was removed from analysis due to model initial conditions. Downstream boundary condition at Niamey is set as a constant water level slope of 10 cm/km, which was derived from average values of SRTM DEM elevation along downstream reaches.

Extraction of drainage networks and sub-grid floodplain topography was carried out using the void-filled SRTM 250 m Digital Elevation Model from the Consortium for Spatial Information (CGIAR; DEM available at http://srtm.csi.cgiar.org/), and all GIS preprocessing steps were performed with the IPH-HydroTools package (Siqueira et al., 2016). The basin was discretized into 4307 unit-catchments of equal reach length (Figure 4.1c), set here to 10 km based on the method presented in Siqueira et al., (submitted paper). Land use and soil type maps were obtained from ECOCLIMAP (Masson et al., 2003), and their combination led to the definition of 11 Hydrological Response Units (Figure 4.1d).

For parameterization of the vertical hydrology module (soil water budget, evapotranspiration and streamflow generation), the basin was divided into 5 sub-basins (Figure 4.1b), so that one set of parameters was applied to Bani River basin, one for each of the three Red Flood tributaries (Gorouol, Dargol and Sirba), and one for the remaining areas of the basin (including all areas along Niger main stem and Inner Delta, since parameters of the latter are defined for one special HRU, see Figure 4.1). Regarding hydrodynamic module parameters, Manning's n coefficient was globally set as 0.03 for simplification, which is a commonly adopted value in large scale models. Channel width was obtained from a simple manual extraction of LANDSAT 8 imagery for the Niger main stem (800 m wide for the first 750 km; 500 m for the following 250 km, 700 m along 100 km; 600 m along 300 km; and 500 m for the last 800 km; see Figure 4.3a). For the other reaches, the following simple geomorphic relationship was used: $w = 0.95 * A^{0.5}$, where w is width (m) and A is the reach upstream drainage area (km²). This relationship adjusted well to in-situ surveyed cross sections. Bankfull depth was calibrated against observed discharge for the Niger main stem reaches and maintaining coherence with a few surveyed cross sections available from Autorité du Bassin du Niger (ABN) (Figure 4.3b). Bankfull depth was subtracted from channel bankfull elevation (computed as average pixels along river reach along a given unit-catchment) to yield channel bed elevation. The following geomorphic relationship was used for the remaining river reaches: $d = 0.15 * A^{0.25}$, where d is bankfull depth (m). It was consistent with surveyed cross sections. Specific parameterization is justified for the Niger main stem since width and depth values do not follow a simple relationship with drainage area in this river. Figures 3a and 3b present the final values of width and bankfull depth.

For river reaches within Inner Delta, the following parameters were adopted: width of 30 m and 200 m for all reaches within Southern and Northern Inner Delta regions, respectively, and bankfull depth of 0.5 m and 1 m. These values were adopted since the drainage in the region does not follow a dendritic pattern with only one upstream-downstream direction and a defined upstream drainage area (as is given by one direction flow direction maps). Width values were coherent with LANDSAT 8 imagery, while depth ones were adopted for simplicity. For each lateral connection channel, width was assumed with the same values as adjacent Delta river reaches (defined as 200 and 30 m for Southern and Northern areas), and bankfull elevation was assumed with the same elevation as the respective connected unit-catchments. Finally, specific parameters were manually extracted from LANDSAT 8 for main distributaries that exist along the Inner Delta: Diaka river, a distributary at the entrance of Southern Delta that drains a significant part of main stem discharge, and three main distributaries that exist downstream of Lac Débo region, at the beginning of Northern Inner Delta (Issa Ber, Bara Issa and Kolikoli branches) (Olivry, 1993).

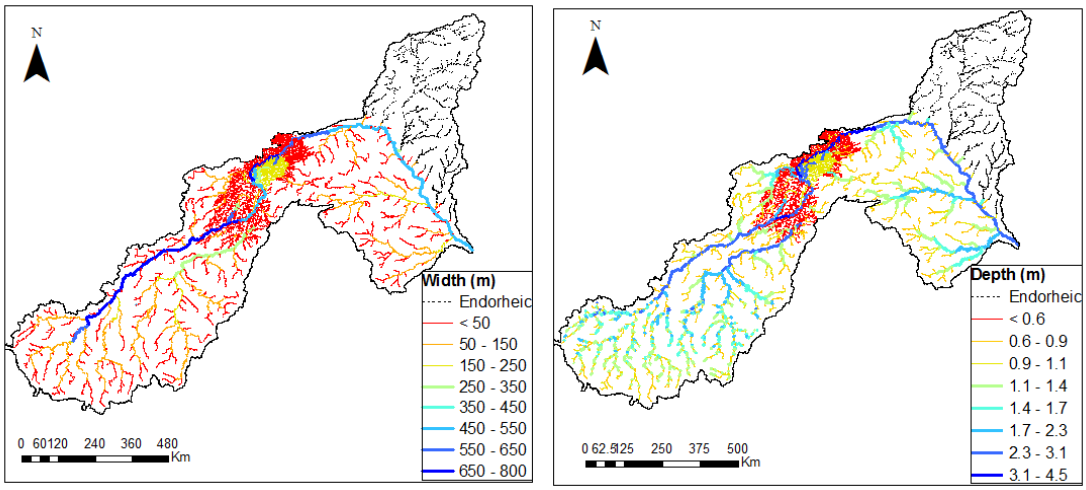

Figure 4.3. (a) Channel width and (b) bankfull depth values used in the model. Width was obtained from LANDSAT 8 manual extraction for Niger main stem (as defined in Figure 4.1, dark blue drainage) and geomorphic relationship for the other river reaches. Depth was calibrated against observed discharge for Niger main stem and defined with geomorphic relationship for the other river reaches.

4.2.5 Model calibration with in-situ observed discharge data

The model was manually calibrated with observed daily discharge provided by the Niger Basin Authority (ABN, http://www.abn.ne/), for the 2000-2014 simulation period (disregarding first year spin-up period for computation of performance metrics). Gauges used for calibration are listed in Table 4.1 (see Figure 4.1a for their location). Calibrated parameters related to hydrological vertical balance are presented in Supplementary Material 4.A1, while Niger main stem calibrated depth is presented in Figure 4.3b.

Table 4.1. In situ discharge gauges in the Upper Niger River basin. See Figure 4.1a for location. Drainage area is related to geoprocessing automatic extraction routine from IPH-HydroTools package, and calculated values include regions that are actually not connected to Niger river (endorheic basins).

ID	Gauge	Latitude (°)	Longitude (°)	Drainage area (km²)
1	Alcongui (Gorouol river)	14.75	0.60	53905
2	Kakassi (Dargol river)	13.85	1.45	7344
3	Garbey (Sirba river)	13.73	1.62	39292
4	Koulikoro	12.86	-7.55	118850
5	Banankoro	11.70	-8.66	71147
6	Kemacina	13.96	-5.35	141524
7	Ansongo	15.53	0.51	519137
8	Niamey	13.50	2.10	657009
9	Faranah	10.03	-10.75	3297
10	Mandiana	10.61	-8.68	22126
11	Diré	16.31	-3.40	358911
12	Douna	13.18	-5.95	99304

4.2.6 Model validation

Model validation was performed using in situ observed water level, satellite altimetry and extent of flooded areas, for the same period of calibration with discharge, as described in the next sections.

In-situ water level data

Daily water levels at Koulikoro, Faranah, Diré, Banankoro and Mandiana (see Table 4.1 and Figure 4.1a for their location) were provided by ABN. Water level anomaly (WLA), computed as the difference between observed level and mean of water level time series ($y - \bar{y}$), was used instead of water surface elevation to avoid discrepancies between datum references.

Altimetry

Daily Water surface elevations (WSE) at seven locations were obtained from the Jason-2, ENVISAT and SARAL/AltiKa satellite altimetry mission. The WSEs are estimated at the virtual stations (VS) defined as places where the satellite ground-track crosses the Niger River, following a manual extraction method presented by Santos da Silva et al. (2010, 2012). The Jason-2 mission provides water level estimates at a 10-day repetition frequency for the [2008-2016] period while the ENVISAT mission provides a 35-day repetition frequency with data between 2002 and 2010. SARAL/AltiKa has the same orbit than ENVISAT and therefore provides data with the same characteristics since 2013. Within the available raw radar echoes retrackers, the ICE-1 retracker has been highlighted to provide the best estimates of the water surface elevation (Frappart et al., 2006). Recent studies have shown that reliable information can be taken from the comparative behavior of water levels gained from satellite altimetry and hydraulic models (Garambois et al., 2016) or hydrological models (Paiva et al. 2013; Paris et al., 2016).

In this study, we focus on seven VSs (Figure 4.1a) located 1- upstream the Inner Delta (VS1), 2- within the Inner Delta (VS4), 3- immediately downstream the Inner Delta (VS2 and VS7) and 4- in the vicinity of Ansongo (VS3, VS5 and VS6). These VSs should provide a variety of locations to assess model performance in terms of water levels estimates. The analysis was performed for water level anomalies.

Flooded area extent

Flooded area estimation was obtained from Bergé-Nguyen & Crétaux (2015) study, based on MODIS imagery classification. The product uses 8-day MODIS data for the period 2000-2013 to yield a 500 m spatial resolution estimation of flooded areas along the Niger Inner Delta, and threshold values for classification of pixels are based on Normalized Difference Vegetation Index (NDVI) and MODIS band 5 (1230-1250 nm) values. This part of the spectra of the Modis Band 5 has the capacity to detect very shallow water and water with high concentration of sediments as it is often rhe case in floodplain in arid regions (Bergé-Nguyen & Crétaux 2015). A total of five classes are provided for the region: open water, mix water/dry land, aquatic vegetation, vegetation and dry land.

4.2.7 Model performance statistics

Model performance was evaluated with the following metrics for daily discharges: Nash-Sutcliffe (NSE), Nash-Sutcliffe of variable logarithm (NSE-log, which enhances

errors in low flows), delay index (DI, time delay that leads to best Pearson correlation between modeled and observed series, Paiva et al., 2013), volume error (DV, long term model bias), and visual inspection. Water level was evaluated with NSE and DI, and flooded areas were evaluated with NSE and Pearson correlation metrics.

4.3 Results

4.3.1 Calibration with discharge observations

MGB-IPH was calibrated with in-situ observed discharge, and calibrated hydrographs are presented in Figure 4.4. Table 4.2 shows performance metrics (NSE, NSElog, DI and DV). Generally, model was considered to have a good performance both upstream and downstream the Inner Delta region, with NSE>0.6 for most gauges.

Gauges upstream of the Inner Delta (Faranah, Mandiana, Banankoro and Koulikoro) presented NSE values between 0.64 and 0.74, while baseflow (reflected by NSElog) were also well simulated. These upstream areas are tropical and present a typical rainfall-runoff mechanism. Relevant discrepancies occurred between simulated years, probably due to error in model forcing data (long-term climatology and daily precipitation). TRMM 3B42 precipitation estimates are known to present some inconsistencies during some years. For instance, 2008 rainfall rates were abnormally high, as reflected in all simulated hydrographs.

In addition, as shown by Diré gauge station (NSE =0.81, NSElog= 0.72), the model also performed well along and downstream of Niger Inner Delta, where floodplain effects and hydrological processes within arid regions play an important role. A Delay Index (DI) of 8 days is also satisfactory, given the months of delay that the flood wave is subjected to along the Delta. However, in almost all years an overestimation of recession limb can be observed, which might be due to important DEM errors in this region. Indeed, large scale NW-SE oriented stripes in the SRTM DEM in the Delta were observed by previous studies (e.g., Neal et al.,2012), which affects floodplain wet and dry processes, especially in such a large, flat area. This volume surplus is also observed in downstream gauges (e.g., Ansongo and Niamey), and one additional explanation may be related to channel and floodplain transmission losses. These may be important in such dryland rivers, and are not considered within the model, since infiltration from flooded areas are always assumed to return to soil column. Finally, it is interesting to note that years with poorest model performance downstream the Delta were also the poorest simulated in Koulikoro gauge station, upstream the Delta and the Niger confluence with Bani river: the low model performance in Bani basin (Douna station) due to reservoir flow regulation did not seem to largely affect the calculated hydrograph at Diré.

The hydrograph shape downstream the Inner Delta is dominated by floodplain attenuation, as shown by its negative skewness (slower receding than rising limb), which is a typically feature of floodplain regulated rivers (Fleischmann et al., 2016). A good hydrograph skewness and timing representation indicates that floodplain storage effects were well simulated, at least along the river main stem. It can be noticed that negative skewness increases downstream of the Delta, since between Diré and Ansongo gauges there are also relevant floodplains that alter flood wave overall shape (floodplain ~4 km long with Quaternary alluvial deposits; Andersen et al., 2005). In this reach, significant water loss occurs due to open water evaporation, as is common in semi-arid rivers with small contribution and high evaporation rates.

In the Niger right bank, downstream of Ansongo, the Red Flood tributaries (Alcongui, Kakassi and Garbey stations) presented low NSE and NSE log performance in comparison to other gauges, possibly due to an incoherence in the model streamflow generation conceptualization: the Arno model variable infiltration capacity model (Todini, 1996) is designed for saturation excess flow, while in these dryland basins, infiltration excess drives runoff generation (Esteves et al., 2003; Mamadou et al., 2015). Addittionally, lower performance of NSElog in Alcongui and Kakassi in comparison to NSE may also be a response to the soil bucket model (only one soil layer) used by MGB-IPH to simulate rainfall-runoff transformation, where first rainfall events in the flood period meet a very dry soil, which takes a long time to fill before generating runoff. Also, results not presented here indicate that the model was extremely sensible to vertical hydrology parameters (Supplementary Material 4.A1) in these areas, e.g., a small change in soil maximum storage (*Wm*) parameter led to much more dispersion than in more tropical regions of the basin.

Lowest NSE performance was obtained for Bani river (Douna station, NSE =0.34) due to flow regulation by Talo dam near Douna location, which started activities in 2005, as shown by atypical volume releases during hydrograph recession in comparison to hydrographs before 2005. NSE for 2000-2004 period is improved up to 0.59.

Finally, we stress that this model application was performed using reasonable and simply defined parameters for the whole Upper Niger basin, in order to avoid model overparameterization. An automatic calibration procedure could definitely improve model performance, but it was not the aim of this paper. Lastly, anthropic influences not considered in the model that may add uncertainty to simulation results are reservoir operation (e.g., Selingué dam in the upper basin) and water abstraction in the Office du Niger area, a large irrigation area upstream the Inner Delta.

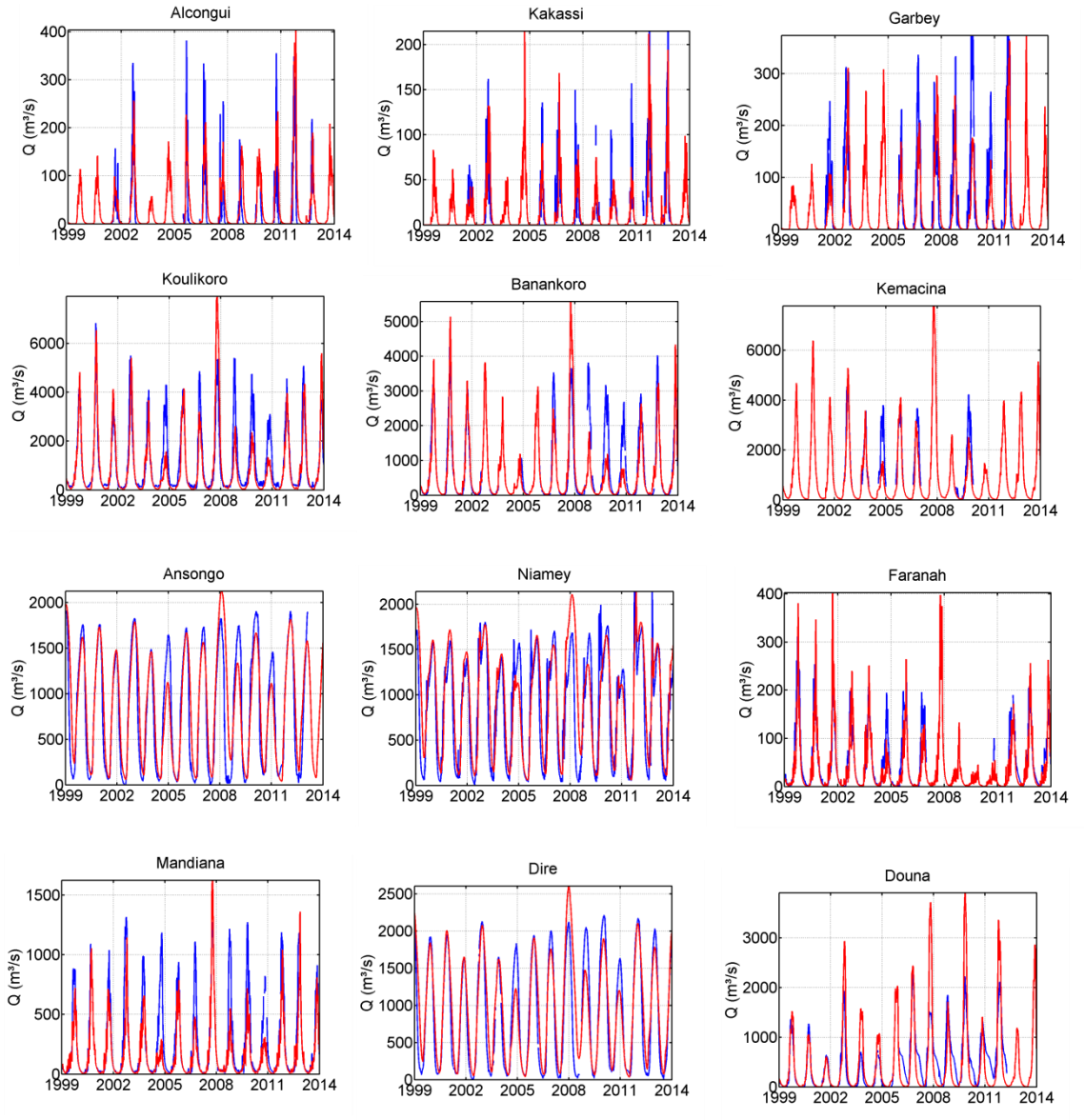

Figure 4.4. Observed (blue) and simulated (red) discharge at Faranah, Kakassi, Mandiana, Garbey, Banankoro, Alcongui, Koulikoro, Douna, Kemacina, Nantaka, Diré, Ansongo and Niamey, described in Table 4.1.

Table 4.2. Performance metrics for simulated discharges. See Figure 4.1a and Table 4.1 for location and description of the gauges. NSE: Nash-Sutcliffe efficiency; NSElog: Nash-Sutcliffe efficiency of logarithm of discharges; DI: Delay Index; DV: Volume error (Bias). Spin-up year (1999) was removed from statistics computation due to initial conditions.

ID	Gauge	NSE	NSElog	DI	DV
1	Alcongui (Gorouol river)	0.51	0.17	11	28
2	Kakassi (Dargol river)	0.68	0.27	2	-11
3	Garbey (Sirba river)	0.51	0.60	14	-26
4	Koulikoro	0.72	0.55	4	-15
5	Banankoro	0.75	0.84	3	-12
6	Kemacina	0.60	0.80	0	-24
7	Ansongo	0.79	0.35	11	8
8	Niamey	0.72	0.68	12	11
9	Faranah	0.69	0.78	-2	-13
10	Mandiana	0.65	0.79	6	-33
11	Diré	0.82	0.73	8	9
12	Douna	0.34	0.27	1	-3

4.3.2 Validation with in-situ water level and satellite altimetry

Simulated and in-situ measured WLA time series are presented Fig. 5 and performance metrics in Table 4.3. Again, the model presented an overall good performance both upstream and downstream the Inner Delta. At Diré gauge, model results were not very satisfactory, with NSE=0.5 and DI=16 days, and the absolute variation of WSE was overestimated. At Faranah, however, NSE was satisfactory while WSE variation was underestimated. Such behavior can be due to:

- The rough values of bankfull width and depth that were used for model simplification. Improving the representation of river cross sections could enhance model results;
- The Manning's coefficient. Simulated water level is sensitive to Manning's *n* coefficient (Paiva et al., 2013; Paris et al., 2016), and in the model a fixed value of 0.03 was applied to the whole basin for simplification of parameters.

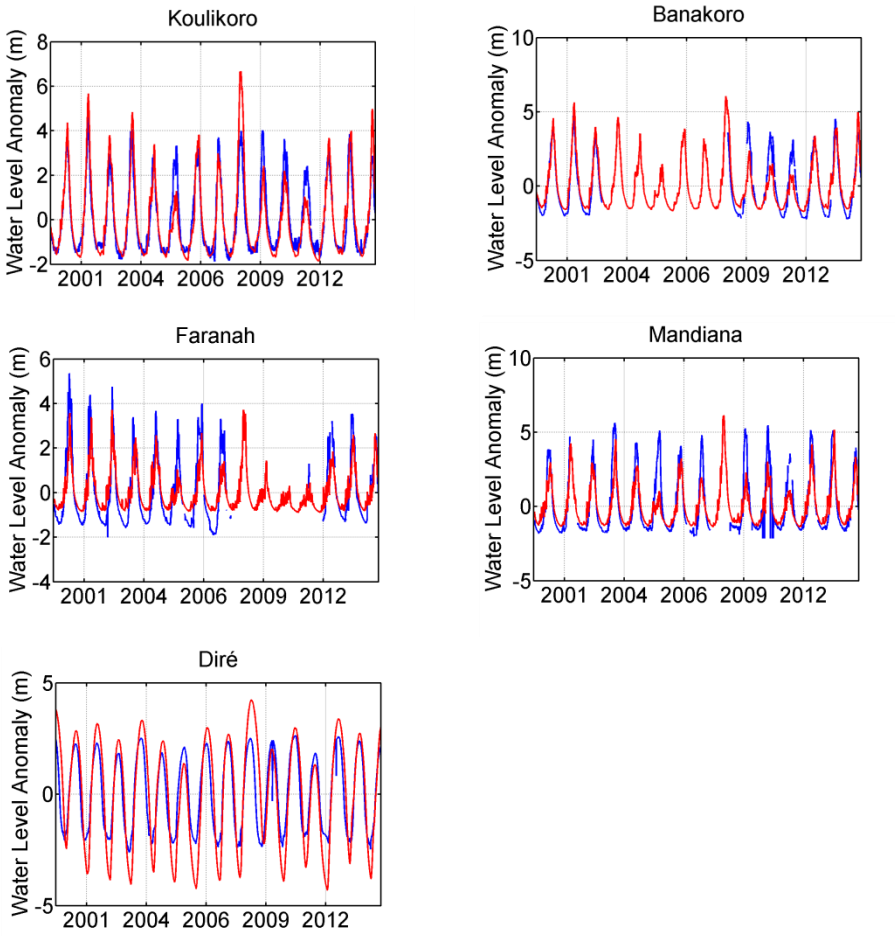

Figure 4.5. In-situ and simulated water level anomaly at Koulikoro, Faranah, Diré, Banankoro and Mandiana. Anomalies were computed as the difference between daily values and long term average. NSE: Nash-Sutcliffe efficiency; DI: Delay Index.

Table 4.3. Performance metrics for simulated and in-situ observed water levels. See Figure 4.1a and Table 4.1 for location and description of the gauges. NSE: Nash-Sutcliffe efficiency; DI: Delay Index. Spin-up year (1999) was removed from statistics computation due to initial conditions.

ID	Gauge	NSE	DI
4	Koulikoro	0.80	4
5	Banankoro	0.83	0
9	Faranah	0.72	-2
10	Mandiana	0.73	5
11	Diré	0.52	16

Time series of water level anomalies from the MGB-IPH model coincident to virtual station VS1-7 (Figure 4.1a) are presented in Fig. 4.6, and performance metrics in Table 4.4.

First, Fig. 6 shows that MGB-IPH model WLAs were in agreement with satellite altimetry ones. For all VSs, the shape is preserved and the peak time is mostly respected. At most of VSs, absolute variation (i.e. the difference between maximum and minimum anomaly) was similar for both model and satellite estimates. At VS2 (Fig. 6b), the model tended to overestimate the water level variation, principally in high waters. At VS4 and VS5 the amplitude was respected but the lower value (e.g. the anomaly at low waters) was underestimated. The specific case of the 2008/2009 hydrologic year should be highlighted. For this period, the model presented a high WLA that was not observed in the WLA time series from satellite altimetry. This point was neither observed on in-situ discharge time series nor on in-situ WLA time series and seems to evidence a possible issue in the precipitation rate for this year.

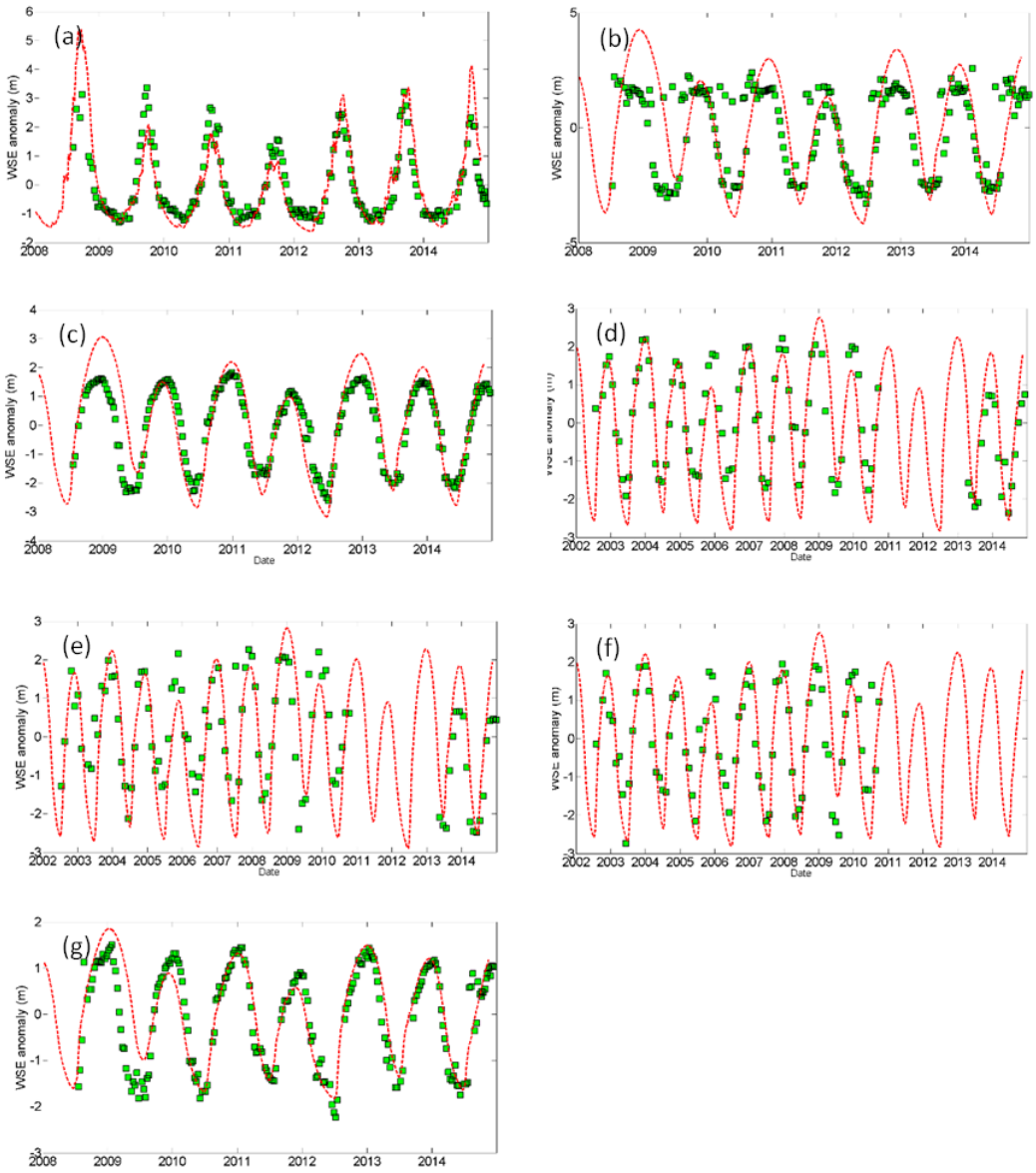

Figure 4.6. Comparison between model and satellite-derived water levels anomaly at VS1 (a), VS2 (b), VS3 (c), VS4 (d), VS5 (e), VS6 (f) and VS7 (g). Modeled WSA are in red dashed line; Satellite altimetry observations are in green squares.

Table 4.4. Performance metrics for simulated water levels and satellite altimetry. See Figure 4.1a for location of virtual gauges. NSE: Nash-Sutcliffe efficiency; RMSE: root mean square error. Spin-up year (1999) was removed from statistics computation due to initial conditions.

Virtual Station	NSE	RMSE (m)
VS1	0.68	0.71
VS2	-0.80	1.77
VS3	0.63	0.83
VS4	0.37	1.08
VS5	0.55	0.90
VS6	0.63	0.81
VS7	0.75	0.52

The performance indicators (Table 4.4) corroborate these conclusions. NSE efficiency coefficient is usually above 0.5, and below it only for VS2 and VS4. For VS2, outliers at high stages are expected to impact negatively NSE, while for VS4, there seems to be a bias between estimated and observed by satellite altimetry WSA. RMSE values present similar behavior, with values below 0.9 m for VS1, VS3, VS5, VS6 and VS7.

Some discrepancies could have been discarded by filtering altimetry WSE time series. There are indeed some outliers that may have been removed. However, we choose to keep the rough time series without any post-processing based on model-estimated time series shape. Also, as the means were calculated over distinct periods (the nominal period for each kind of data, e.g. 1999-2014 for the model, 2008-2014 for Jason-2 and 2002-2010 and 2013-2014 for ENVISAT and Saral/AltiKa), and as the time sampling is not the same neither, it is expected that anomalies do not completely agree in terms of absolute value. Despite these difficulties, the model performed very well regarding to estimating WLA.

The comparison of model and satellite-derived WLAs underlines the fact that modeling discharges and heights with information taken principally from raw DEM are uncertain. As a matter of fact, the shape and amplitude of the WSE time series is highly sensitive to the shape and characteristics of the cross-section, through parameters such as width, bankfull depth and Manning's roughness coefficient (e.g., Paiva et al., 2013). Hence, WSEs gained from satellite altimetry (and, in our case, from three different altimeters: Poseidon-3 on Jason-2, RA-2 on Envisat and Ka-band AltiKa on Saral) offers an independent source of information that could be used to constraint the geometrical representation of the river reaches along the basin.

4.3.3 Validation of flooded areas in Niger Inner Delta

Simulated and observed time series of flooded areas are presented in Figure 4.7a, while monthly climatology of these areas is shown in Figure 4.7b. Figure 4.7c shows calculated flooded areas separately for Northern and Southern Delta regions. In general,

there was a good agreement between simulated and observed flooded areas (MODIS classified product from Bergé-Nguyen & Crétaux, 2015), with NSE=0.60 and r=0.85. Maximum simulated flooded area was ~11,000 km² (excluding anomalous 2008/2009 year) for the whole Delta region, while maximum observed was ~12,000 km². Peaks were slightly higher for most years in remotely sensed observations, and a pronounced overestimation of flooded area recession occurred (as shown by monthly climatology). Southern and Northern Delta regions showed different flooding dynamics. While the former had the largest flooded area (>8,000 km²) and typically peaks at late October, the latter had peak flooded areas (~3,000 km²) occurring in late December.

Estimates based on a hydrological balance method (Mahé et al., 2009) suggested a total flooded area for the whole Delta of 24,000 km², while a MODIS-based estimation Ogilvie et al. (2015) indicated flooded areas in the area to range between >3,000 km² and 20,000 km² which are considerably higher than our values. However, one must notice that the definition of the area of interest in each of these studies is also different, so that a direct comparison of values is not possible.

Assuming that water level within a single unit-catchment is uniform (Paiva et al. 2011; Yamazaki et al. 2011, 2013), flood extent (or water depth) maps are created by subtracting the unit-catchment simulated water level from the HAND model computed using a high resolution DEM (SRTM 250 m), and reclassifying all negative depths to null values (Siqueira et al., Submitted paper). Figure 4.8 shows maps of flood water depth for 1st Jun 2001 (low flow), 1st Sep 2001 (mid-rising), 20th Oct 2001 (flooded areas peak), 1st Jan 2002 (mid-falling limb) and the maximum flood for Southern and Northern Delta regions. It can be seen how both areas differ in terms of flooding processes: while the Southern Delta presents a more diffuse flooding pattern, the Northern Delta has flooding mainly along floodplain channels that meander through Erg of Nianfunké dunes, a set of stationary sand dunes running from west to east (Davies et al., 1996). The seasonal flooding cycle is also evident (Figure 4.7b), with low stage in June (basically channel surfaces yielding flooded areas), and peak floods in late October (late December) for Southern (Northern) Delta. By early January, most Southern delta flooding areas have already been drained. Also, flooding in Northern Delta lasts longer than in south (Figure 4.7c), presenting a higher residence time, as noted by remote sensing studies (Ogilvie et al., 2015; Bergé-Nguyen and Crétaux, 2015). This model result was only achievable by representation of flood hydrodynamic along floodplain channels in the Delta. Finally, several lakes (especially Lac Débo; see bottom-left part of Northern Delta flood maps in Figure 4.8) in the Southern-Northern Delta border were kept flooded during several months, although they have dried out during low-stage period, what is in contrast with remote sensing observations, which indicated that several permanent lakes exist in this area (Bergé-Nguyen and Crétaux, 2015).

There was some model uncertainty related to low stage flooded areas. MGB-IPH does not represent estimated permanent flooded areas (low stage flood estimated as ~3,000 km² by Ogilvie et al., 2015), since neither lakes nor eventual ponds are included in the model. For instance, isolated flooded areas cannot occur within the model, since

the same elevation is considered between channel and floodplain, and all drainage network is somehow connected.

Model errors in estimation of flooded areas may be explained by several factors. Firstly, there is a high sensitivity to DEM inaccuracies and estimation of channel cross section parameters in such large scale hydrodynamic models (e.g., Paiva et al., 2013). It is known that SRTM presents SE-NE stripes in the Inner Delta (Neal et al., 2012), which are evident in the Southern Delta flood maps of Figure 4.8. Also, SRTM 90 m presents elevation errors in Africa in the order of 5 m (Rodriguez et al., 2006), although DEM upscaling as used in this study (SRTM 250 m) decreases DEM errors. As presented in the MGB-IPH sensitivity analysis (section 4.3.4), model results are highly dependent on adopted channel hydraulic geometry (width and bankfull depth values), and our simple approach of parameter estimation, with the same width and depth for the whole Northern and Southern Delta regions, may have led to erroneous model outputs. Improving channel bathymetry of floodplain and main stem channels is an important way forward for large scale hydrodynamic models (e.g., by assimilating future SWOT, Biancamaria et al., 2016). In very flat areas such as the Niger Inner Delta, a variation of one to few meters in Niger main stem may largely change simulation results by altering river-floodplain exchange flows and then hydrograph shape. Finally, there is some uncertainty related to simulated evaporation and infiltration, and respective model parameterization, what is addressed in the sensitivity analysis presented in section 4.3.4.

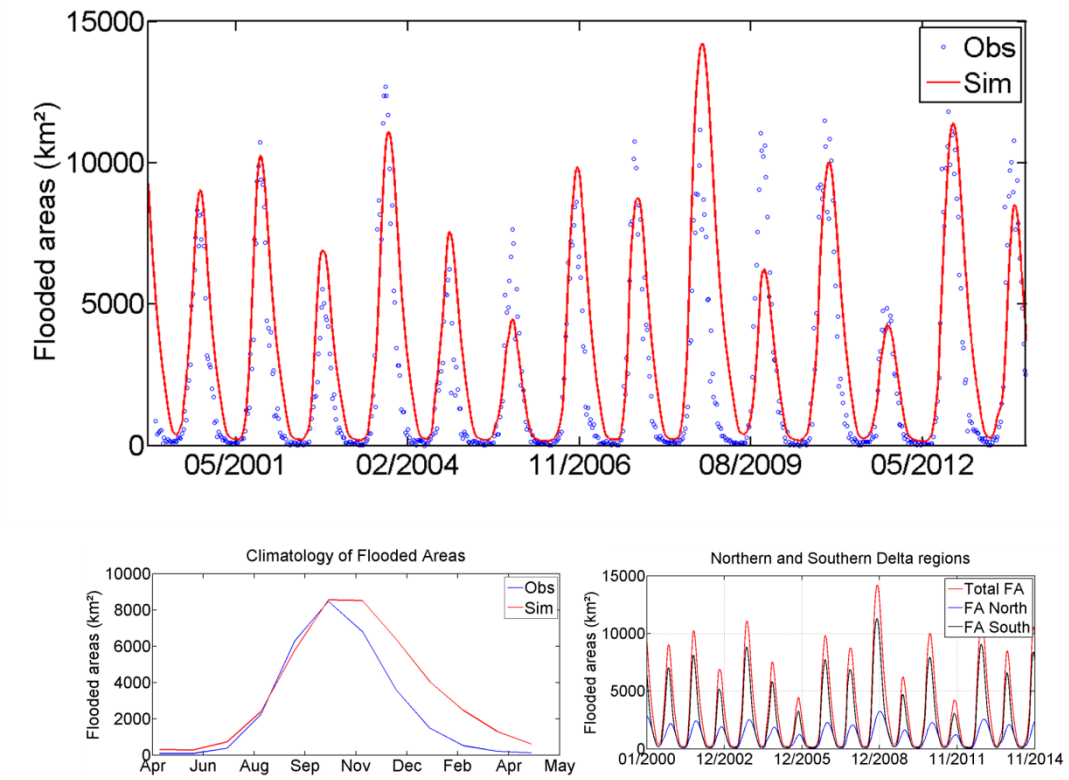

Figure 4.7. (a) Comparison between (open water + aquatic vegetation class) from Bergé-Nguyen & Crétaux (2015) study and simulated flooded areas. (b) Monthly climatology of flooded areas in the whole Delta and (c) time series of flooded areas in Northern (blue) and Southern (black) Delta regions. Total flooded area (Northern + Southern) is also plotted (red).

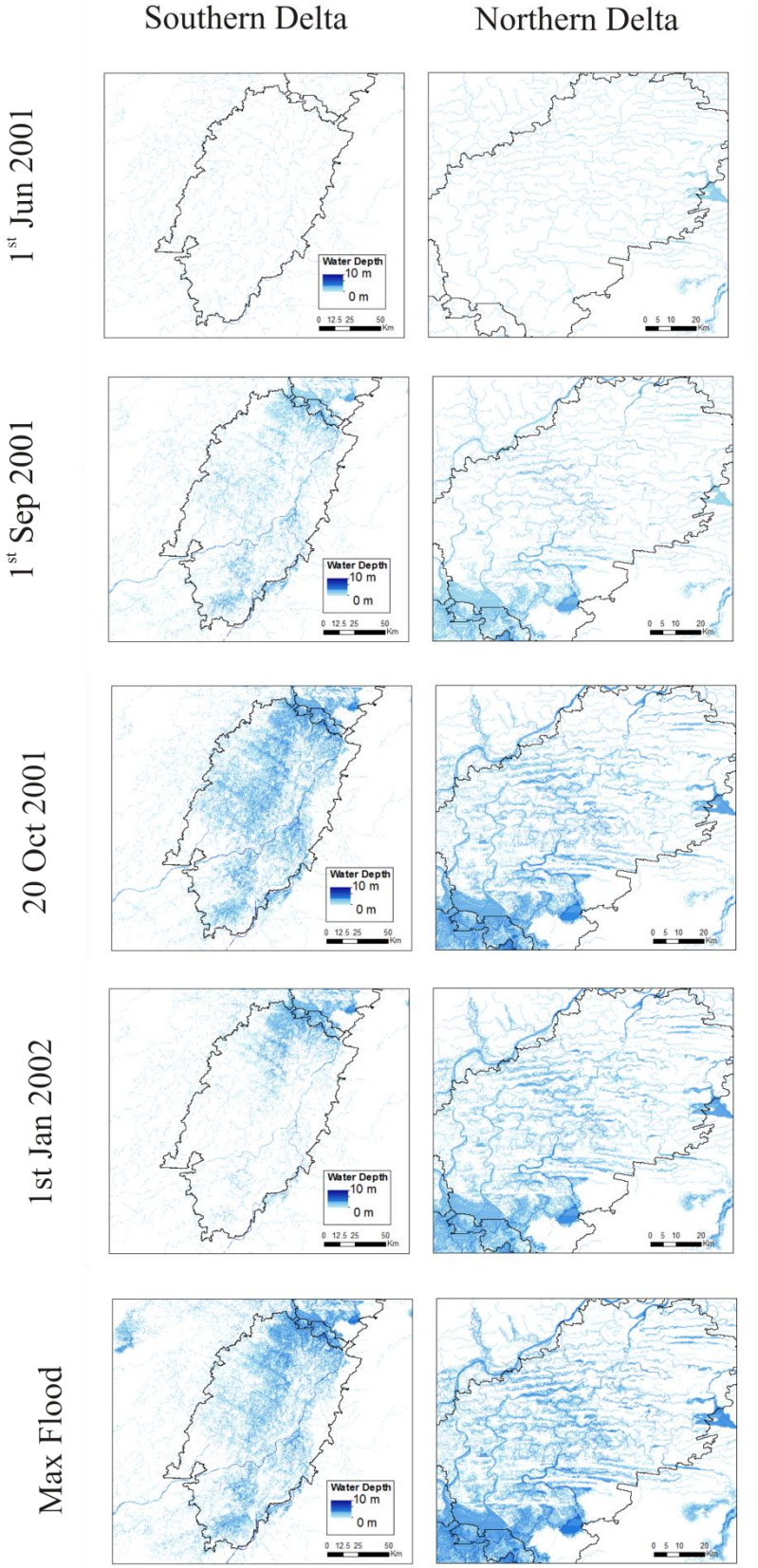

Figure 4.8. Simulated flooded area extent for 1st Jun 2001 (low flow), 1st Sep 2001 (mid-rising), 20th Oct 2001 (flooded areas peak), 1st Jan 2002 (mid-falling limb) and maximum flooding. Maps are provided for Southern (left column) and Northern Delta regions (right column).

4.3.4 Sensitivity Analysis of Upper Niger River Basin model

A sensitivity analysis was performed to investigate the impact of parameter estimation on the model results, as well as to explore the basin hydrological functioning (Figure 4.9). Sensitivity analysis of MGB-IPH hydrological vertical balance was performed by Collischonn et al. (2001) and Paiva et al. (2013), while sensitivity of the hydrodynamic routing model was evaluated by Paiva et al. (2013) for an Amazon basin MGB-IPH application and by Yamazaki et al. (2011) for a global application of CaMa-Flood model. In this study we focus on the model sensitivity in the Niger Inner Delta region, given its complex hydrodynamics and the new formulation implemented for floodplain simulation in arid wetlands, including infiltration from floodplains and lateral connections between neighbor unit-catchments. Evaluated parameters are KINF (Infiltration from floodplain into soil column; KINF=0, 10, 20, 30 and 40 mm/day), lateral connection width for Northern and Southern Delta regions (±50%, ±100%, +500% variation), and channel width and depth (±20, ±50% variation). Sensitivity results are evaluated for climatology of evapotranspiration (ET), discharge (Q) and flooded areas (FA). Default simulation values, as presented in section 4.2.4, are Infiltration (*KINF*) = 20 mm/day, Northern Delta Connection Width (*NDeltaWidth*) = 200 m; Southern Delta Connection Width (*SDeltaWidth*) = 30 m. Channel width and depth values are presented in Figure 4.3.

Model discharge and flooded areas were more sensitive to channel width, followed by channel bankfull depth values, which drive similarly calculated ET, Q and FA. Smaller values of these parameters lead to more water stored on floodplains and thus more attenuation in the hydrograph, more water evaporated in the Niger Inner Delta and larger flooded. Similar results were presented by Paiva et al. (2013) in a MGB-IPH model application for Amazon Basin, where a 50% decrease in channels width reduced peak discharge in Manacapuru (Amazon main stem) by 20%. In Niger, a 50% decrease led to a 25% reduction in peak discharge in Diré due to increased floodplain attenuation.

Infiltration parameter KINF largely influenced evapotranspiration. Water transferred from floodplain into unsaturated soil became available for soil evapotranspiration, systematically increasing ET rates. In contrast, considering no infiltration into unsaturated soil (KINF=0) led to a distinct behavior in Q than did changes in channel width and depth. Evaporation of soil infiltrated water occurred after the rainfall period, since during it soil saturation was relatively high, and thus neglecting infiltration processes led to an overestimation of hydrograph recession (from peak discharge to low water stage period). Also, there was an upper limit for model sensitivity on this parameter, since at very high infiltration rates soil became saturated and thus no more infiltration occurred.

A change on the widths of lateral connections led to different behaviors of Q and FA between Northern and Southern Delta regions. High uncertainty is related to this

parameter given its conceptual nature, and thus a wide range of parameter variation was performed (from -100% to +500%). Generally, the model presented higher sensitivity in Southern Delta than in the Northern one. While a comparison between scenarios -100% (no lateral connection) and +500% in the Southern area showed a peak discharge alteration of ~500m³/s, in the Northern one a change of less than 200³/s was observed. In the Southern part, smaller connections led to smaller flooded areas across the region and higher flooding along the Niger mainstem. Without connections, Diaka River distributary could not be represented, since in the single downstream connectivity defined by a 1D upstream-downstream flow direction (i.e., simulations without bifurcations) such distributaries are not defined. In this scenario, flooding was restricted to Niger main stem, leading to reduced total flooded areas across the whole Delta and attenuated hydrograph in Diré. In turn, sensitivity to Northern Delta parameters was much smaller and showed a considerably different pattern. Along this area, flows are channelized between dunes. In the original flow direction map with single downstream connectivity, many Northern Delta channels are connected to Lac Débo region, and thus the simulations without lateral connection led to water storage in these channels through backwater from Niger main stem and an overall large flooded area at this region (see discussion in next paragraph). By implementing lateral connections, water was allowed to propagate from the Lac Débo region towards Diré gauge throughout the Northern Delta channels. It then decreased flooding across the region, by draining its water downstream.

Figure 4.10 shows flooding maps for five different simulation scenarios: (a) No lateral connections across the whole basin; (b) no lateral connection in Southern Delta; (c) no lateral connection in Northern Delta; (d) lateral connection only for Diaka river distributary; and (e) default simulation. The results contribute to the sensitivity analysis by showing spatial patterns of flooding across the Delta. Simulation without lateral connections (scenario a) increased flooding along the Niger main stem and in Lower Bani River, possibly due to main stem backwater. Lateral connection also ensured important bifurcation that exists in the Southern Delta entrance (Diaka river), although its only representation (scenario d) was not enough to flood the whole Southern Delta area. In the Northern Delta, smaller sensitivity was observed to lateral connections, although their implementation (default simulation) was able to flood the eastern part of the region, as shown by detail maps in Figure 4.10f. A comparison between ET, Q and FA is also presented for the same five scenarios. These results clearly show how important are the establishment of lateral connections along the Niger Inner Delta to ensure connectivity along the floodplains and bifurcations, and are in accordance with conclusions by Yamazaki et al. (2014), Mateo et al. (2016) and Pontes et al. (2017) for large scale modeling with bifurcation schemes for floodplains in Mekong, Chao Phraya and Araguaia river basins, respectively. If only a dendritic drainage network was represented within the model, with only one pre-defined upstream-downstream direction (as presented in many previous large scale hydrological models of Niger river basin), Niger main stem flood attenuation and delay would not be satisfactorily simulated.

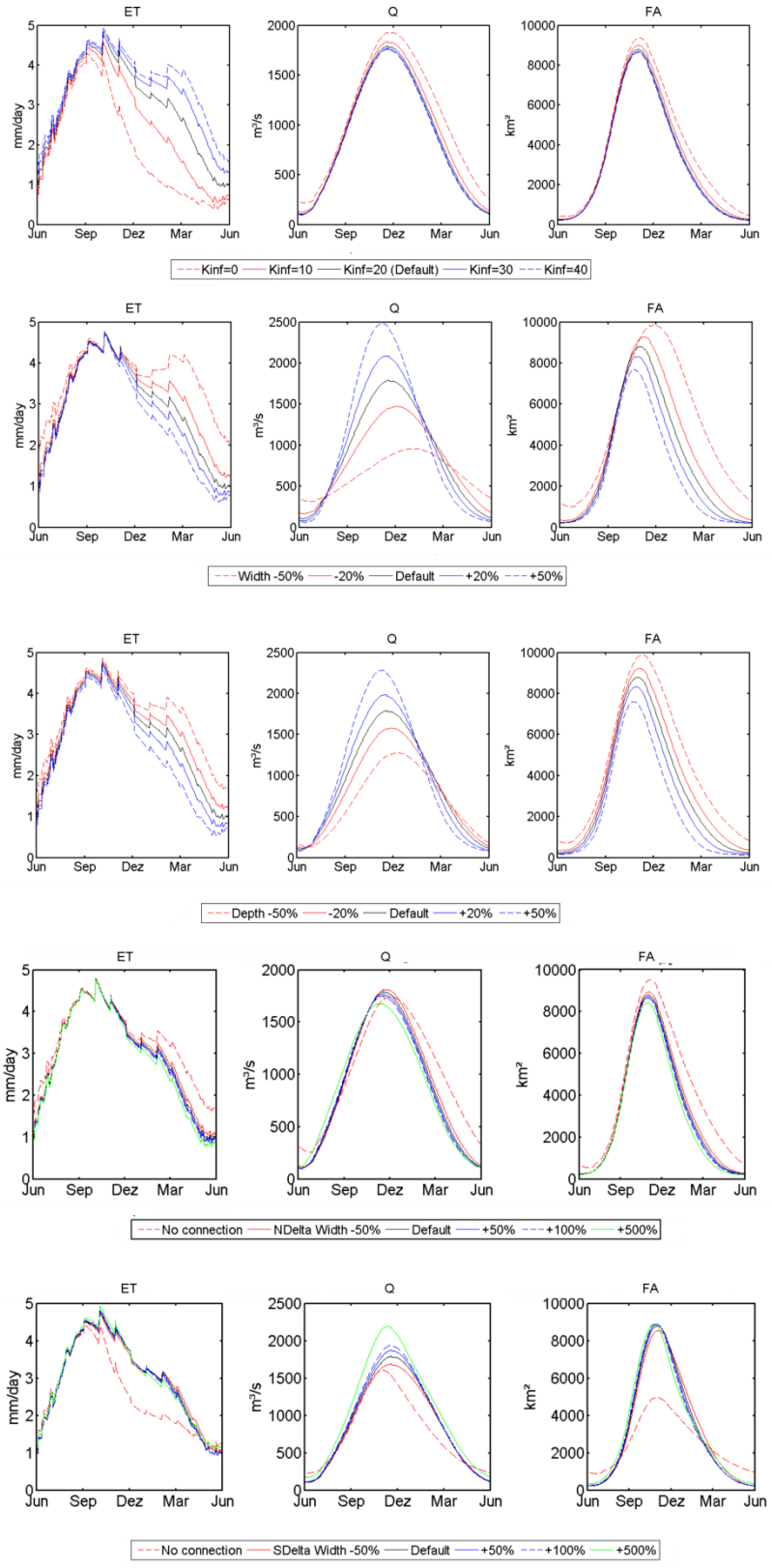

Figure 4.9. Sensitivity analysis for parameters KINF (0, 10, 20, 30, 40 mm/day), channel width and depth (±20, ±50%) and lateral connection width for South and Northern Deltas (±50%, ±100%, +500%). Model results are presented for climatology of daily real evapotranspiration in Niger Inner Delta (ET), daily discharge at Diré gauge location (Q) and daily flooded areas (FA).

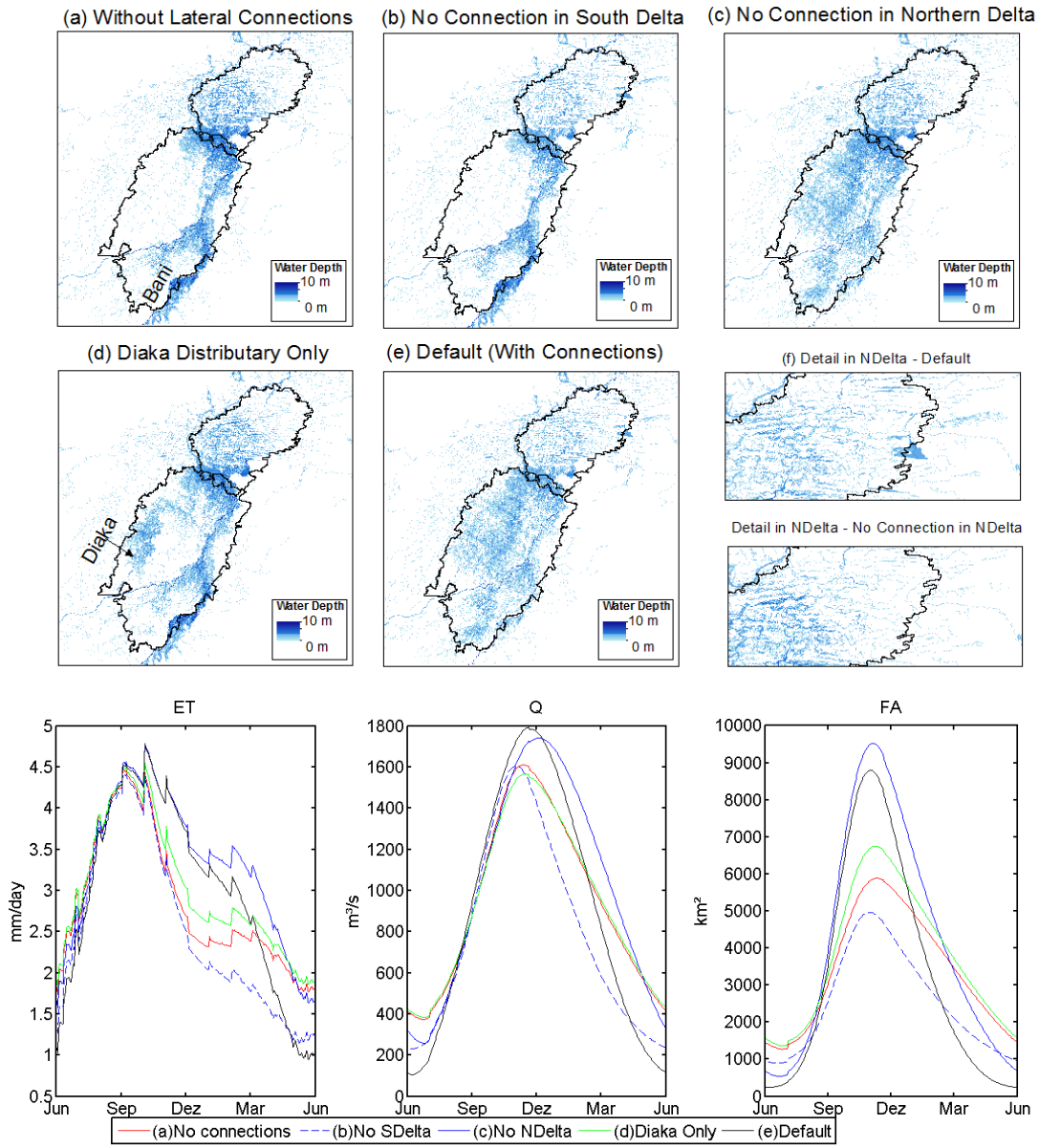

Figure 4.10. Sensitivity analysis results of five simulation scenarios in terms of flood extent, evapotranspiration (ET), discharge at Diré (Q) and total Delta flooded areas (FA): (a) No lateral connections across the whole basin; (b) no lateral connection in Southern Delta; (c) no lateral connection in Northern Delta; (d) lateral connection only for Diaka river distributary; and (e) default simulation. Detail of flooding in Northern Delta is presented in (f). Bani and Diaka rivers are also shown in the figures (a) and (d), respectively.

4.4 Discussion: flood dynamics and hydrological processes in the Niger Inner Delta

Which hydrological processes should we represent in large scale models of Upper Niger River Basin? Which model structure should we employ to improve simulations along the basin, and thus our capability of prediction?

Previous sections indicated that MGB-IPH model results in the Niger Inner Delta satisfactorily represented discharge, water level and dynamics of flooded areas, given uncertainties in model input data and parameterization (e.g., SRTM DEM vertical accuracy and simple adopted cross section geometry). Processes of floodplain infiltration into unsaturated soil column, together with explicit simulation of the floodplain channels and diffuse flow across the Northern and Southern Delta regions seemed to be important for the adequate representation of flooding dynamics. In this section, we evaluate the impact of model structure and process representativeness on the Niger Inner Delta hydrology, by exploring the role of vertical hydrology (infiltration, rainfall), hydrodynamics (lateral connections, distributaries, flow bifurcation, backwater flow) and the coupling between them (infiltration, open water evaporation) on the Delta hydrological response.

Figure 4.11 presents model results of monthly and annual evapotranspiration, with and without infiltration from floodplains into unsaturated soil, together with TRMM precipitation data. ET was always larger than P along the Delta due to open water evaporation that came from upstream catchments, but the inclusion of floodplain infiltration largely increased it. Annual P varied between 250 mm/yr and 600 mm/yr, while ET without infiltration ranged from 420 mm/yr to 720 mm/yr, and ET with infiltration from 760 mm/yr to 1130 mm/yr. Calculated evapotranspiration is coherent with Mahé et al. (2009) who estimated evapotranspiration averaging 800 mm/yr in the Delta, and varying between 400 mm/yr in 1984/1985 and 1300 mm/yr in 1924/1925, and our results agree with previous studies which state that Niger Inner Delta is involved in important land-atmosphere feedback processes (Dadson et al., 2010; Taylor, 2010). In the region, wet season precedes Niger flood arrival and is important in driving soil saturation. Thus, alterations in precipitation regime may affect antecedent soil moisture and then flood extent in the region.

In this study, CRU long-term monthly mean climate data were used for computation of Penman-Monteith equation, which led to some plateaus in daily ET (see Figure 4.9 with sensitivity analysis) due to constant adopted climate variables during whole months. It may certainly contribute to model uncertainty. For instance, Ogilvie et al. (2015) showed that CRU potential evapotranspiration values are slightly lower than observed ones along the Delta.

Table 4.5 presents water losses in Southern and Northern Delta regions in terms of total ET, soil ET and flooded areas open water evaporation. Total ET had an annual maximum of 31.6 km^3/yr and a monthly maximum of 10 km^3/month. Northern and

Southern regions had a similar seasonal cycle. Monthly ET-Flood peaked in November for both, while ET-Soil showed two peaks: the first occurring in October due to local rainfall and the second one in January due to soil infiltration from floodplains. Losses through ET-soil were higher than ET-flood: maximum ET-soil calculated values were 0.9 and 1.9 km³/yr for Northern and Southern regions, respectively, and ET-flood values were 0.5 and 1.8 km³/yr. Also, Northern region had always lower evapotranspiration losses than Southern, although observed data indicate that the opposite situation tends to occur (Mahé et al., 2009). This may be explained by the CRU long-term monthly mean climate data used here. Finally, calculated values were in the same order as estimated by Ogilvie et al. (2015) (annual evaporation losses between 12 km³ and 21 km³) and Mahé et al. (2009) (annual losses between 11.4 and 29.5 km³/yr).

Soil infiltration from flooded areas seems to be an important process to be modeled, as highlighted by a water balance for the Inner Delta computed by Ogilvie et al. (2015). Furthermore, Mahé et al. (2009) argued that infiltration may be important in Northern Delta (or at least higher than in South region), where there are sandy soils and sandhills. The importance of infiltration to unsaturated soil was also found in the Okavango Delta (Botswana), where it is generally accepted that large volumes infiltrate into very permeable soils during flooding arrival and lead to groundwater level increase (Milzow et al., 2009).

In our model, we considered for simplicity the same KINF value for the whole Delta, but further refinement could be carried out. Without soil infiltration, total ET was much smaller during January-March period, as shown by KINF sensitivity analysis in Figure 4.9. In this case, flooding water was drained away from Inner Delta without staying long enough to evaporate.

It is also possible that the representation of floodplain infiltration compensated the non-inclusion of water storage in local depressions and ponds along the Delta, which are considered to be relevant in the evaporation process along the region (Mahé et al., 2009). An additional relevant process is related do deep infiltration to groundwater (Pedinotti et al., 2012), although groundwater recharge is believed to be insignificant along the Delta (Dadson et al., 2010; Neal et al., 2012).

Local rainfall in the Delta has little impact on Niger main stem discharge, but is important for evapotranspiration estimation, and thus for land-atmosphere modeling. MGB-IPH simulations considering zero rainfall in the Delta (not presented here) led to very small changes in Diré calculated hydrograph and Delta flooded areas, but decreased annual total ET in the Delta from 912 ± 114 mm/yr (mean ± SD) to 612 ± 114 mm/yr.

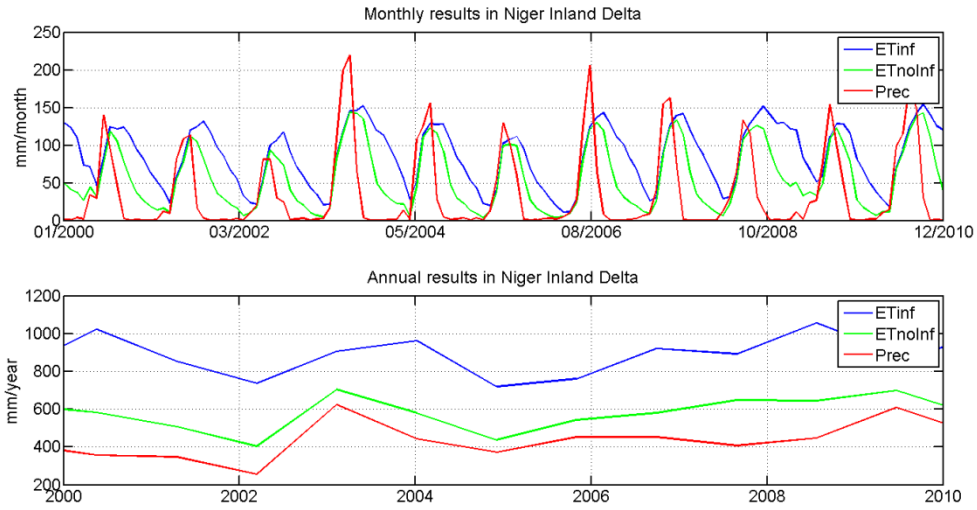

Figure 4.11. Monthly (upper panel) and annual (bottom panel) values of observed precipitation and calculated total evapotranspiration (with and without infiltration from floodplains) for Niger Inner Delta region. Values are considered based on the whole Delta area. See Table 4.5 for specific values for Northern and Southern areas.

Table 4.5. Water loss through evapotranspiration from soil and floodplain for Southern, Northern and whole Delta regions.

Region	**ET type**	**Monthly water loss (km^3/month)**			**Annual water loss (km^3/yr)**		
-	-	Min	Max	Average	Min	Max	Average
Northern Delta	ET-Flood	0.0	0.5	0.2	1.2	2.8	2.0
	ET-Soil	0.0	0.9	0.4	4.3	7.1	5.8
	Total ET	0.1	1.2	0.6	6.1	10.0	8.0
Southern Delta	ET-Flood	0.0	1.8	0.4	2.2	7.5	4.7
	ET-Soil	0.1	1.9	1.0	9.6	16.4	13.0
	Total ET	0.2	2.5	1.4	13.7	21.7	18.1
Whole Delta	ET-Flood	0.0	2.2	0.6	3.4	10.1	6.7
	ET-Soil	0.2	2.8	1.5	14.5	23.5	18.8
	Total ET	0.2	3.6	2.1	20.1	31.6	26.1

Regarding Delta hydraulics, Ogilvie et al. (2015) argued that distributed hydrodynamic models of the Inner Delta need to take into account the spatial differences in timing and duration of flooding along the region, while simplified routing models (e.g., one large reservoir for the whole Delta) are not able to represent it. Our model results and sensitivity analysis corroborate it. It is necessary to represent flow

connectivity, flooding along floodplain channels and diffuse flow across the Delta area, instead of representing a single upstream-downstream direction, as shown by Neal et al. (2012). Northern and Southern lateral connections considerably improved model simulation (as showed in Sensitivity Analysis, Figures 9 and 10) in terms of discharge and flooded areas. One important role of lateral connections was to allow flow bifurcation and representation of important distributaries along the Delta, that would not be possible in commonly adopted 1D upstream-downstream model approaches. For instance, Diaka river distributary, at the entrance of Southern Delta (Figure 4.2, bottom-right figure), diverted around 15% of main stem flow (long term simulation average), and annual peaks in Diaka varied between 5% and 25% of main stem peak in simulations. This value is, however, highly sensitive on the assumed hydraulic geometry along Diaka river. The inclusion of lateral connections is expected to improve model prediction in the case of applications with finer resolution, since flow capacity in floodplains and river channels can differ considerably across multiple scales when assuming only single dowstream connectivities (Mateo et al., 2016).

Different behaviors were observed between Southern and Northern Delta areas. Flood attenuation along a diffuse flow pattern occurs mainly in the south, while channelized flow along stationary west-east oriented dunes are predominant in the north. This is visible in simulated flooded areas (Figure 4.8).

Given the flat terrain along Niger Inner Delta, backwater flow is also relevant. In the Delta region, based on SRTM elevation, main stem bed elevation decreased 10 meters in a 510 km long reach (~2 cm/km). Figure 4.12 presents simulated water level across several unit-catchments in a transect along the Northern Inner Delta (transect shown in Figure 4.2 as a dashed black line). While Niger main stem level fell seasonally from ~264 m to ~257 m elevation (EGM96 vertical datum as used by SRTM), floodplain channels between Erg of Nianfunké dunes had smaller variations during low flows, when most of them dried out (261 m, 260 m and 259 m level plateaus indicate stream bed level). However, during high water period, all unit-catchments presented roughly the same water level, and thus were directly linked to Niger main stem and dependent on backwater flow conditions.

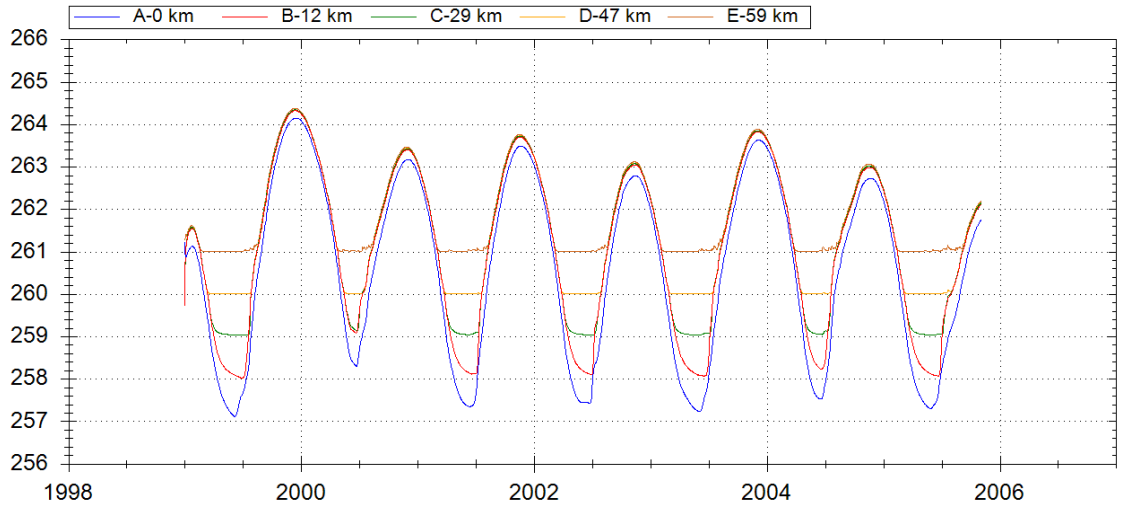

Figure 4.12. Modeled water level time series (m) for five catchments (A-E) along a transect in Northern Inner Delta (location presented in Figure 4.2). Figure 4.legend refers to catchment location and distances (0-59 km) from Niger main stem along the transect.

Previous large scale models of the Niger basin which considered rather coarse flow paths, with only one defined upstream-downstream direction, seemed to overpredict discharges in downstream gauges (e.g., Dadson et al., 2010; Pedinotti et al., 2012). Dadson et al. (2010) argued that it may have occurred due to (i) water abstraction by humans, (ii) groundwater recharge, (iii) uncertainty in discharge observations, (iv) underestimation of evapotranspiration, (v) uncertainty in precipitation, or (vi) uncertainty in flow paths at 0.5° spatial resolution. Water abstraction and observed data (precipitation, discharge, climate variables) uncertainty may certainly have contributed to our model errors. However, from our results, it seems that main processes needed to be simulated in order to achieve good modeled discharges are related to (i) distributed flow paths along floodplain channels in Northern Delta as well as diffuse flow in the South Delta (as shown by Neal et al., 2012), (ii) infiltration from those flooded areas to ensure water availability for soil evapotranspiration, and (iii) representation of flow hydrodynamics (flood wave diffusion, backwater, floodplain storage) across the vast Niger Inner Delta. We expect that this study provides new insights on the way forward for large scale modeling efforts on the Niger River Basin or other global arid wetlands.

4.5 Conclusions

In this study, we presented a first coupled hydrologic and hydrodynamic model of the Upper Niger River Basin in West Africa. The MGB-IPH was run from 1999 to 2014, forced with TRMM daily precipitation and 10' CRU monthly mean climate data. The basin was discretized into 4307 unit-catchments, with 4307 simulated river reaches. A vertical hydrology module was coupled to a hydrodynamic one (inertial model, Bates

et al., 2010), where feedbacks such as floodplain open water evaporation and infiltration into soil were represented. The model was calibrated with a simplified parameter estimation approach, with only five parameter sets for the whole basin, while Niger main stem channel width and depth values were assumed constant for long reaches to avoid overparameterization. The Niger Inner Delta, a vast wetland area within the Sahel Desert, was satisfactorily simulated due to a set of model implementations: (i) higher drainage density along the Delta in comparison to other areas of the basin, allowing an explicit simulation of floodplain channels; (ii) lateral connections between unit-catchments along the Delta, representing diffuse flows in Southern Delta region and the flooding dynamics of distributaries which convey large amounts of water; (iii) satisfactory hydrograph attenuation due to floodplain storage and long residence time along the Delta with the representation of floodplain channels; and (iv) floodplain water infiltration to unsaturated soil column, which improved calculation of evapotranspiration and water loss along the Delta.

Model results were satisfactory, reaching Nash-Sutcliffe efficiency during calibration higher than 0.6 for most discharge gauges. The model was then validated with in-situ water level, remote sensing altimetry and flooded areas, yielding equally good results.

Flood dynamics of the Niger Inner Delta was also studied, showing the different flooding patterns in Southern and Northern Delta regions, and the relevant contribution of different implemented processes, such as floodplain hydrodynamics (water storage, backwater flows, river bifurcations, distributaries and lateral connections), local rainfall and different timing of soil evapotranspiration and open water evaporation, as well as the interaction between flooded areas and their underneath soil.

Finally, the development of a hydrologic-hydrodynamic basin scale model for the Niger may be useful for water management issues, where the effects of alterations at upstream regions (e.g., building of dams and climate change) on the Niger Delta region and downstream reaches may be more satisfactorily simulated. The developed model may also be interesting for other large scale, complex floodplain systems in arid regions, such as those found in African continent (e.g., Okawango Delta) and elsewhere (e.g., Chaco wetlands in South America). This study adds to hydrological research on which processes should be included in large scale models of Upper Niger Basin, in order to correctly represent floodplain attenuation. Interesting possibilities towards model improvement are related to better parameter estimation, especially those related to cross section hydraulic parameters (e.g., width, depth, Manning) along main stem and floodplain channels, for which remote sensing data may be very useful (e.g., estimation of channel widths from satellite imagery and depths from altimetry), given the poorly gauged character and the scale of the Niger River Basin. Missions such as the forthcoming SWOT may provide monitoring of such environments at unprecedented spatio-temporal resolutions.

Supplementary material 4.A: Model calibrated parameters

All model calibrated parameters for the hydrologic vertical balance (soil water budget) are presented in Table 4.A.1. Parameters related to hydrodynamic routing (width, depth and Manning parameters) are discussed in the "2.2.2 Model input data and parameterization". Additionally, KINF infiltration parameter was defined as KINF=20 mm/day for the whole basin. For each one of the five sub-basins (Figure 4.1), one set of parameters is defined, which different values for each Hydrological Response Unit (HRU) within the same sub-basin. Parameters CS, CI and CB are related to surface, sub-surface and groundwater linear reservoirs (hillslope propagation module within catchment), and are defined as constant for all catchments within a sub-basin.

Table 4.A.1. Model calibrated parameters. ForShal : Forest with shallow soil ; ForDeep: Forest with deep soil; InnerDel: Niger Inner Delta area; SavaShal: Savanna with shallow soil; SavaDeep: Savanna with deep soil; AgrShal: Agriculture with shallow soil; AgrDeep: Agriculture with deep soil; BareShal: Bare soil with shallow soil ; BareDeep: Bare soil with deep soil; Water: open water.

Sub-basin/ HRU	**Wm**	**b**	**Kbas**	**Kint**	**CAP**	**CS**	**CI**	**CB**
Sub-basin	1					10	80	150
ForShal	550	0.15	0.2	3	0	-	-	-
ForDeep	750	0.15	0.2	3	0	-	-	-
InnerDel	1050	0.15	0.2	3	2	-	-	-
SavaShal	550	0.15	0.2	3	0	-	-	-
SavaDeep	800	0.15	0.2	3	0	-	-	-
AgrShal	900	0.15	0.2	3	0	-	-	-
AgrDeep	750	0.15	0.2	3	0	-	-	-
BareShal	950	0.15	0.2	3	0	-	-	-
BareDeep	950	0.15	0.2	3	0	-	-	-
Wetland	650	0.15	0.2	3	0	-	-	-
Water	0	0	0	0	0	-	-	-
Sub-basin 2 (Gorouol river)						8	50	150
ForShal	650	0.2	0.05	1	0	-	-	-
ForDeep	500	0.15	0.2	2	0	-	-	-
InnerDel	800	0.15	0.2	2	2	-	-	-
SavaShal	700	0.15	0.2	2	0	-	-	-
SavaDeep	650	0.2	0.05	1	0	-	-	-
AgrShal	700	0.15	0.2	2	0	-	-	-
AgrDeep	650	0.25	0.05	1	0	-	-	-
BareShal	700	0.15	0.2	2	0	-	-	-
BareDeep	700	0.15	0.2	2	0	-	-	-
Wetland	400	0.15	0.2	2	0	-	-	-
Water	0	0	0	0	0	-	-	-

Sub-basin 3 (Dargol river)						20	80	300
ForShal	350	0.8	0.05	8	0	-	-	-
ForDeep	350	0.8	0.05	8	0	-	-	-
InnerDel	350	0.8	0.05	8	2	-	-	-
SavaShal	350	0.8	0.05	8	0	-	-	-
SavaDeep	300	0.8	0.05	8	0	-	-	-
AgrShal	350	0.8	0.05	8	0	-	-	-
AgrDeep	350	0.8	0.05	8	0	-	-	-
BareShal	350	0.8	0.05	8	0	-	-	-
BareDeep	350	0.8	0.05	8	0	-	-	-
Wetland	350	0.8	0.05	8	0	-	-	-
Water	0	0	0	0	0	-	-	-
Sub-basin 4 (Sirba river)						20	30	40
ForShal	300	0.15	0.2	2	0	-	-	-
ForDeep	500	0.15	0.2	2	0	-	-	-
InnerDel	800	0.15	0.2	2	2	-	-	-
SavaShal	500	0.15	0.2	2	0	-	-	-
SavaDeep	470	0.12	0.05	0.5	0	-	-	-
AgrShal	700	0.15	0.2	2	0	-	-	-
AgrDeep	470	0.12	0.05	0.5	0	-	-	-
BareShal	700	0.15	0.2	2	0	-	-	-
BareDeep	700	0.15	0.2	2	0	-	-	-
Wetland	400	0.15	0.2	2	0	-	-	-
Water	0	0	0	0	0	-	-	-
Sub-basin 5 (Bani river)						10	80	120
ForShal	275	0.05	0.2	1	0	-	-	-
ForDeep	575	0.05	0.2	1	0	-	-	-
InnerDel	575	0.05	0.2	1	2	-	-	-
SavaShal	275	0.05	0.2	1	0	-	-	-
SavaDeep	525	0.05	0.2	1	0	-	-	-
AgrShal	475	0.05	0.2	1	0	-	-	-
AgrDeep	375	0.05	0.2	1	0	-	-	-
BareShal	475	0.05	0.2	1	0	-	-	-
BareDeep	475	0.05	0.2	1	0	-	-	-
Wetland	175	0.05	0.2	1	0	-	-	-
Water	0	0	0	0	0	-	-	-

5 Conclusão

Grandes áreas inundáveis prestam importantes serviços ambientais, como regulação de clima, cheias e ciclos biogeoquímicos e manutenção da biodiversidade, e estão presentes nas mais variadas regiões geográficas, desde úmidas áreas tropicais como na Amazônia, até locais áridos como os grandes deltas internos da África. Complexos processos hidrológicos e hidrodinâmicos ocorrem nestas áreas, onde existe intensa interação entre áreas inundadas, biosfera e atmosfera.

Neste trabalho, foram estudados alguns aspectos relacionados ao papel das grandes áreas inundáveis na dinâmica hidrológica de bacias hidrográficas. No Capítulo 3, foi explorado o papel das planícies de inundação na alteração da onda de cheia afluente. Além de aspectos já conhecidos como a atenuação de picos e suavização de hidrogramas devido ao efeito de armazenamento das planícies, mostrou-se o efeito destas na alteração da assimetria das ondas de cheia: hidrogramas tendem a apresentar assimetria negativa, com ascensão mais lenta que a recessão, ao passar por grandes planícies de inundação. Através de análises numéricas, analíticas e empíricas, concluiu-se que a relação entre celeridade da onda de cheia e vazão (C x Q) está diretamente relacionada a este fenômeno, ocasionado devido à relação inversa entre C e Q existente em áreas de armazenamento (planície de inundação). Um estudo de caso na Amazônia evidenciou potencialidades deste estudo, onde grandes rios com áreas inundadas por extravasamento da calha fluvial (e.g., rios Purus, Juruá e trecho principal do Amazonas) tenderam a apresentar assimetria negativa e uma significativa correlação entre áreas inundadas e o índice de assimetria proposto. Por sua vez, rios com grandes áreas interfluviais, inundadas por chuva local (e.g., rio Negro), não apresentaram tal correlação. Como recomendação para trabalhos futuros, a avaliação de assimetria de séries temporais de altimetria espacial pode auxiliar na compreensão dos processos de inundação em regiões mal monitoradas.

Uma importante ferramenta para compreensão da dinâmica hidrológica destas grandes áreas inundáveis é a modelagem matemática. No Capítulo 4, foi apresentado o desenvolvimento e validação de um modelo hidrológico-hidrodinâmico de grande escala para a bacia do Alto Rio Níger, onde está localizado o Delta Interno do Níger, uma grande planície inundada sazonalmente no meio do Deserto do Sahel, e onde importantes perdas por evaporação ocorrem. O modelo desenvolvido acoplou de forma satisfatória processos hidrodinâmicos de inundação de canais ao longo das planícies com processos hidrológicos de evapotranspiração e infiltração de água no solo. Foi então avaliado o papel relativo destes diversos processos, evidenciando importantes elementos da dinâmica de inundação da região, como o distinto comportamento das áreas norte e sul do Delta. A pesquisa desenvolvida contribui também para o desenvolvimento de modelos hidrológicos de grande escala em outras regiões inundáveis, apresentando processos cuja implementação e representação faz-se necessária para uma melhor capacidade preditiva dos modelos. O modelo desenvolvido é aplicável a outras grandes áreas inundáveis.

Por fim, frente ao contexto atual de aumento da disponibilidade de dados de sensoriamento remoto para monitoramento de grandes áreas inundáveis, como a missão SWOT para monitoramento de águas superficiais em escala global e prevista para lançamento em 2021, espera-se que a presente dissertação contribua para o conhecimento e compreensão de processos hidrológicos existentes nestas áreas, e que propicie novas possibilidades de uso destas novas fontes de dados.

5.1 Recomendações

Algumas recomendações podem ser propostas para desenvolvimento futuro da pesquisa desenvolvida nesta dissertação em relação a estudos sobre grandes áreas inundáveis.

Em relação ao Capítulo 3 sobre assimetria negativa observada em hidrogramas de rios com planície, recomenda-se pesquisas no sentido de:

- Aprofundar o papel de diferentes geometrias hidráulicas na assimetria de hidrogramas, com variadas características de larguras, ângulo de inclinação, etc.;
- Analisar assimetria de hidrogramas e curvas celeridade-vazão em outras regiões além das aqui estudadas (principalmente bacia Amazônica);
- Avaliar o uso de altimetria espacial para estimativa de assimetria de hidrogramas em rios mal monitorados cujo comportamento hidrodinâmico ainda é pouco conhecido, de forma a compreender e/ou diferenciar processos distintitos de inundação.

Em relação ao Capítulo 4 sobre modelagem hidrológica-hidrodinâmica de grandes áreas inundáveis, recomenda-se pesquisas no sentido de:

- Melhorar a estimativa de geometria hidráulica de canais (profundidade e largura de calha cheia, coeficiente de Manning) a partir de técnicas de otimização ou de sensoriamento remoto;
- Aprofundar estudos em relação à forma de representar fluxos bidimensionais e difusos em regiões bastante planas, como as conexões laterais utilizadas no modelo do Alto Rio Níger, cujas premissas adotadas podem ser melhor avaliadas;
- Comparar modelo *quasi*-2D utilizado nesta pesquisa (através das conexões laterais entre minibacais) com modelo 2D de grade retangular, a fim de avaliar vantagens e desvantagens entre as diversas abordagens;
- Explorar outras formas de validação de modelos hidrológicos-hidrodinâmicos com produtos de sensoriamento remoto, como os recentemente disponibilizados de umidade do solo (e.g., missões SMOS e

SMAP), além de dados de altimetria espacial com cada vez maior resolução espacial e temporal, e dados de evapotranspiração real a partir de modelos de balanço de energia.

6 Referências

Aires, F., Papa, F., Prigent, C., Crétaux, J-F., Berge-Nguyen, M.. (2014). Characterization and Space–Time Downscaling of the Inundation Extent over the Inner Niger Delta Using GIEMS and MODIS Data. Journal of Hydrometeorology, 15(1), 171-192.

Äkesson, A., A. Wörman, A. Bottacin-Busolin. (2015). Hydraulic response in flooded stream networks. Water Resources Research, 51, 213-240.

Almeida-Filho, R., Miranda, F. (2007). Mega capture of the Rio Negro and formation of the Anavilhanas Archipelago, Central Amazônia, Brazil: evidences in and SRTM digital elevation model. Remote Sensing of Environment 110, 387-392.

Alsdorf, D. E. (2003). Water storage of the central Amazon floodplain measured with GIS and remote sensing imagery. Ann. Assoc. Am. Geogr. 93(1), 55–66.

Alsdorf, D,. Lettenmaier, D. (2003). Tracking freshwater from space. Science 301, 1491-1494.

Alsdorf, D., Dunne, T., Melack, J., Smith, L., Hess, L. (2005). Diffusion modeling of recessional flow on central Amazonian floodplains. Geophysical Research Letters 32, L21405, doi:10.1029/2005GL024412.

Alsdorf, D., P. Bates, J. Melack, M. Wilson, T. Dunne. (2007a). Spatial and temporal complexity of the Amazon flood measured from space. Geophysical Research Letters 34, L08402, 1-5.

Alsdorf, D., Rodríguez, E., Lettenmaier, D. (2007b). Measuring surface water from space. Review of Geophysics 45, 1-24.

Andersen, I., Dione, O., Jarosewich-Holder, M., Olivry, J.C., Golitzen, K.G., (2005). The Niger River Basin: a vision for sustainable management. Directions in development, World Bank, Washington DC.

Aquino, S.; Latrubesse, E. M.; Souza Filho, E. E. (2008). Relações entre o regime hidrológico e os ecossistemas aquáticos da planície aluvial do rio Araguaia. Acta Sci. Biol. Sci. Maringá, 30(4), 361-369.

Bastiaanssen, W., Menenti, M., Feddes, R.A., Holtslag, A. (1998). A remote sensing surface energy balance algorithm for land (SEBAL). 1. Formulation. Journal of Hydrology, 212-213, 198-212.

Bates, P., De Roo, A.P.J. (2000). A simple raster-based model for flood inundation simulation. Journal of Hydrology 236, 54-77.

Bates, P., Horritt, M., Fewtrell, T. (2010). A simple inertial formulation of the shallow water equations for efficient two-dimensional flood inundation modelling. Journal of Hydrology 387, 33-45.

Bauer, P., Gumbricht, T., Kinzelbach, W., (2006). A regional coupled surface water/groundwater model of the Okavango Delta, Botswana. Water Resources Research, 42, W04403.

Bergé-Nguyen, M. & Crétaux, J.-F. (2015). Inundations in the Inner Niger Delta: monitoring and analysis using MODIS and Global Precipitation Datasets. Remote Sensing 7, 2127-2151,

Beven, K. (2012). Parameter Estimation and Predictive Uncertainty. In: Beven, K. (Org). Rainfall-Runoff Modelling. Wiley-Blackwell, Chichester, UK, 2012.

Biancamaria, S., P. D. Bates, A. Boone, N. M. Mognard. (2009). Large scale coupled hydrologic and hydraulic modelling of the Ob river in Siberia, J. Hydrol., 379(1–2), 136–150.

Biancamaria, S., D.P. Lettenmaier, T.M. Pavelsky (2016), The SWOT Mission and Its Capabilites for Land Hydrology, Surveys in Geophysics, 1-31.

Bonnet, M.P., Barroux, G., Martinez, J.M., Seyler, F., Moreira-Turcq, P., Cochonneau, G., Melack, J.M., Maurice-Bourgoin, L., León, J.G., Roux, E., Calmant, S., Kosuth, P., Guyot, J.L., P. Seyler. (2008). Floodplain hydrology in an Amazon floodplain lake (Lago Grande de Curuaí). Journal of Hydology 349, 18-30.

Borma, L.S., da Rocha, H.R., Cabral, O.M., Von Randow, C., Collicchio, E., Kurzatkowski, D., Brugger, P.J., Freitas, H., Tannus, R., Oliveira, L., Rennó, C.D., Artaxo, P. (2009). Atmosphere and hydrological controls of the evapotranspiration over a floodplain forest in the Bananal Island region, Amazonia. Journal of Geophysical Research 114, G01003, doi:10.1029/2007JG000641.

Botter, G. and A. Rinaldo. (2003). Scale effect on geomorphologic and kinematic dispersion. Water Resources Research, 39(10), doi:10.1029/2003WR002154.

Breda et al., submitted paper. Assimilation of altimetry data to improve channel bottom level estimates

Bourrel, L., L. Phillips, S. Moreau. (2009). The dynamics of floods in the Bolivian Amazon Basin. Hydrological Processes 23 (22), 3161–3167.
Brasil, Ministério do Meio Ambiente. (2001). Plano de Manejo do Parque Nacional do Araguaia – TO.

Brasil, Ministério do Meio Ambiente, Instituto Chico Mendes. PARNA do Pantanal Mato-Grossense. Disponível em: < http://www.icmbio.gov.br/portal/biodiversidade/unidades-de-conservacao/biomas-brasileiros/pantanal/unidades-de-conservacao-pantanal/2232-parna-do-pantanal-matogrossense.html>. Último acesso em 13 de Abril de 2016.

Bravo, J. M., D. Allasia, A. R. Paz, W. Collischonn, C.E.M. Tucci. (2012). Coupled Hydrologic-Hydraulic Modeling of the Upper Paraguay River Basin. Journal of Hydrologic Engineering, 17, 635, 2012.

Callede, J., J.L. Guyot, J. Ronchail, N, Molinier, E. De Oliveira. (2002). L'Amazone à Óbidos (Brésil): étude statistique des débits et bilan hydrologique. Hydrological Sciences Journal, 47 (2), 321–333.

Cao, Z., J. Meng, G. Pender, S. Wallis. (2006). Flow resistance and momentum flux in compound open channels. Journal of Hydraulic Engineering, 132(12), 1272-1282.

Cardoso, J.M. & Bates, J.M. (2002). Biogeographic patterns and conservation in the South American Cerrado: a tropical savanna hotspot. BioScience 52(3), 225-233.

Casse, C., M. Gosset, T. Vischel, G. Quantin, B.A. Tanimoun. (2015). Model-based study of the role of rainfall and land use land cover in the changes in Niger Red floods occurrence and intensity in Niamey between 1953 and 2012. Hydrology and Earth System Sciences Discussions, 12, 12039–12087.

Centre National d'études spatiales (CNES). (2017). SWOT. Disponível em: https://swot.cnes.fr/fr. Último acesso em 18 de fevereiro de 2017.

Chow, V.T. (1988). Applied Hydrology. McGraw-Hill.

Cochrane, M.; Barber, C. (2008). Climate change, human land use and future fires in the Amazon. Global Change Biology 15(3), 610-612.

Collischonn, W. (2001). Simulação hidrológica de grandes bacias. Tese de Doutorado. IPH/UFRGS, Porto Alegre, Brasil.

Collischonn, W., Allasia, D., Silva, B., Tucci, C. (2007). The MGB-IPH model for large-scale rainfall-runoff modelling. Hydrological Sciences 52(5)878-895.

Conway, D., Mahé, G., (2009). River flow modelling in two large river basins with non-stationary behaviour: the Paraná and the Niger. Hydrological Processes 23(22), 3186-3192.

Costabile, P. and F. Macchione. (2012). Analysis of One-Dimensional Modelling for Flood Routing in Compound Channels. Water Resources Management, 26(5), 1065-1087.

Costa, A.C., Bronstert, A., Araújo, J.C., (2012). A channel transmission losses model for different dryland rivers. Hydrol. Earth Syst. Sci., 16, 1111–1135.

Dadson, S., Ashpole, I., Harris, P., Davies, H.N., Clark, D., B., Blyth, E., Taylor, C.M., (2010). Wetland inundation dynamics in a model of land surface climate:
Evaluation in the Niger inland delta region. Journal of Geophysical Research, VOL. 115, D23114.

Da Rocha, H. et al,. (2009). Patterns of water and heat flux across a biome gradient from tropical forest to savanna in Brazil. Journal of Geophysical Research 114, G00B12, doi:10.1029/2007JG000640.

Davies, S., (1996). Adaptable Livelihoods : Coping with Food Insecurity in the Malian Sahel. New York: St. Martin's Press, 335 pp.

Descroix, L., Mahé, G., Lebel, T., Favreau, G., Galle, S., Gautier, E., Olivry, J.C., Albergel, J., Amogu, O., Cappealaere, B., Dessouassi, R., Diedhiou, A., Le Breton, E., Mamadou, I., Sighomnou, D. (2009). Spatio-temporal variability of hydrological regimes around the boundaries between Sahelian and Sudanian areas of West Africa: A synthesis. Journal of Hydrology 375, 90-102.

Di Baldassarre, G., A. Castellarin, A. Brath. (2009). Analysis of the effects of levee heightening on flood propagation: example of the River Po, Italy. Hydrological Sciences, 54(6), 1007-1017.

Dingman, S. L. (2009). Fluvial Hydraulics. Oxford: Oxford University Press.

Durand, M., L.L. Fu, D.P. Lettenmaier, D.E. Alsdorf, E. Rodrígue, D.E. Fernandez. (2010). The surface water and ocean topography mission: Observing terrestrial surface water and oceanic submesoscale eddies. Proceedings Of the IEEE, 98(5) 766−779.

Entekhabi, D., Eni G. Njoku, Peggy E. O'Neill, Kent H. Kellogg, Wade T. Crow, Wendy N. Edelstein, Jared K. Entin, Shawn D. Goodman, Thomas J. Jackson, Joel Johnson, John Kimball, Jeffrey R. Piepmeier, Randal D. Koster, Neil Martin, Kyle C. McDonald, Mahta Moghaddam, Susan Moran, Rolf Reichle, J. C. Shi, Michael W. Spencer, Samuel W. Thurman, Leung Tsang, Jakob Van Zyl, (2010). The Soil Moisture Active Passive (SMAP) Mission. Proceeding of the IEEE 98(5), 704-716.

Espinoza, J.C., Ronchail, J., Guyot, J.L., Cocheneau, G., Filizola, N., Lavado, W., Oliveira, E., Pombosa, R., Vauchel, P. (2009a). Spatio-temporal rainfall variability in the Amazon Basin Countries (Brazil, Peru, Bolivia, Colombia and Ecuador). International Journal of Climatology 29, 1574-1594.

Espinoza, J.C., Guyot, J.L., Ronchail, J., Cocheneau, G., Filizola, N., Fraizy, P., Labat, D., de Oliveira, E., Ordonez, J.J., Vauchel, P. (2009b). Constrasting regional discharge evolutions in the Amazon Basin. Journal of Hydrology 375, 297-311.

Esteves, M., Lapetite, J.M., (2003). A multi-scale approach of runoff generation in a Sahelian gully catchment: a case study in Niger. Catena 50, 255-271.

Fan, Y., Miguez-Macho, G. (2011). A simple hydrologic framework for simulating wetlands in climate and earth system models. Climate Dynamics 37, 253-278.

Fan, F. M., Collischonn, W., Sorribas, M. V., Pontes, P. R. M, (2013). Sobre o início da rede de drenagem definida a partir dos modelos digitais de elevação. Brazilian Journal on Water Resources 18, 241-257.

Farr, T.G., Rosen, P.A., Caro, E., Crippen, R. et al (2007) The Shuttle Radar Topography Mission. Rev. Geophys. doi:10.1029/2005RG000183.

Fernández, A., Najafi, M.R., Durand, M., Mark, B.G., Moritz, M., Jung, H.C., Neal, J., Shastry, A., Laborde, S., Phang, S.C., Hamilton, I.M., Xiao, N., 2016. Testing the skill of numerical hydraulic modeling to simulate spatiotemporal flooding patterns in the Logone floodplain, Cameroon. Journal of Hydrology 539, 265.280.

Filizola, N., Latrubesse, E., Fraizy, P., Souza, R., Guimarães, V., Guyot, J.-L. (2014). Was the 2009 flood the most hazardous or the largest ever recorded in the Amazon? Geomorphology 215, 99–105.

Fleischmann, A., Paiva, R., Collischonn, W., Sorribas, M., Pontes, P, (2016). On river-floodplain interaction and hydrograph skewness. Water Resources Research 52(10), doi: 10.1002/2016WR019233.

Frappart, F., Seyler, F., Martinez, J.-M., Léon, J., Cazenave, A. (2005). Floodplain water storage in the Negro River basin estimated from microwave remote sensing of inundation area and water levels. Remote Sensing of Environment 99, 387-399.

Frappart, F., Calmant, S., Cauhopé, M., Seyler, F., & Cazenave, A. (2006). Preliminary results of ENVISAT RA-2-derived water levels validation over the Amazon basin. Remote sensing of Environment, 100(2), 252-264.

Forsberg, B., Devol, A., Richey, J., Martinelli, L., dos Santos, H. (1998). Factors controlling nutrient concentrations in Amazon floodplain lakes. Limnology & Oceanography 33(1), 41-56.

Gao, B. (1996). NDWI – a normalized difference water index for remote sensing of vegetation liquid water from space. Remote Sensing of Environment, 58(3), 257-266.

Garambois, P.A., Calmant, S., Roux, H., Paris, A., Monnier, J., Santos da Silva, J., (2016). Hydraulic visibility: using satellite altimetry to parameterize a hydraulic model of an ungauged reach of a large braided river, Hydrol. Process., doi:10.1002/hyp.11033.

Garbrecht, J., G. Brunner. (1990). Hydrologic channel-flow routing for compound sections. Journal of Hydraulic Engineering 117(5), 629-642.

Getirana, A., Bonnet, M.P., Rotunno Filho, O., Collischonn, W., Guyot, J.L., Seyler, F., Mansur, W.J. (2010). Hydrological modelling and water balance of the Negro River basin: evaluation based on in situ and spatial altimetry data. Hydrological Processes 24, 3219–3236.

Getirana, A., Paiva, R. (2013). Mapping large-scale river flow hydraulics in the Amazon Basin. Water Resources Research 49(5), 2437-2445.

Grimaldi, S., A. Petroselli, G. Alonso, F. Nardi. (2010). Flow estimation with spatially variable hillslope velocity in ungauged basins. Advances in Water Resources, 33, 1216-1223.

Gupta, V.K., E. Waymire, C.T. Wang. (1980). A representation of instantaneous unit hydrograph from geomorphology. Water Resources Research, 16(5), 855–862.

Hamilton, S. K., S.J. Sippel, J. Melack. (2002). Comparison of inundation patterns among major South American floodplains. Journal of Geophysical Research 107(D20), 5-1 – 5-14.

Hannah, D.M., B.P.G. Smith, A.M. Gurnell, G.R. McGregor. (2000). An approach to hydrograph classification. Hydrological Processes, 14, 317-338.

Hess, L., Melack, J., Novo, E., Barbosa, C., Gastil, M. (2003). Dual-season of wetland inundation and vegetation for the Central Amazon basin. Remote Sensing of Environment 87, 404-428.

Hrachowitz, M., H.H.G. Savenije, G. Blöschl, J.J. McDonnell, M. Sivapalan, J.W. Pomeroy, B. Arheimer, T. Blume, M.P. Clark., U. Ehret, F. Fenicia, J.E. Freer, A. Gelfan, H.V. Gupta, D.A. Hughes, R.W. Hut, A. Montanari, S. Pande, D. Tetzlaff, P.A. Troch, S. Uhlenbrook, T. Wagener, T., H.C. Winsemius, R.A. Woods, E. Zehe, and C. Cudennec, (2013), A decade of Predictions in Ungauged Basins (PUB): a review, Hydrological Sciences Journal 58(6), 1198-1255.

Huffman, G., Adler, R., Bolvin, D., Gu, G., Nelkin, E., Bowman, K., Hong, Y., Stocker, E., Wolff, D. (2007). The TRMM Multisatellite Precipitation Analysis (TMPA): Quasi-Global, Multiyear, Combined-Sensor Precipitation Estimates at Fine Scales. Journal of Hydrometeorology 8, doi 10.1175/JHM560.1.

Hung, N. N., J.M. Delgado, V.K. Tri, L.M. Hung, B. Merz, A. Bárdossy, H. Apel. (2012). Floodplain hydrology of the Mekong Delta, Vietnam. Hydrological Processes 26, 674-686.

Joyce, R., Janowiak, J., Arkin, P., Xie, P. (2004). CMORPH: a method that produces global precipitation estimates from passive microwave and infrared data at high spatial and temporal resolution. Journal of Hydrometeorology 5, 487-503.

Jothityangkoon, C. and M. Sivapalan. (2003). Towards estimation of extreme floods: examination of the roles of runoff process changes and floodplain flows. Journal of Hydrology, 281(3), 206-229.

Junk, W., P.B. Bayley, R.E. Sparks. (1989). The flood pulse concept in river-floodplain systems, Proceedings of the International Large River Symposium. Can. Spec. Publ. Fish. Aquat. Sci. 106, 110-127.

Junk. W. and K. Furch. (1993). A general review of tropical South American floodplains. Wetlands Ecology and Management 2(4), 231-238.

Junk, W., M.G. Soares, P.B. Bayley. (2007). Freshwater fishes of the Amazon River basin: their biodiversity, fisheries, and habitats. Aquatic Ecosystem Health & Management 10(2), 153-173.

Junk, W., M.T. Piedade, J. Schöngart, M. Cohn-Haft, J. Adeney, F. Wittman. (2011). A classification of major naturally-occuring Amazonian lowland wetlands. Wetlands 31(4), 623-640.

Junk, W. (2012). Current state of knowledge regarding South America wetlands and their future under global climate change. Aquatic Sciences 75(1), 113-131.

Junk, W., Piedade, M.T., Lourival, R., Wittman, F., Kandus, P., Lacerda, L., bozelli, R., Esteves, F., da Cunha, C.N., Maltchik, L., Schöngart, J., Schaeffer-Novelli, Y., Agostinho, A. A., Nóbrega, R.L.B. (2015). Definição e Classificação das Áreas Úmidas (AUs) Brasileiras: Base Científica para uma Nova Política de Proteção e Manejo Sustentável. Instituto Nacional de Pesquisa e Tecnologia em Áreas Úmidas (INCT-Áreas Úmidas).

Keddy, P. A., L.H. Fraser, A.I. Solomeshch, W.J. Junk, D.R. Campbell, M.T. Arroyo, C.J. Alho. (2009). Wet and Wonderful: The World's Largest Wetlands Are Conservation Priorities.Bioscience 59(1), 39-51.

Knight, D.W. and J.D. Demetriou. (1983). Flood Plain and Main Channel Flow Interaction. Journal of Hydraulic Engineering 109(8), 1073-1092.

Knight, D. and K. Shiono. (1996). River channel and floodplain hydraulics. In: Anderson, M., Wallind, D., Bates, P. (Org.). Floodplain Processes, Chichester: John Wiley & Sons, 1996.

Kuppel, S., J. Houspanossian, M.D. Nosetto, E.G. Jobbágy. (2015). What does it take to flood the Pampas? Lessons from a decade of strong hydrological fluctuations. Water Resources Research 51(4), 2937-2950.

Lai, C-J., C.-L., Liu, C-L., Y-Z., Lin. (2000). Experiments on flood-wave propagation in compound channel. J. Hydraul. Eng. 126, 492-501.

Latrubesse, E. (2008). Patterns of anabranching channels: the ultimate end-member adjustment of mega rivers. Geomorphology 101(1-2), 130-145.

Latrubesse, E. (2012). Amazon lakes. In: Bengtsson, L., Herschy, R., Fairbridge, R. (Org). Encyclopedia of lakes and reservoirs (Encyclopedia of Earth Science Series). Springer, New York City.

Latrubesse, E. & Rancy, A. (2000). Neotectonic influence on tropical rivers of southwestern Amazon during the late Quaternary: the Moa and Ipixuna river basins, Brazil. Quaternary International 72, 67-72.

Latrubesse, E. & Franzinelli, E. (2002). The Holocene alluvial plain of the middle Amazon River, Brazil. Geomorphology 44, 241–257.

Latrubesse, E. & Franzinelli, E. (2005). The late Quaternary evolution of the Negro River, Amazon, Brazil: Implications for island and floodplain formation in large anabranching tropical systems. Geomorphology 70, 372– 397.

Latrubesse, E., Stevaux, J.C. (2008). The Anavilhanas and Mariuá Archipelagos: fluvial wonders from the Negro River, Amazon Basin. In: Vieira, B.C. (org). Landscapes and Landforms of Brazil, World Geomorphological Lanscapes. Springer, Dordrecht.

Lee, H., Beighley, R., Alsdorf, D,. Jung, H.C., Shum, C.K., Duan, J., Guo, J., Yamazaki, D., Andreadis, K. (2011). Characterization of terrestrial water dynamics in the Congo Basin using GRACE and satellite radar altimetry. Remote Sensing of Environment 115, 3530-3538.

Lesack, L. F. W., & J. M. Melack. (1995). Flooding hydrology and mixture dynamics of lake water derived from multiple sources in an Amazon floodplain lake, Water Resour. Res. 31(2), 329–345.

Lehner, B. & Döll, P. (2004). Development and validation of a global database of lakes, reservoirs and wetlands. Journal of Hydrology 296(1-4), 1-22.

Li, H. and M. Sivapalan. (2011). Effect of spatial heterogeneity of runoff generation mechanisms on the scaling behavior of event runoff responses in a natural river basin. Water Resources Research, 47(3), doi 10.1029/2010WR009712.

Mahé, G., Bamba, F., Soumaguel, A., Orange, D., Olivry, J.C., 2009. Water losses in the inner delta of the River Niger : water balance and flooded area. Hydrological Processes 23, 3157-3160.

Malhi, Y., Roberts, J., Betts, R., Killeen, T., Wenhong, L., Nobre, C. (2008). Climate change, deforestation, and the fate of the Amazon. Science 319(5860), 169-172.

Mamadou, I., Gautier, E., Descroix, L., Noma, I., Moussa, I.B., Maiga, O.F., Genthon, P., Amogu, O., Abdou, M.M., Vandervaere, J.P., (2015). Exorheism growth as an explanation of increasing flooding in the Sahel. Catena 131, 130-139

Martins, A.K. (2004). Ipucas da planície do Araguaia, Estado do Tocantins: ambiente físico de ocorrência, solos e uso da terra. Tese de Doutorado. Viçosa: Universidade Federal de Viçosa.

Masson, V., Champeaux, J.L., Chauvin, F., Meriguet, C., Lacaze, R., 2003. A global database of land surface parameters at 1-km resolution in meteorological and climate models. Journal of Climate 16(9), 1261-1282

McCartney, M.P. and P.S. Naden. (1995). A semi-empirical investigation of the influence of flood-plain storage on flood flow. Water and Environment Journal 9(3), 236-246.

McCarthy, T.S., Bloem, A., Larkin, P.A. (1998). Observations on the hydrology and geohydrology of the Okavango Delta. South African Journal of Geology 101(2), 101-117.

McDonnell, J., R. Woods. (2004). On the need for catchment classification. Journal of Hydrology 299, 2-3.

Meade, R.H. (1991). Backwater Effects in the Amazon River Basin of Brazil. Environ. Geol. Water Sci. 18(2), 105–114.

Mejia, A.I.,nM. Reed. (2011). Role of channel and floodplain cross-section geometry in the basin response. Water Resources Research, 47(9), doi 10.1029/2010WR010375.

Melack, J.M., L.L. Hess, M. Gastil, B. Forsberg, S. Hamilton, I.B.T. Lima. (2004). Regionalization of methane emissions in the Amazon Basin with microwave remote sensing. Glob. Chang. Biol., doi:10.1111/j.1529-8817.2003.00763.x

Melack, J., E. Novo, B. Forsberg, M. Piedade, L. Maurice. (2009). Floodplain ecosystem processes. In: Keller, M., M. Bustamante, J. Gash and P. Dias (org). Amazonia and Global Change, American Geophysical Union, Geophysical Monograph Series, vol. 186.

Melack, J.M., L. Hess. (2010). Remote sensing of the distribution and extent of wetlands in the Amazon basin. In W.J. Junk and M. Piedade (org.). Amazonian floodplain forests: Ecophysiology, ecology, biodiversity and sustainable management. Ecological Studies, Springer.

Mertes, L.A.K. (1997). Documentation and significance of the perirheic zone on inundated floodplains. Water Resources Research 33(7), 1749–1762.

Mertes, L.A.K., Daniel, D., Melack, J., Nelson, B., Martinelli, L.A., Forsberg, B. (1995). Spatial patterns of hydrology, geomorphology, and vegetation on the floodplain of the Amazon River in Brazil from a remote sensing perspective. Geomorphology 13, 215-232.

Michaelides, K., Wilson, M. (2007). Connectivity as a concept for characterising hydrological behaviour. Hydrological Processes 23, 517-522.

Miguez-Macho, G., Fan, Y. (2012a). The role of groundwater in the Amazon water cycle: 1. Influence on seasonal streamflow, flooding and wetlands. Journal of Geophysical Research 117, doi:10.1029/2012JD017539.

Miguez-Macho, G., Fan, Y. (2012b). The role of groundwater in the Amazon water cycle: 2. Influence on seasonal soil moisture and evapotranspiration. Journal of Geophysical Research 117, doi:10.1029/2012JD017540.

Milzow, C., Kgotlhand, L., Bauer-Gottwein, P., Meier, P., Kinzelbach, W, (2009). Regional review : the hydrology of the Okavnago Delta, Botswana – processes, data and modelling. Hydrogeology Journal 17, 1297-1328.

Moussa, R., C. Bocquillon. (2009). On the use of the diffusive wave for modelling extreme flood events with overbank flow in the floodplain. Journal of Hydrology, 374(1-2), 116-135.

Musy, A., C. Higy. (2011). Hydrology: a science of nature. Science Publishers, 326pp.

NASA-JPL. SMAP Mission Description. Available at < http://smap.jpl.nasa.gov/mission/description/>. Last access in 15th August 2015.

Natural Environment Research Council (NERC). (1975). Flood studies report, NERC, London.

Neal, J., Fewtrell, T., Trigg, M. (2009). Parallelisation of storage cell flood models using OpenMP. Environmental Modelling & Software 24, 872-877.

Neal, J., Schumann, G., Bates, P. (2012a). A subgrid channel model for simulating river hydraulics and floodplain inundation over large and data sparse áreas. Water Resources Research 48, W11506, doi:10.1029/2012WR012514.

Neal, J., Villanueva, I., Wright, N., Willis, T., Fewtrell, T., Bates, P. (2012b). How much physical complexity is needed to model flood inundation? Hydrological Processes 26, 2264-2282.

New, M., Lister, D., Hulme, M., Makin, I., (2002). A high-resolution data set of surface climate over global land areas. Climate Research 21, 1-25.

O'loughlin, F., Paiva, R., Durand, M., Alsdorf, D.E., Bates, P. (2016). A multi-sensor approach towards a global vegetation corrected SRTM DEM product. Remote Sensing of Environment 182, 49-59.

Olivera, F. and S. Koka. (2004). Hydrodynamic Dispersive and Advective Processes in Watershed Responses. Journal of Hydrologic Engineering, 9(6), 534-543.

Ogilvie, A., Belaud, G., Delenne, C., Bailly, J.S., Bader, J.C., Oleksiak, A., Ferry, C. Martin, D., (2015). Decadal monitoring of the Niger Inner Delta flood dynamics using MODIS optical data. Journal of Hydrology 523, 368–383.

Olivry, J.C., (1994). Fonctionnement hydrologique de la cuvette lacustre du Niger et essai de modelisation de l'inondation du delta interieur. In: Colloque "Grands Bassins Fluviaux", Paris.

Ovando, A., J. Tomasella, D.A. Rodriguez, J.M. Martinez, J.L. Siqueira-Junior, J.L.,G.L.M. Pinto, P. Passy, P., Vacuhel, L. Noriega, C. Von Randow. (2015). Extreme flood events in the Bolivian Amazon wetlands. Journal of Hydrology: Regional Studies, 5, 293-298.

Paiva, R. (2009) Modelagem hidrológica e hidrodinâmica de grandes bacias. Estudo de caso: bacia do rio Solimões. Dissertação de Mestrado. IPH/UFRGS, Porto Alegre, Brasil.

Paiva, R., Collischonn, W., Tucci, C. (2011). Large scale hydrologic and hydrodynamic modeling using limited data and a GIS based approach. Journal of Hydrology 406, 170-181.

Paiva, R. C. D., D.C. Buarque, W. Collischonn, M.-P. Bonnet, F. Frappart, S. Calmant, S., C.A. Mendes. (2013). Large-scale hydrologic and hydrodynamic modelling of the Amazon River basin. Water Resources Research 49(3), 1226-1243.

Papa, F., Guntner, A., Frappart, F., Prigent, C., Rossow, B. (2008). Variations of surface water extent and water storage in large river basins: a comparison of different global data sources. Geophysical Research Letters 35, L11401.

Parajka, J., V. Andréassian, S. Archfield, A. Bárdossy, F. Chiew, Q. Duan, A. Gelfan, K. Hlavčová, R. Merz, N. McIntyre, L. Oudin, C. Perrin, M. Rogger, J. Salinas, H. Savenije, J.O. Skøien, T. Wagener, E. Zehe, Y. Zhang. (2013). Predictions of runoff hydrographs in ungauged basins, In: Blöschl, G., M. Sivapalan, T. Wagener, A. Viglione, H. Savenije (org.). Runoff Predictions in Ungauged Basins: Synthesis across processes, places and scales. Cambridge: Cambridge University Press, 2013.

Paris, A., Paiva, R., Silva, J.S., Moreira, D.M., Calmant, S., Garambois, P.A., Collischonn, W., Bonnet, M.O., Seyler, F., (2016). Stage-discharge rating curves based on satellite altimetry and modeled discharge in the Amazon basin. Water Resources Research 52, 3787-3814.

Pavan, L. Ilha do Bananal: a maior ilha de rio do mundo. Disponível em: < http://www.temporadalivre.com/blog/ilha-do-bananal-a-maior-ilha-de-rio-do-mundo/>. Último acesso em: 13 de Abril de 2016.

Paz, A. R., W. Collischonn, C. E. M. Tucci, C. R. Padovani. (2011). Large-scale modelling of channel flow and floodplain inundation dynamics and its application to the Pantanal (Brazil). Hydrol. Processes 25(9), 1498–1516.

Paz , A. R. (2010). Simulação hidrológica de rios com grandes planícies de inundação. Tese de Doutorado, IPH, UFRGS. Porto Alegre.

Paz, A., W. Collischonn, J.M. Bravo, P. Bates, C. Baugh. (2014). The influence of vertical water balance of modelling Pantanal (Brazil) spatio-temporal inundation dynamics. Hydrological Processes 28, 3539-3553.

Pedinotti, V., Boone, A., Decharme, B., Crétaux, J.F., Mognard, N., Panthou, G., Papa, F., Tanimoun, B.A., (2012). Evaluation of the ISBA-TRIP continental hydrologic system over the Niger basin using in situ and satellite derived datasets. Hydrol. Earth Syst. Sci., 16, 1745–1773.

Perumal, M., E. O'Connell, K.G.R Raju. (2001). Field Applications of a Variable-Parameter Muskingum Method. Journal of Hydrologic Engineering, 6(3), 196-207.

Pidwirny, M. (2013). Remote Sensing, The Encyclopedia of Earth. Available at http://www.eoearth.org/view/article/155700/. Last access in 17th August 2015.

Pfeffer, J., Seyler, F., Bonnet, M.-P., Calmant, S., Frappart, F., Papa, F., Paiva, R., Satgé, F., Silva, J. (2014). Low-water maps of the groundwater table in the central Amazon by satellite altimetry. Geophysical Research Letters 41, 1981-1987.

Ponce, V. (1989). Engineering Hydrology: principles and practices. Prentice Hall, Englewood Cliffs, New Jersey.

Pontes, P., Collischonn, W., Fan, F., Paiva, R., Buarque, D. (2015). Modelagem hidrológica e hidráulica de grande escala com propagação inercial de vazões. Revista Brasileira de Recursos Hídricos 20(4), 888-904.

Pontes, P., Fan, F., Fleischmann, A., Paiva, R., Buarque, D., Siqueira, V., Jardim, P., Sorribas, M., Collischonn, W. (2017). MGB-IPH model for hydrological and hydraulic simulation of large floodplain river systems coupled with open source GIS. Environmental Software & Modelling 94, 1-20.

Price, R. (2009). Volume-conservative nonlinear flood routing. Journal of Hydraulic Engineering 135(10), 838-845.

Pringle, C. (2001). Hydrologic connectivity and the management of biological reserves: a global perspective. Ecological Applications 11(4), 981-998.

Rast, M., Johannessen, J., Mauser, W. (2014). Review of undersdanding of Earth`s hydrological cycle: observations, theory and modelling. Surv Geophys 35, 491-513.

Richey, J.E., Mertes, L.A.K., Dunne, T., Victoria, R., Forsberg, B., Tancredi, A., Oliveira, E. (1989). Sources and routing of the Amazon River flood wave. Global Biogeochemical Cycles 3(3), 191-204.

Richey, J.E., J.M. Melack, A.K. Aufdenkampe, V.M. Ballester, L.L. Hess. (2002). Outgassing from Amazonian rivers and wetlands as a large tropical source of atmospheric CO2. Nature 416, 617-620

Richey, A., Thomas, B., Lo, M-H., Reager, J.T., Famiglietti, J., Voss, K., Swenson, S,. Rodell, M. (2015). Quantifying renewable groundwater stress with GRACE. Water Resources Research 51, 1-22.

Rinaldo, R., A. Marani, R. Rigon. (1991). Geomorphological dispersion. Water Resources Research, 27(4), 513-525.

Rinaldo, A., G.K. Vogel, R. Rigon, I. Rodriguez-Iturbe. (1995). Can one gauge the shape of a basin? Water Resources Research 31(4), 1119-1127.

Rinaldo, R. and I. Rodriguez-Iturbe. (1996). Geomorphological theory of the hydrological response. Hydrological Processes, 10(6), 803-829.

Robinson, J., M. Sivapalan, J. Snell. (1995). On the relative roles of hillslope processes, chanel routing, and network geomorphology in the hydrologic response of natural catchments. Water Resources Research, 31(12), 3089-3101.

Rodriguez, E., Morris, C.S., Eric Belz, J., (2006). A global assessment of SRTM performance. Photogrammetric Engineering & Remote Sensing 72(3), 249–260.

Rodriguez-Iturbe, I. and J. Valdes. (1979). The geomorphologic structure of hydrologic response. Water Resources Research, 15(6), 140-1420.

Rowland, J.C., Dietrich, W.E., Day, G., Parker, G. (2009). Formation and maintenance of single-thread tie channels entering floodplain lakes: observations from three diverse river systems. Journal of Geophysical Research 114, F02013.

Rozante, J., Moreira, D., Gonçalves, L., Vila, D. (2010). Combining TRMM and Surface Observations of Precipitation: Tecnhique and validation over South America. Weather and Forecasting 25, 885-894.

Rudorff, C., Melack, J., Bates, P. (2014a). Flooding dynamics on the lower Amazon floodplain: 1. Hydraulic controls on water elevation, inundation extent, and river-floodplain discharge. Water Resources Research 50, 619-634.

Rudorff, C., Melack, J., Bates, P. (2014b). Flooding dynamics on the lower Amazon floodplain: 2. Seasonal and interannual hydrological variability. Water Resources Research 50, 1-15.

Saco PM, Kumar P. (2002). Kinematic dispersion in stream networks. 1. Coupling hydraulic and network geometry. Water Resources Research 38(11):1244, doi:10.1029/2001WR000694.

Santos da Silva, J., Calmant, S., Seyler, F., Rottuno, O., Cochonneau, G., Mansur, W. (2010). Water levels in the Amazon basin derived from the ERS 2 and ENVISAT radar altimetry missions. Remote Sensing of Environment 114, 2160-2181.

Santos da Silva, J. S., Seyler, F., Calmant, S., Rotunno Filho, O. C., Roux, E., Araujo, A. A. M., Goyot, J. (2012). Water level dynamics of Amazon wetlands at the watershed scale by satellite altimetry. International Journal of Remote Sensing 33, 3323-3353.

Sawicz, K., T. Wagener, M. Sivapalan, P.A. Troch, G. Carrillo. (2011). Catchment classification: empirical analysis of hydrologic similarity based on catchment function in the eastern USA. Hydr. Earth Syst. Sci, 15, 2895-2911.

Schöngart, J., Junk, W., Piedade, M.T., Ayres, J.M., Hüttermann, A., Worbes, M. (2004). Teleconnection between tree growth in the Amazonian floodplains and the El Niño-Southern Oscillation effect. Global Change Biology 10(5), 683-692.

Schöngart, J. & Junk, W. (2007). Forecasting the flood-pulse in Central Amazonia by ENSO-indices. Journal of Hydrology 335, 124-1332.

Schumann, G., Bates, P., Horritt, M., Matgen, P., Pappenberger, F. (2009). Progress in integration of remote sensing-derived flood extent and stage data and hydraulic models. Review of Geophysics, 47, RG4001.

Serra, J. (2006). Estimación de crecidas máximas en paisajes de meseta. Tese de Doutorado, Universidad Nacional de Rosario, Rosario, Argentina.

Siqueira, V., A., Fleischmann, A., S., Jardim, P. F., Fan, F. M., Collischonn, W. (2016). IPH-Hydro Tools: uma ferramenta open source para determinação de informações topológicas em bacias hidrográficas integrada a um ambiente SIG. Revista Brasileira de Recursos Hídricos 21(1), 274-287.

Siqueira et al., 2017. Submitted Paper. Issues on spatial discretizations of large scale hydrological and hydrodynamic models.

Snell, J., M. Sivapalan, B. Bates. (2004). Nonlinear kinematic dispersion in channel network response and scale effects: application of the meta-channel concept. Advances in Water Resources, 27, 141–154.

Sholtes and Doyle. (2011). Effect of Channel Restoration on Flood Wave Attenuation. Journal of Hydraulic Engineering, 137(2), 196-208.

Sivapalan, M., K. Takeuchi, S.W. Franks, V.K. Gupta, H. Karambiri, V. Lakshmi, X. Liang, J. Mcdonnell, E.M. Mendiondo, P.E. O'Connell, T. Oki, J.W. Pomeroy, D. Schertzer, S. Uhlenbrook, and E. Zehe (2003), IAHS Decade on Predictions in Ungauged Basins (PUB), 2003–2012: Shaping an exciting future for the hydrological sciences, Hydrological Sciences 48(6), 857-880.

Sorribas, M., Paiva, R., Melack, J., Bravo, J., Jones, C., Carvalho, L,. Beighley, E., Forsberg, B., Costa, M. (2016). Projections of climate change effects on discharge and inundation in the Amazon basin. Climate Change, doi:10.1007/s10584-016-1640-2.

Stephenson, D., P.Kolovopoulos. (1990). Effects of momentum transfer in compound channels. Journal of Hydraulic Engineering 116(12), 1512-1522.

Sutcliffe, J.V., Parks, Y. P., (1989). Comparative water balances of selected African wetlands. Hydrological Sciences 34, 49-62.

Tang, X., D. Knight, P.G. Samuels. (1999). Variable parameter Muskingum-Cunge method for flood routing in a compound channel. Journal of Hydraulic Research 37(5), 591-614.

Tapley, B.D., Bettadpur, S., Watkins, M., Reigber, C. (2004). The gravity recovery and climate experiment: mission overview and early results. Geophysical Research Letters 31(9), 10.1029/2004GL019920.

Taylor, C. M., (2010). Feedbacks on convection from an African wetland. Geophysical Research Letters, 37, L05406, doi:10.1029/2009GL041652.

Thompson, J.R., Crawley, A., Kingston, D.G. (2016). GCM-related uncertainty for river flows and inundation under climate change: the Inner Niger Delta. Hydrological Sciences Journal 61(13), 2325-2347.

Todini, E., (1996). The ARNO rainfall-runoff model. Journal of Hydrology 175, 339-382.

Tourian, M.J., Schwatke, C., Sneeuw, N. (2017). River discharge estimation at daily resolution from satellite altimetry over an entire river basin. Journal of Hydrology 546, 230-247.

Trigg, M., Wilson, M., Bates, P., Horritt, M., Alsdorg, D., Forsberg, B., Vega, M. (2009). Amazon flood wave hydraulics. Journal of Hydrology 374, 92-105.

Trigg, M., Bates, P., Wilson, M., Schumann, G., Baugh, C. (2012). Floodplain channel morphology and networks of the middle Amazon River. Water Resources Research 48, W10504, doi:10.1029/2012WR01188.

Trigg, M., K. Michaelides, J. Neal, P. Bates. (2013). Surface water connectivity dynamics of a large scale extreme flood. Journal of Hydrology 505, 138-149.

Turner-Gillespie, D., J.A. Smith, P. Bates. (2003). Attenuating reaches and the regional flood response of an urbanizing drainage basin. Advances in Water Resources, 26(6), 673-684.

U.S. Army Corps of Engineers (USACE). (2010). HEC-RAS River Analysis System: Hydraulic Reference Manual, Version 4.1. US Army Corps of Engineers, Hydrologic Engineering Center. <http://www.hec.usace.mil>.

Valente, C.R., Latrubesse, E. M., Ferreira, L.G.. Relationships among vegetation, geomorphology and hydrology in the Bananal Island tropical wetlands, Araguaia River basin, Central Brazil. Journal of South American. Earth Sciences, v. 46, p. 150-160. 2013.

Villanueva I, Wright NG. (2006). Linking Riemann and storage cell models for flood prediction. Proceedings of the Institution of Civil Engineers, Journal of Water Management 159, 27–33.

Wagener, T., G. Blöschl, D. Goodrich, H.V. Gupta, M. Sivapalan, Y. Taschikawa, P. Troch, M. Weiler. (2013). A synthesis framework for runoff prediction in ungauged basins, In: Blöschl, G., M. Sivapalan, T. Wagener, A. Viglione, H. Savenije (org.). Runoff Predictions in Ungauged Basins: Synthesis across processes, places and scales. Cambridge: Cambridge University Press, 2013.

Wagener, T., M. Sivapalan, P. Troch, R. Woods. (2007). Catchment classification and hydrologic similarity. Geography Compass 1/4, 901-931.

Whalen, S.C. (2005). Biogeochemistry of Methane exchange between natural wetlands and the atmosphere. Environmental Engineering Science 22(1).

White, A. B., P. Kumar, P. Saco, B. L. Rhoads, B. C. Yen. (2004). Hydrodynamic and geomorphologic dispersion: scale effects in the Illinois River Basin. Journal of Hydrology, 288, 237-257.

Wigmosta, M. S., Vail, L. W., Lettenmaier, D. P., 1994. A distributed hydrology–vegetation model for complex terrain. Water Resour. Res. 30(6), 1665–1679.

Wilson, M., Bates, P., Alsdorf, D., Forsberg, B., Horritt, M., Melack, J., Frappart, F., Famiglietti, J. (2007). Modeling large-scale inundation of Amazonian seasonality wetlands. Geophysical Research Letters 34, L15404, doi:10.1029/2007GL030156.

Winter, T.C. & LaBaugh, J.W. (2003). Hydrologic considerations in defining isolated wetlands. Wetlands 23(3), 535-540.

Wolff, C.G., S.J. Burges. (1994). An analysis of the influence of river channel properties on flood frequency. Journal of Hydrology 153, 317-337.

Wong, T. and E. Laurenson. (1983). Wave speed-discharge relations in natural channels. Water Resources Research 19(3), 701-706.

Yamazaki, D., S. Kanae, H. Kim, T. Oki. (2011). A physically based description of floodplain inundation dynamics in a global river routing model. Water Resources Research, 47, W04501.

Yamazaki, D., Almeida, G., Bates, P. (2013). Improving computational efficiency in global river models by implementing the local inertial flow equation and a vector-based river network map. Water Resources Research 49, 7221-7235.

Yamazaki, D., Sato, T., Kanae, S., Hirabayashi, Y., Bates, P. (2014). Regional flood dynamics in a bifurcating mega delta simulated in a global river model. Geophysical Research Letters 41, 3127-3135.

Zulkafli, Z., Buytaert, W., Onof, C., Manz, B., Tarnavsky, E., Lavado, W., Guyot, J-L. (2014). A comparative performance analysis of TRMM 3B42 (TMPA) Versions 6 and 7 for hydrological applications over Andean-Amazon River basins. Journal of Hydrometeorology 15, 581-592.

Zwarts, L., Beukering, P., Kone, B., Wymenga, E.. (2005). The Niger, a Lifeline: Effective Water Management in the Upper Niger Basin. Lelystad RIZA. The Netherlands.